Spiral and Striped Phases in Cuprates: The Role of Disorder

Dissertation
zur Erlangung des Doktorgrades
des Fachbereichs Physik
der Universität Hamburg

vorgelegt von
Nils Hasselmann
aus Hamburg

Hamburg
2001

Gutachterin/Gutachter der Dissertation:	Prof. Dr. H. Schmidt Prof. Dr. C. de Morais Smith Prof. Dr. D. Pfannkuche Prof. Dr. T. M. Rice
Gutachterin/Gutachter der Disputation:	Prof. Dr. C. de Morais Smith Prof. Dr. D. Fay
Datum der Disputation:	28.06.2001
Sprecher des Fachbereichs Physik und Vorsitzender des Promotionsausschusses:	Prof. Dr. F.-W. Büßer

Summary

In this thesis, the physics of two dimensional spiral and striped phases of doped Mott-insulators, cuprates and nickelates in particular, is investigated. The main emphasis is on the study of the influence of dopant induced disorder on these phases.

In the first part of this work we develop a phenomenological model for the spin glass phase of $La_{2-x}Sr_xCuO_4$. In this model it is assumed that holes doped into the CuO_2 planes localize near their Sr dopants where they cause a dipolar frustration of the antiferromagnetic environment. In absence of long range antiferromagnetic order, the spin system can reduce frustration, and also its free energy, by forming a state with an ordered orientation of the dipolar moments which leads to the appearance of spiral spin correlations. To investigate this model, a non-linear sigma model is used in which disorder is introduced via a randomly fluctuating gauge field. A renormalization group study of this model shows that the collinear fixed point of the model is destroyed through the disorder and that the only stable fixed point is governed by a $O(4)/O(3)$ symmetry. The disorder coupling leads to an additive renormalization of the order parameter stiffness. Further, the stability of the spiral state against the formation of topological defects is investigated with the use of the replica trick. A critical disorder strength is found beyond which topological defects proliferate. Comparing our results with experimental data, it is found that for a hole density $x > 0.02$, i. e. in the entire spin glass regime, the disorder strength exceeds the critical threshold.

In the second part of the thesis, we derive a continuum model which allows to describe and analyze striped phases. Using field theoretical tools, the influence of both disorder and lattice perturbations are investigated. Besides a free phase of the stripes, which is characterized by gaussian fluctuations, the analysis shows the existence of a disorder dominated phase as well as the existence of a lattice pinned phase in which transversal fluctuations of the stripes are suppressed. Comparison with experimental data from cuprates and nickelates shows qualitative agreement with the theoretical phase diagram. Furthermore, the influence of stripe fluctuations on spin fluctuations is investigated. Using dimensional estimates, a depinning transition of disordered stripes subject to an externally applied field is studied. Finally, the interplay between transverse stripe excitations and longitudinal charge and spin fluctuations along the stripe is studied with bosonization techniques. The stability of a phase characterized by a zig-zag form of the transverse displacements and a simultaneous occurrence of longitudinal charge density wave order is demonstrated.

Zusammenfassung

In dieser Arbeit wird die Physik zweidimensionaler Spiral- und Streifenphasen von dotierten Mott-Isolatoren, speziell von Kupraten und Nickelaten, untersucht. Der Schwerpunkt liegt hierbei auf der Analyse des Einflusses von Unordnung, welche durch zufällig verteilte ionisierte Donatoren erzeugt wird.

Im ersten Teil der Arbeit wird ein phänomenologisches Modell für die Spinglas-Phase von $La_{2-x}Sr_xCuO_4$ entwickelt. In diesem Modell wird angenommen, dass die durch die Sr Dotierung erzeugten Löcher in den CuO_2-Ebenen nahe den Sr Donatoren lokalisiert sind und dort eine dipolartige Frustration der antiferromagnetisch geordneten Umgebung hervorrufen. In Abwesenheit von langreichweitiger antiferromagnetischer Ordnung kann das Spinsytem die Frustration, und damit die freie Energie, minimieren, indem es die Dipole ausrichtet, was zu spiralartigen Spinkorrelationen führt. Der Einfluss der Unordnung auf eine solche Spiralphase wird mit Hilfe eines nichtlinearen Sigma-Modells untersucht, in welches die Unordnung durch ein zufällig fluktuierendes Eichfeld eingeführt wird. Unter Verwendung einer Renormierungsgruppen-Analyse wird das Skalenverhalten der Steifigkeit des Ordnungsparameters der Spiralphase sowie der Unordnungsstärke untersucht. Es wird gezeigt, dass der kollineare Fixpunkt des Systems durch die Unordnung zerstört wird, und dass der einzige stabile Fixpunkt des Systems eine $O(4)/O(3)$ Symmetrie besitzt. Die Unordnung führt zu einer additiven Renormierung der Steifigkeit des Ordnungsparameters. Weiterhin wird die Stabilität der Spiralphase gegenüber der Ausbildung topologischer Defekte mit Hilfe des Replika-Tricks untersucht. Die kritische Unordnungsstärke wird berechnet, jenseits derer topologische Defekte durch die Unordnung induziert werden. Der Vergleich mit experimentellen Daten zeigt, dass für eine Lochdichte $x > 0.02$, d. h. in der gesamten Spinglas-Phase, die kritische Unordnungsstärke überschritten ist.

Im zweiten Teil der Arbeit leiten wir zunächst ein Kontinuumsmodel zur Beschreibung der Streifenphase her. Mit Hilfe feldtheoretischer Methoden wird der Einfluss sowohl der Unordnung als auch des Gitterpotentials untersucht. Neben einer freien Phase der Streifen, welche durch Gausssche Quantenfluktuationen der Streifen charakterisiert ist, zeigt die Analyse die Existenz einer ungeordneten Phase, in welcher die Streifen durch die Unordnung gepinnt werden, als auch die Existenz einer Gitter-gepinnten Phase, in welcher die Streifenfluktuationen durch das korrelierte Potential des Gitters unterdrückt werden. Der Vergleich mit Daten von Kupraten und Nickelaten zeigt eine gute qualitative Übereinstimmung des theoretischen Phasendiagramms mit dem Experiment. Weiterhin wird der Einfluss der Streifenfluktuationen auf die Spinfluktationen untersucht. Ein Depinning der ungeordneten Streifen aufgrund extern angelegter Felder wird mit Hilfe dimensionaler Abschätzungen berechnet. Schließlich wird die Wechselwirkung zwischen den transversalen Streifenfluktuationen und den longitudinalen Ladungs- und Spindichtefluktuationen entlang der Streifen mit der Bosonisierungstechnik analysiert. Diese Untersuchung zeigt die Stabilität einer Zick-Zack Form des Streifens bei gleichzeitiger Ausbildung einer longitudinalen Ladungsdichtewelle.

Contents

Chapter 1

Introduction

This thesis is chiefly concerned with the influence of disorder on the properties of striped and spiral states of hole doped cuprate materials, compounds which display high temperature superconductivity at moderate doping concentrations. In cuprates, the superconducting state emerges through chemical doping of a parent compound which is insulating and shows antiferromagnetic (AF) order with a high critical Néel temperature of typically a few hundred Kelvin. As a consequence of the chemical doping, the compounds are intrinsically disordered. Especially at weak doping concentrations disorder is experimentally known to strongly influence the behavior of these materials. This is evident for example in the simplest cuprate superconductor, $La_{2-x}Sr_xCuO_4$, where the superconducting phase emerges via doping directly from a low temperature spin glass phase (see Fig. 1.1) and in which glassy characteristics were detected even inside the superconducting phase.

Cuprates are layered compounds, consisting of weakly coupled CuO_2 planes, and understanding the properties of these planes is central for a description of these materials. In the planes, AF correlations are strong and survive also when the compound is weakly doped. As explained in more detail in the next section, the hole doped CuO_2 planes are well described by a relatively simple model in which each Cu site carries either a spin $\frac{1}{2}$ degree of freedom or a spinless hole which can hop to neighboring sites. Neigboring spins interact via an AF exchange. It is easy to understand that the mobility of holes is directly affected by the desire of the material to form AF correlations. To illustrate this, let us briefly consider a simple toy model mimicking the physics of the CuO_2 planes, where the spin $\frac{1}{2}$ are represented by Ising spins and we consider a state with one missing spin, or hole. When the hole hops, it creates a string of frustration in the AF background which strongly limits the hole's mobility, see Fig. 1.2. While this simple picture would suggest a localization of the hole through strings, both transverse fluctuations of the spins and the existence of retraceable paths which do not cause frustration [2] actually lead to a finite but small mobility.

The single hole properties seem now to be quite well understood and early theories of high temperature superconductivity were constructed from these one-hole wave functions.

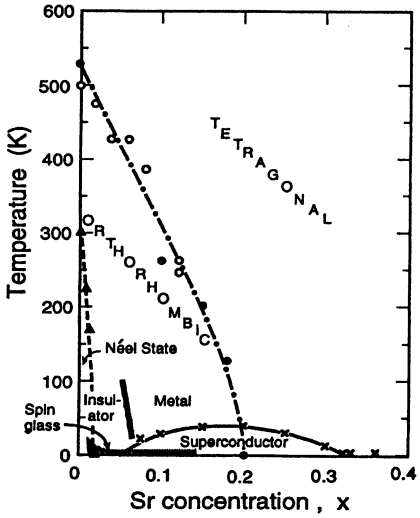

Figure 1.1: Phase diagram of $La_{2-x}Sr_xCuO_4$, from [1].

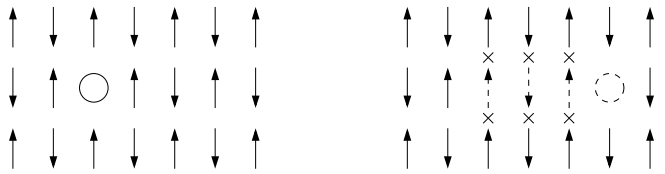

Figure 1.2: String of frustrated AF bonds (crosses) created by moving the hole three lattice sites to the right.

Shraiman and Siggia [3, 4] proposed a theory of interacting hole-quasiparticles based on the one-hole picture and predicted the formation of spiral correlations with a pitch proportional to the hole density. Experiments have to date however not found any evidence of such spiral correlations inside the superconducting phase. The pairing mechanism suggested by the one-hole picture, arising from a dipole-dipole interaction of the holes [5], does not seem to be a satisfactory model of the high T_c phenomenon. One shortcoming of this theory is that it treats the spins in the semi-classical approximation which is only justified in presence of fairly large AF correlation lengths. Generally, a homogenous distribution of a finite density of mobile holes reduces the AF correlations and eventually this is believed to lead to the formation of a spin liquid in which the spins are disordered by quantum fluctuations. In such a state the scattering of the hole from spin excitations is qualitatively different than for the case of ordered AF moments.

At sufficiently low hole concentrations where static AF correlations are still dominant,

i. e. in the spin glass and AF phase, one nonetheless expects an approach based on the semiclassical description of the spins to be a good approximation. In these regimes, dopant disorder is however known to be strong and any description of these phases must account for a quenched distribution of charges, i. e. holes. In the first part of this thesis, chapter 3, we propose a theory of the spin glass regime in which the entire charge distribution is assumed to be quenched. Each hole, localized close to an ionized dopant, is assumed to produce a long ranged dipolar-shaped frustration of the AF, similar to the one known to be produced by delocalized holes. A polarization of the dipole moments leads to the appearance of spiral correlations. Because of the quenched charge distribution, disorder is of fundamental importance in this phase. We therefore develop a renormalization approach for disordered spiral phases, where we study the scaling of the spin stiffness and the disorder. The importance of topological defects of the spiral texture is analysed and their relevance for the physics of the spin glass phase is discussed.

A large amount of theoretical work has been devoted to the properties of the superconducting phase. In most approaches, a homogeneous distribution of mobile holes is assumed. However, one suggestion, which has been put forward by Emery and Kivelson, is that an AF with a finite and homogeneous hole density is in fact a thermodynamically unstable phase, the stable one being rather a phase separated state, in which hole depleted and hole rich phases are formed. Such a clustering of holes would minimize the number of broken bonds at the expense of the kinetic energy of the holes which favors a homogeneous distribution. At present it is not clear, whether the tendency to phase separation really plays an important role in cuprate materials. However, some experiments suggest it does. Phase separation has been observed in oxygen doped cuprates. In these materials, stable homogeneous phases were only found in overdoped samples. The reason why phase separation is observed in oxygen doped materials but not in e. g. Sr doped ones is that oxygen dopants are relatively mobile. Thus, they can screen the long range Coulomb interaction between holes, which would otherwise always prevent macroscopic phase separation to take place. As argued by Emery and Kivelson, for a quenched distribution of dopants the tendency to phase separation is therefore always frustrated, but phase separation may nonetheless appear at a mesoscopic scale. This may lead to the formation of striped phases, in which holes cluster into one dimensional stripes which act as AF domain walls of the undoped AF environment. In this scenario of stripe formation, an immobile distribution of dopants is thus directly responsible for the appearance of stripes. Experimentally, immobile dopants are however always disordered, i. e. the disordered distribution of dopants aquires a dominant role in the frustrated phase separated state. Therefore, in chapter 4, where we analyze the nature of striped phases, we discuss in detail the importance of quenched disorder. We use a phenomenological description of the stripes to investigate the stability of stripes again both pinning by disorder and pinning by the lattice within a renormalization group approach. We further investigate the possibility of a depinning of disorder pinned stripes by externally applied

electric fields. Because superconductivity in cuprate materials has been linked to dynamical fluctuating striped phases, and because stripes in cuprates seem to be characterized by a finite charge density, we also investigate the importance of a coupling between transverse stripe fluctuations and the charge and spin fluctuations along the stripe in the last section of chapter 4.

We begin with an overview over the magnetic properties of weakly doped $La_{2-x}Sr_xCuO_4$ in chapter 2, and develop a phenomenological model for the spin glass regime in chapter 3. Chapter 4, which begins with a review of some key theoretical and experimental results on striped phases, is concerned mainly with the pinning of striped phases by either lattice or disorder perturbation. We compare our results with data from underdoped cuprates and also doped nickelate materials, which are known to display well developed striped phases. In the same chapter we also discuss the interplay between stripe fluctuations and longitudinal charge and spin fluctuations which live on the one dimensional stripes. Finally, we summarize our results in chapter 5 which includes an outlook for possible future investigations.

Chapter 2

Primer: The magnetic phase diagram of weakly doped $La_{2-x}Sr_xCuO_4$

$La_{2-x}Sr_xCuO_4$ (LSCO) has the simplest structure among the family of cuprate high temperature superconductors (HTSC's) and for that reason is one of its best studied members. Common among all cuprates is their layered structure and the presence of CuO_2 layers which are widely believed to be responsible for the unusual properties of these materials. In LSCO the CuO_2 layer are isolated from each other by insulating La(Sr)O layers and the structure is shown schematically in Fig. 2.1. Each Cu site is surrounded by octahedra of oxygen ions, with however imperfect symmetry as the in-plane Cu-O distance (∼1.9 Å) is considerably shorter than the out of plane Cu-O distance (∼2.6 Å). While the prime research interest in

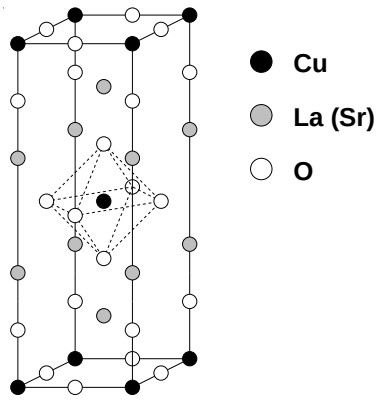

Figure 2.1: Chemical structure of $La_{2-x}Sr_xCuO_4$

HTSC's is related to their superconducting properties, it is generally understood that the magnetism of these materials should play a key role in the mechanism of superconductivity. This has led to detailed studies of the doping dependence of magnetic properties and some

surprising results.

2.1 Chemical structure

Undoped La_2CuO_4 is a charge transfer insulator with an antiferromagnetically ordered groundstate. In this material, lanthanum is in an ionized La^{3+} (closed shell) configuration, oxygen has a closed p-shell and valence state O^{2-} while copper enters a Cu^{2+} state, loosing a $4s$ and one of its $3d$ electrons. The net result is that Cu is one electron short of a closed $3d$ shell and thus a hole with spin $\frac{1}{2}$ is created at the copper site. The two p_x and p_y oxygen orbitals and the Cu $d_{x^2-y^2}$ orbital hybridize to form the hole state with mainly $d_{x^2-y^2}$ character. The undoped CuO_2 planes can thus be effectively described as a simple square lattice (representing the copper sites) with a single spin per lattice site (half filling). A double exchange between charge carriers on neighboring copper sites then leads to an effective antiferromagnetic interaction between neighboring spins. The magnetism of these planes can then to a good approximation be described within a simple square lattice spin-$\frac{1}{2}$ Heisenberg model,

$$H_H = J \sum_{\langle ij \rangle} \mathbf{S}_i \cdot \mathbf{S}_j, \tag{2.1}$$

with an antiferromagnetic $J \sim 1200$K. The sum is over nearest neighbor pairs of sites and $\mathbf{S}_i$ are spin-$\frac{1}{2}$ operators.

Doping of the CuO_2 planes can be achieved e.g. through Sr, which replaces La in the lattice structure. Thus, La^{3+} is replaced by Sr^{2+} and one electron is removed from the CuO_2 planes. This extra hole is mainly localized on the oxygen shells. As argued by Zhang and Rice [6], this extra hole then forms a singlet with the hole localized on the Cu and thus effectively removes one spin from the Cu sites. Hence, doping can be understood as introducing spinless holes into the half filled system. Based on this picture, they argued that the doped CuO_2 planes are well described by a t-J Hamiltonian of the form

$$H_{tJ} = J \sum_{\langle ij \rangle} \mathbf{S}_i \cdot \mathbf{S}_j - t \sum_{\langle ij \rangle, \alpha} \left\{ c^\dagger_{i\alpha} \left(1 - n_{i\bar{\alpha}}\right) \left(1 - n_{j\bar{\alpha}}\right) c_{j\alpha} + h.c. \right\} \tag{2.2}$$

where $c_{i\alpha}$ is a Fermi operator and removes one electron with spin α from site i ($\bar{\alpha}$ has its spin opposite to α). t is the hopping parameter and the $1 - n_{i\bar{\alpha}}$ factors forbid double occupancy.

2.2 Antiferromagnetism of the parent compound

In the study of the magnetism of La_2CuO_4, an approach based on the quantum-non-linear-σ (QNLσM) model has been highly successful. It correctly describes the long wavelength hydrodynamic modes (spin waves) of the Heisenberg model (2.1) [7]. In this continuum

model, it is assumed that the antiferromagnetic correlation length is much larger than the lattice spacing and the model describes slow fluctuations of the locally well defined staggered magnetisation $\mathbf{n}$ (normalized such that $\mathbf{n}^2 = 1$) which, for Heisenberg models, is a three component unit vector. The effective Euclidean action of the QNLσM is

$$\frac{S_{eff}}{\hbar} = \frac{\rho_S}{2\hbar} \int_0^{\hbar\beta} d\tau \int d^2\mathbf{x} \left\{ (\partial_\mu \mathbf{n})^2 + \frac{1}{c^2} (\partial_\tau \mathbf{n})^2 \right\}. \tag{2.3}$$

The spin stiffness ρ_S and the spin wave velocity c should be viewed as phenomenological parameters to be determined either from experiment or from other techniques such as spin wave theory or numerical simulations. The fact that the QNLσM has two parameters already implies that it is more general than the one-parameter model (2.1). The behavior of this model depends strongly on the value of its isotropic coupling constant $g = \hbar c \Lambda / \rho_s$ (Λ is a high frequency cutoff). There is a zero temperature quantum phase transition at $g = g_c \sim 4\pi$. The model has long range order for $g < g_c$ ("renormalized classical regime") whereas for $g > g_c$, the ground state is quantum disordered with only finite spin correlations and no static magnetic order. At finite temperatures there is further an intermediate regime between these two phases which is governed by the nearby quantum critical point and thus characterized by a single scale set by the temperature ("quantum critical regime") [7]. A schematic phase diagram of the model is shown in Fig. 2.2. It is now firmly believed that the Heisenberg model described by (2.1) has $g < g_c$ and that additional frustrating next-nearest neighbor coupling terms are required to reach the disordered regime. Indeed, measurements of the correlation length of La_2CuO_4 have been fitted extremely well with the QNLσM predictions for the renormalized classical regime. The fit can be done without any adjustable parameters assuming only the validity of the model (2.1) and using quantum Monte-Carlo results for ρ_S and c [8].

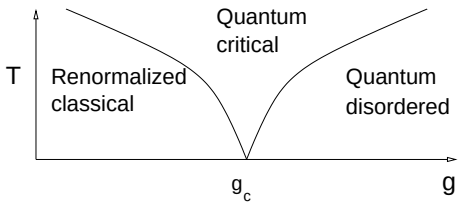

Figure 2.2: Phase diagram of the two dimensional QNLσM

The Néel temperature, which is about 300 K for La_2CuO_4, can also be obtained approximately within a mean field approach, in which 3D ordering should appear roughly at a temperature $T_N \sim [\xi_{2D}(T_N)/a]^2 J_\perp$, where $J_\perp$ is the antiferromagnetic coupling perpendicular to the planes. Even though $J_\perp/J \sim 10^{-4} - 10^{-5}$ is very small, T_N can be fairly large because of the dominant $\xi_{2D} \sim \exp(2\pi\rho_S/T)$ behavior of the 2D correlation length in the renormalized classical regime [7].

2.3 Magnetism at finite doping

Once holes are added to the CuO_2 planes, the magnetism becomes more complicated. Fig. 2.3 summarizes the magnetic phase diagram at weak doping concentrations of $La_{2-x}Sr_xCuO_4$ and $Y_{1-x}Ca_xBa_2CuO_4$. Here, we briefly discuss the phase diagram concentrating on $La_{2-x}Sr_xCuO_4$. For very small Sr concentration, the most dramatic effect is a rapid reduction of T_N with the complete destruction of long range order occurring at a very small critical doping value of roughly $x_g \sim 0.02$. Further, a spin freezing is observed inside the AF phase below a temperature T_f which scales linearly with the Sr concentration, $T_f \sim (815\text{K})x$ for $0 < x < x_g$. This spin freezing is inferred from a broad distribution of extremely slow relaxation times measured with local probes such as ^{139}La nuclear quadrupole resonance (NQR) [9] and muon spin resonance (μSR) [10]. Surprisingly, while at higher temperatures doping leads to a reduction of the local staggered moments, at temperatures lower than about 30 K the staggered moments recover and at zero temperature they are practically doping independent and approach the value of the undoped compound [9, 10]. However, the distribution of staggered moments is broad at finite doping, with a variance which is again simply linear in x [11]. Both the recovery of the staggered moments and the broad distribution of relaxation times is reminiscent of a transverse spin glass state, in which the transverse spin wave modes of the AF freeze in a static but random pattern. Hence, there are unambiguous signatures of disorder in the weakly doped AF phase. This is further corroborated by transport measurements, which show a behavior typical for random systems. At temperatures below ∼50 K the conductivity roughly follows variable range hopping characteristics while at higher temperatures a thermally activated conductivity is observed, with activation energies of about 19 meV [12]. This indicates that the holes localize near their randomly distributed Sr donors.

Both the presence of finite staggered magnetic moments and the broad distribution of slow relaxation times persist also above $x > x_g$ [11], where the long range AF order is destroyed. Again, there is a recovery of the staggered moments at very low temperatures, although the zero temperature moment is now slightly smaller than in the undoped compound. The x dependence of T_f follows now roughly a $1/x$ scaling. The regime $0.02 < x < 0.05$ is well described as a conventional spin glass (SG) and shows characteristic non-ergodic behavior [13]. The freezing transition temperature T_f in this regime can thus be identified as a SG transition temperature T_g.

The fact that staggered moments persist also above $x = 0.02$ is a very important finding and excludes the possibility that the transition at $x = 0.02$ is a disordering transition driven by quantum fluctuations as described in the QNLσM formulation above. It has sometimes been argued that upon hole doping, the reshuffeling of the spins by the mobile holes leads to frustration and enhances quantum fluctuations of the spins. Within such a scenario, it would be possible to reach the quantum critical point of the QNLσ model which would drive the AF into a spin liquid phase. While a renormalization of the effective spin stiffness does

occur, the transition at $x = 0.02$ is not followed by a spin liquid phase but rather a SG. The transition therefore seems to be driven by randomness and not by quantum fluctuations.

Only recently, it was found that the short ranged magnetic order in the SG regime is incommensurate, with a maximum of the imaginary part of the susceptibility located at the in-plane wave vector $(\frac{1}{2} \pm \frac{\delta}{\sqrt{2}}, \frac{1}{2} \pm \frac{\delta}{\sqrt{2}})$, in units of $\frac{2\pi}{a}$ where a is the Cu lattice spacing [14]. Here, δ is the incommensurability which roughly follows $\delta \simeq x$, see Fig. 2.4. A possible explanation for such an incommensurability is diagonal stripe formation. We will argue however that a more likely explanation is the formation of short ranged spiral order.

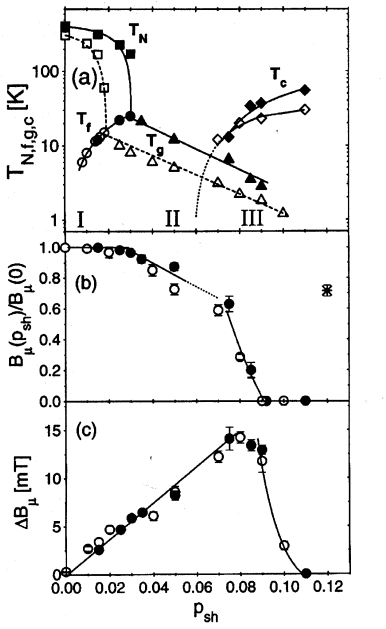

Figure 2.3: Phase diagram as seen by μ-SR, with data obtained from $La_{2-x}Sr_xCuO_4$ (open symbols) and $Y_{1-x}Ca_xBa_2CuO_3$ (closed symbols), p_{sh} is the hole concentration. (a) Doping dependence of the Néel temperature T_N, freezing transition temperature T_f, spin glass transition temperature T_g and superconducting transition temperature T_c. (b) Normalized average internal field at T=1 K. (c) RMS deviation ΔB at T=1 K. Fig. from Niedermayer *et al.* [11].

Superconductivity appears first at a critical doping concentration $x_c \simeq 0.05$. It is interesting that this transition occurs directly from an insulating state and not from a metallic one. Precisely at x_c, there is also a marked change in the magnetic incommensurability. First, the incommensurability changes from diagonal to horizontal, i.e. the dominant peak position of the neutron scattering structure factor changes from $(\frac{1}{2} \pm \frac{\delta}{\sqrt{2}}, \frac{1}{2} \pm \frac{\delta}{\sqrt{2}})$ to $(\frac{1}{2}, \frac{1}{2} \pm \delta)$ and $(\frac{1}{2} \pm \delta, \frac{1}{2})$. Further, while the incommensurate scattering observed in the SG regime is quasi-elastic with the main weight located at zero frequency [14], the incommensurability

seen in the superconducting regime is usually only observed in inelastic scattering experiments with a finite energy transfer [15]. Short ranged static antiferromagnetic correlations, although weaker, are nonetheless observable well inside the superconducting phase and seem to disappear only at relatively high doping concentrations of about $x \sim$0.10-0.12 [11], as can be seen in Fig. 2.3. Again, because of the presence of static moments also for $x > x_c$ there is no clear-cut evidence of a sharp quantum disordering transition of the spins. The strong decrease of static moments well inside the superconducting phase as well as the reduction of low frequency weight of the magnetic susceptibility does however indicate some slow crossover to a spin liquid phase. The most likely scenario is that the quantum transition is replaced by a smooth crossover in the presence of disorder.

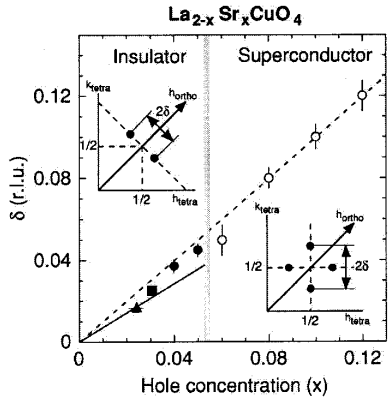

Figure 2.4: Incommensurability of $La_{2-x}Sr_xCuO_4$, from [14]. Insets show the geometry of the IC fluctuations in both the insulating and superconducting phases.

As an unexpected surprise came the observation of static magnetism at $x = 0.12$, with an incommensurability of $\delta \simeq \frac{1}{8}$. This was first observed in a co-doped $La_{1.6-x}Nd_{0.4}Sr_xCuO_4$ sample [16, 17], but later a similar static order was also found in $La_{1.88}Sr_{0.12}CuO_4$ [18, 19, 20] and also in oxygen doped samples [21]. The $La_{1.6-x}Nd_{0.4}Sr_xCuO_4$ sample is further characterized by a charge density wave with half the periodicity of the magnetic periodicity. These experimental data are consistent with a striped phase, in which holes localize in periodically spaced anti-phase domain walls of the antiferromagnet (AF). The presence of stripe-like charge and spin density ordering is believed to be responsible for the anomalous suppression of superconductivity around $x = 1/8$ in these materials. It is interesting, that a similar, although weaker, suppression of T_c near $x = 1/8$ occurs also in $La_{2-x}Sr_xCuO_4$. This suppression, together with the appearance of static spin density order [18], again suggest a formation of a striped phase, although charge order in this compound has not yet been detected.

The experimental indications of static stripe order near $x = 1/8$ have also led to sugges-

tions that the incommensurabilities seen in the dynamic spin fluctuations at lower doping levels may be signatures of fluctuating stripes, i.e. slowly fluctuating anti-phase domain walls. The question whether or not fluctuating stripes are really present in underdoped cuprates is to date still open. A strong evidence for fluctuating stripes would be the detection of incommensurate charge density fluctuations, which are however very difficult to observe because of the small cross section associated with the hole.

Chapter 3

Phenomenological theory of the spin glass phase

Understanding the very weak doping regime of cuprates, in particular the insulating AF and SG regime, should be considerably simpler than the superconducting (SC) or metallic regimes. This optimism is based on the belief that this regime is dominated by the behavior of isolated holes in presence of well developed AF moments. As discussed in the beginning, static AF moments are indeed very strong in $La_{2-x}Sr_xCuO_4$ for small x and the holes seem to be well localized at low temperatures where transport experiments indicate a relatively weakly bound hole with a localization length of a few lattice constants. Thus, one might hope to gain considerable insight into these phases by solving the one-hole problem first and to proceed from there on. Fortunately, the understanding of the behavior of one hole in an antiferromagnetic background is by now quite mature [3, 22, 23]. The coupling of the hole to the spin waves leads to a spin-polaron state. For the $t-J$ model, the bottom of the dressed hole band lies at the zone face centers $\mathbf{k} = (\pm\pi/2, \pm\pi/2)$ and the bandwidth scales with J. Because of the presence of two sublattices, there are two degenerate states per $\mathbf{k}$ vector and one can assign a "spin" to the quasiparticle. An important characteristic of the hole wave function is that it describes a long ranged dipolar distortion of the AF order which arises from a coupling of the spin current carried by the hole to the magnetization current of the AF background [3]. It is however not at all clear whether a dipolar frustration is also produced by localized holes. It has been argued for the case of Sr doping that a chiral spin current is induced on the four Cu sites closest to the Sr impurity and that such a current would induce a distortion of the AF which is Skyrmion like, where the mechanism of frustration is again the coupling between spin and background magnetization currents [24]. The Sr impurity position, located above the center of a Cu plaquette, has a high symmetry and couples to both sublattices in the same way (see Fig. 3.1), so that the "spin" degeneracy mentioned above should survive also in the bound hole state. For a sufficient weakly bound hole, it is quite likely that coupling to the background magnetization will produce frustration

and in the following we shall simply assume that dipolar like frustration is produced by the hole, without discussing the microscopic details of the hole bound state. The symmetry of the Sr position would in fact suggest a quadrupolar frustration, which we can describe as a superposition of two degenerate dipole states. This is similar to the just mentioned spin degeneracy of the bound state and allows for a polarization of the dipolar moments. As we discuss below, the dipole model can quite well explain all the important characteristics of the magnetism of the weakly doped AF and SG phase.

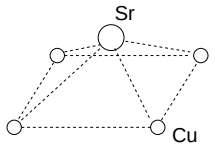

Figure 3.1: Lattice position of the Sr impurity

In section 3.1 we introduce the dipolar frustration model and summarize the main results of previous studies on this model and discuss how they compare with experiments. In section 3.2 we then first derive an extension of the model to allow for non-collinear correlations which arise from dipole ordering and perform a RG analysis to understand the influence of disorder. The importance of topological defects of the spin texture is analysed and finally our results are compared with neutron scattering data on the SG phase of $La_{2-x}Sr_xCuO_4$. We find that the SG phase can be described as a strongly disordered spiral phase in which topological defects proliferate.

3.1 The AF phase and dipolar frustration models

We briefly sketch here the basis of the dipolar frustration model and the results of previous studies of this model in the collinear limit. The model as presented in this section is applicable only for the antiferromagnetic phase in which the dipoles do not have a preferred direction. At high temperatures, the collinear theory can then be used. We will show in the next section however, that the collinear model is not able to describe the low temperature and/or strong disorder regime, where non-collinear behavior emerges.

In the dipole model, it is assumed that each localized hole produces dipolar frustration. It is then possible to study the magnetism of the hole doped materials completely ignoring the charge degrees of freedom and to work with the spin sector only. Further, as there are clear indications of static AF correlations for $x < 0.05$, the antiferromagnet should be well described within the renormalized classical regime of the QNLσM. In this regime, quantum fluctuations simply lead to a renormalization of the spin stiffness of the classical model. A classical model should thus suffice to describe the relevant physics in the AF and SG regime.

3.1.1 Ferromagnetic bonds as an example of dipolar frustration

Dipolar frustration was first discussed in the general context of insulating spin glasses by Villain [25]. The simplest way of producing dipolar spin textures is by placing a ferromagnetic bond in an otherwise AF magnet, whose order parameter we denote by $\mathbf{n}$. At a distance $\mathbf{x}$ away from the ferromagnetic bond, this leads to a deviation of the Néel order $\delta\mathbf{n} \sim \mathbf{f}_\mu x_\mu / x^2$. Here, $\mathbf{f}_\mu$ is a vector both in spin and lattice space, where $\mu = 1{,}2$ are the indices of the 2D lattice vector. The spin part corresponds to the local ferromagnetic moment (with $\mathbf{f}_\mu \perp \mathbf{n}$) produced by the bond and the lattice part corresponds to the orientation of the bond on the lattice (see Fig. 3.2). This can be easily derived in a harmonic continuum approximation, where the energy density of the magnet away from the impurity is proportional to $[\partial_\mu(\delta\mathbf{n})]^2$ and the saddle point solutions satisfy $\nabla^2(\delta\mathbf{n}) = 0$. For any impurity distribution, the solution for $\delta\mathbf{n}$ can thus be written in a multipole expansion. As the Coulomb part is energetically too expensive [25], the lowest order contributions, consistent with the symmetry of the one-bond problem, are dipolar.

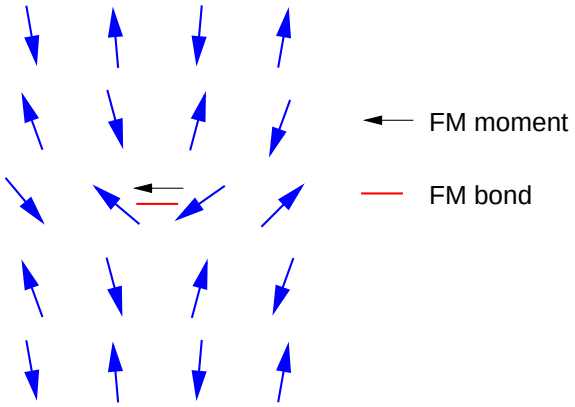

Figure 3.2: Dipolar distortions produced by a ferromagnetic bond

3.1.2 Collinear Model

Because of the long range nature of dipolar frustration, a continuum field theory, such as a (classical) non-linear σ-model (NLσM), should be well suited for a treatment of this problem. While the dipole spin structure discussed above is a saddle point solution of the harmonic theory, it is not a solution of the saddle point equations of the 2D NLσM. Nonetheless one can study the dipole model within the NLσM, if one introduces the dipolar frustration through a minimal coupling scheme. As mentioned in [26], the dipolar frustration can be reproduced (on the harmonic level) via a coupling of the dipoles to the gradient of the order

parameter $\mathbf{n}$ of the NLσM. Thus, within a NLσM approach, the reduced Hamiltonian of the model can be written as [26, 27] (the factor $\beta = T^{-1}$ is included in the Hamiltonian and we set k_B=1)

$$H_{\rm col} = \frac{\rho_s}{2T}\int d^2\mathbf{x}\,(\partial_\mu \mathbf{n})^2 + \frac{\rho_s}{T}\int d^2\mathbf{x}\;\mathbf{f}_\mu\cdot\partial_\mu\mathbf{n}\;, \quad \mathbf{n}^2 = 1 \tag{3.1}$$

where ρ_s is the spin stiffness (renormalized by quantum fluctuations), T the temperature, $\mathbf{n}$ a three component unit vector representing the local staggered moment and $\mathbf{f}_\mu$ is a field representing the dipoles. For a random distribution of localized dipoles

$$\mathbf{f}_\mu(\mathbf{x}) = \mathcal{M}\sum_i \delta(\mathbf{x}-\mathbf{x}_i)a_\mu(\mathbf{x}_i)\mathbf{M}_i \tag{3.2}$$

where the sum is over the impurity sites, $\mathbf{a}_i$ are lattice unit vectors, $\mathbf{M}_i$ unit vectors in spin space, and $\mathcal{M}$ measures the strength of the dipoles. While there is no dipole-dipole interaction term in Eq. (3.1), fluctuations of the $\mathbf{n}$ field generate a spin wave mediated interaction. This can be seen once short scale fluctuations are integrated out under a renormalization procedure [26]. An integration over the short scale fluctuations up to a scale $L \gg 1/\sqrt{x}$ (but $L \ll \xi$ where ξ is the 2D spin correlation length) leads to an effective interaction term of the form

$$H[\{\mathbf{M}_i\}] = \frac{\rho_s\mathcal{M}^2}{2T}\sum_{i,j} J_{ij}\mathbf{M}_i\cdot\mathbf{M}_j \tag{3.3}$$

with

$$J_{ij} = \frac{1}{2\pi x_{ij}^2}\left(2\frac{(\mathbf{x}_{ij}\cdot\mathbf{a}_i)\quad(\mathbf{x}_{ij}\cdot\mathbf{a}_j)}{x_{ij}^2} - \mathbf{a}_i\cdot\mathbf{a}_j\right), \qquad \mathbf{x}_{ij} = \mathbf{x}_i - \mathbf{x}_j. \tag{3.4}$$

Thus, for an average separation of dipoles $\sim 1/\sqrt{x}$ there is a random interaction among dipoles with a characteristic energy $U \sim \rho_s\mathcal{M}^2 x/4\pi$. It was further shown [26] that at high temperatures, $U \ll T$, the presence of dipoles lead to a renormalized effective stiffness $\rho_{\rm eff} = \rho_s(1 - U/T)$. Thus, the correlation length at high temperatures (and small x) has the form

$$\xi \sim \exp\left(\frac{2\pi\rho_{\rm eff}}{T}\right) = \exp\left(\frac{2\pi\rho_s}{T} - \frac{2\pi\rho_s U}{T^2}\right). \tag{3.5}$$

This result agrees to lowest order in x with that obtained by Cherepanov *et al.* [27] in a related renormalization group calculation where they calculated $\rho_{\rm eff}$ up to order x^2. From a comparison with correlation lengths obtained from neutron scattering data at high temperatures, they estimated $U \sim 20\rho_s x$. The doping dependence of T_N was also found to be consistent with the dipole model.

A second and completely independent test of the value of U is to look at the spin relaxation times inside the AF phase. While the relaxation can be understood already within the

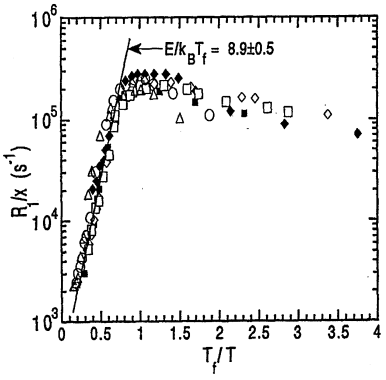

Figure 3.3: $R_1 = (T_1^*)^{-1}$ data from ^{139}La NQR relaxation measurements for $La_{2-x}Sr_xCuO_4$ and various $x < 0.02$, from [9].

theoretical framework just presented, this has so far been overlooked. The relaxation rates inside the AF phase can be explained within the dipole theory if one assumes that the relaxation is driven by the interaction among dipoles and hence controlled by the parameter U. At temperatures well above the actual freezing temperature, an Arrhenius law is observed, with a characteristic energy $E = 8.9T_f \sim 7250\text{K}x$ [9] (see Fig. 3.3). The above estimate of U correctly reproduces not only the linear scaling of the relaxation energy with x but also can account roughly for the prefactor. With $U = 20\rho_s x$, $\rho_s \sim 24$ meV [27] one obtains $U \sim 5500\text{K}x$. Considering that this is a very rough approximation, the value is not too far off from the experimental one. We mention further that the linear scaling of the width of the distribution of local staggered moments is also consistent with a dipole model, as shown in [28]. Thus the dipole model can describe all key experimental data on the magnetism of the AF phase quite well.

3.2 Non-collinear correlations and dipole ordering

While the dipole model presented above can well explain the temperature and doping dependence of the correlation length not just in the AF but also, to some extent, in the SG regime [27], theoretical investigations of the model have always predicted (or rather assumed) short ranged commensurate antiferromagnetism. The recent observation of incommensurate (IC) correlations for the regime $0.02 < x < 0.05$ requires therefore a new approach to the SG phase [29, 30].

As a possible explanation for the presence of IC correlations a disordered striped phase has been proposed, similar to the ordered striped phase found near $x \sim 1/8$. While, as we show in our work on the striped phase in the next section, there is indeed an instability in

the striped phase towards a disordered phase at low x, it is unlikely that the stripes will survive in presence of strong disorder.

In the spin glass regime, there are two competing length scales. The first is related to the average separation between disorder centers (Sr ions) ℓ_d which scales as $\ell_d \sim 1/\sqrt{x}$. The other is the scaling of the periodicity ℓ_s associated with the incommensurability, which scales as $\ell_s \sim 1/x$. For small x, $\ell_d \ll \ell_s$. In a stripe scenario the charge distribution would also have a (short ranged) periodicity which scales with ℓ_s. Thus, in a striped phase the charge can not take full advantage of the disorder. The stripes must either break up into short segments or reduce their on-stripe charge density considerably to take advantage of the disorder potential. Instead we propose here a theory in which the charges are completely disordered and the incommensurability exists only in the spin sector. Then, there is no conflict between the two scales ℓ_s and ℓ_d as ℓ_s relates only to the spins whereas ℓ_d characterizes the charge distribution.

Notice that even in the case that short segments of stripes should be present, these stripes would lose their antiphase domain wall character and instead act like a row of ferromagnetic bonds, again causing dipolar frustration. Thus, the theory we present here applies both to the case of localized hole states which produce dipolar frustration as it does to a system of randomly placed stripe segments. We view the scenario of localized holes however as the more plausible one.

3.2.1 Dipole ordering

It is easy to see how the dipole model can lead to IC correlations [4]. The Hamiltonian Eq. (3.1) favors the formation of a spiral phase, with a non-zero average twist $\partial_\mu \mathbf{n}$ of the AF order and a simultaneous alignment of the dipoles, $\langle \mathbf{f}_\mu \rangle \neq 0$, as long as the lattice and spin degrees of freedom of the dipoles are annealed and free to orient themselves. The lattice position of the Sr dopants (located above the center of a Cu plaquet), which pin the holes, suggests that this freedom indeed exists. We emphasize that a spatially homogeneous distribution of the dipoles is not required for the formation of spiral correlations.

The preferred orientation of the lattice part of the $\mathbf{f}_\mu$ vector is determined by the nature of the localized hole state and therefore should reflect the symmetries of the underlying lattice. Thus a discrete set of favored lattice vectors for the formation of the spiral exists. The a-b (or square lattice) symmetry breaking associated with the formation of spiral correlations can therefore have truly long range order. The continuous symmetry of spin space on the other hand inhibits long range magnetic order in the 2D system for either finite temperatures or disorder. The experimental observation of a macroscopic a-b asymmetry [31] but very short spin correlation lengths thus clearly motivate the study of the dipole model.

3.2.2 Continuum description of spiral phases

We here investigate the dipole model allowing for the presence of non-zero ordered moments but assume a random spatial distribution of the dipoles. First, however, we need a proper theoretical description of the homogeneous spiral phase.

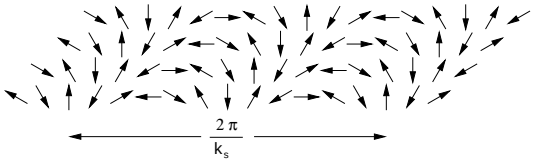

Figure 3.4: Spin texture of an AF spiral.

In collinear magnets, the rotational $O(3)$ symmetry of the system is broken down to a ground state with $O(2)$ symmetry, as rotations around the magnetization axis leave the ground state invariant (this is schematically shown on the left hand side of Fig. 3.5). The order parameter of collinear magnets is then an element of $O(3)/O(2)$. This group is isomorphic to the group of three dimensional unit vectors $\mathbf{n}$, which is the representation used in the Hamiltonian Eq. (3.1). Further, in absence of dipoles, the Hamiltonian Eq. (3.1) is invariant with respect to $O(2)$ rotations of the lattice variables. The spin and lattice symmetries are decoupled and independent for the collinear AF. A spiral ground state on the other hand breaks the $O(3)$ spin symmetry completely. Moreover, in a spiral state the lattice symmetries and the spin symmetries are no longer decoupled and the order parameter space of such a state becomes more involved.

For spirals, the combined symmetry of lattice and the spin space is $O(3) \times O(2)$. As discussed in detail by Azaria *et al.* [32], the coupling of the spin and lattice degrees of freedom in frustrated spin systems leads to an order parameter which results from a symmetry breaking of the combined lattice and spin degrees of freedom and is in general of the form $O(3)\times O(q)/O(q)$ where q depends on the symmetries of the lattice. For a spiral phase, it was found $q = 2$ [33] and thus the order parameter of a spiral is an element of $O(3) \times O(2)/O(2)$.

A convenient representation of the order parameter is in terms of orthonormal $\mathbf{n}_k$, $k = 1 \ldots 3$, with $n_k^a n_q^a = \delta_{kq}$. Klee and Muramatsu [33] have derived a continuum field theory for the $\mathbf{n}_k$ order parameters from the lattice Heisenberg model Eq. (2.1), assuming an IC spiral state with an ordering wave vector $\mathbf{k}_S = (\frac{\pi}{a}, \frac{\pi}{a}) + \mathbf{q}_S$. Here, $\mathbf{q}_S$ measures the deviation from the commensurate AF wave vector. The lattice spins $\mathbf{S}_i$ at sites $\mathbf{r}_i$ can be parametrized in a spiral configuration with the use of the n_k^a as (with $\mathbf{n}_3 = \mathbf{n}_1 \times \mathbf{n}_2$)

$$\mathbf{S}_i/S = \mathbf{n}_1 \cos(\mathbf{k}_S \cdot \mathbf{r}_i) - \mathbf{n}_2 \sin(\mathbf{k}_S \cdot \mathbf{r}_i). \tag{3.6}$$

A perfectly ordered spiral is described by Eq. (3.6) with constant, i.e. space independent, $\mathbf{n}_k$. To allow for spatial fluctuations of the spins around the spiral order, Klee and Muramatsu

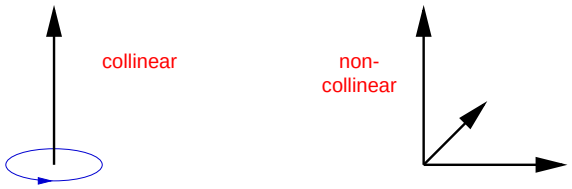

Figure 3.5: The order parameter of collinear magnets, which are invariant under rotations around the collinear axis, can be represented by a unit vector (left), whereas non-collinear order parameters require three orthonormal vectors (right).

introduced a slowly varying field $\mathbf{L}$ via (see also [34])

$$\begin{aligned} \frac{\mathbf{S}(\mathbf{r}_i)}{S} &= \frac{\mathbf{n}_1 \cos(\mathbf{k}_S \cdot \mathbf{r}_i) - \mathbf{n}_2 \sin(\mathbf{k}_S \cdot \mathbf{r}_i) + a\mathbf{L}}{\sqrt{1 + 2a[\mathbf{n}_1 \cos(\mathbf{k}_S \cdot \mathbf{r}_i) - \mathbf{n}_2 \sin(\mathbf{k}_S \cdot \mathbf{r}_i)] \cdot \mathbf{L} + a^2 L^2}} \\ &= \mathbf{N} + a\left[\mathbf{L} - (\mathbf{N}\cdot\mathbf{L})\right] - a^2\left[(\mathbf{N}\cdot\mathbf{L})\,\mathbf{L} + \frac{1}{2}\mathbf{L}^2\mathbf{N} - \frac{3}{2}(\mathbf{N}\cdot\mathbf{L})^2\,\mathbf{N}\right] + \mathcal{O}(a^3), \end{aligned} \tag{3.7}$$

where $\mathbf{N} = \mathbf{n}_1 \cos(\mathbf{k}_S \cdot \mathbf{r}_i) - \mathbf{n}_2 \sin(\mathbf{k}_S \cdot \mathbf{r}_i)$. The continuum theory can then be found upon expressing in the lattice Heisenberg model the spin operators in terms of the $\mathbf{n}_k$ and $\mathbf{L}$ fields, expanding the terms up to order a^2 and taking the limit $a \to 0$ in the end. After integrating out the $\mathbf{L}$ fields, one finds an effective Hamiltonian which can be written in the classical limit in the general form [33] (again we include the factor $\beta = T^{-1}$ into H)

$$H = \frac{1}{2}\int d^2\mathbf{x}\; p_{k\mu}(\partial_\mu \mathbf{n}_k)^2 + s_\mu \int d^2\mathbf{x}\; \mathbf{n}_1 \cdot \partial_\mu \mathbf{n}_2. \tag{3.8}$$

This description is valid for length scales larger than $|\mathbf{q}_S|^{-1}$. The stiffnesses of the order parameter $\mathbf{n}_k$ are given initially by $p_{1\mu} = p_{2\mu} = JS^2 \cos(q_{S\mu}a)/(2T)$ and $p_{3\mu} \simeq 0$, but will change under a renormalization of the model. We will ignore for the most part the small anisotropy (of order $|\mathbf{q}_S|^2 a^2$) in the stiffnesses $p_{k\mu}$ and just write p_k. The vector $\mathbf{s}$ is to lowest order given by $\mathbf{s} = J\mathbf{q}_S/T$. The term with the s_μ pre-factor makes this Hamiltonian unstable, which simply expresses the fact that the pure Heisenberg model does not support a spiral phase ground state. The s_μ term will however be cancelled by a similar term originating from the coupling of the spins to the ordered fraction of the dipoles, relating the incommensurability self-consistently to the ordered moment of the dipoles. In other words, the ordered dipoles stabilize the spiral phase, as expected.

It must be stressed that because the continuum model is only valid at length scales larger than the period of the IC structure, there is a relatively large uncertainty in the estimates of the $p_{k\mu}$. There is always a fundamental problem in relating the continuum model parameters to those of the original microscopic lattice model, but in this case this problem is especially severe. The continuum model parameters must be obtained from an average over one period

of the spiral which, for small incommensurabilities, can be rather large. Thus, the above estimates for the $p_{k\mu}$'s should be taken with care.

3.2.3 Disorder coupling: a gauge glass model

We now must include the coupling of the dipolar frustration centers to the spiral order parameter. While there is no microscopic derivation of this coupling at hand, the fact that the coupling in the collinear model can be expressed within a minimum coupling scheme allows for a simple generalization of the model to non-collinear spin states. We first observe that the ordering wave vector of the spiral, $\mathbf{q}_S$, is entirely determined by the average orientation of the dipoles. Similarly, local variations of the density or orientation of the dipoles should also modify the local ordering wave vector. Further, to reproduce the strong canting produced by the dipoles, the coupling should be of first order in the spatial derivative of the spiral order parameter. To generate the frustration produced by the dipoles we thus introduce a minimal coupling [35] in the first term of Eq. (3.8), i.e. we replace $(\partial_\mu \mathbf{n}_k)^2$ with $[(\partial_\mu - i\mathbf{B}_\mu \cdot \mathbf{L})\mathbf{n}_k]^2$ where $\mathbf{B}_\mu$ is a random gauge field, representing the dipoles. The components of $\mathbf{L}$ are 3×3 matrix representations of angular momenta which generate rotations about the three spin axes, with

$$-i\mathbf{B}_\mu \cdot \mathbf{L}\ \mathbf{n}_k = \mathbf{B}_\mu \times \mathbf{n}_k. \tag{3.9}$$

This coupling has the advantage of relative simplicity combined with a clear physical interpretation: the dipolar fields define the locally preferred wave vector of the spiral, and fluctuations of the dipole fields lead to fluctuations of the wave vector. Further, it reproduces the correct form of the dipole coupling in the collinear limit, as shown below. Let us write $\mathbf{B}_\mu = [\mathbf{B}_\mu]_D + \mathbf{Q}_\mu$ so that $[\mathbf{Q}_\mu]_D = 0$, where $[\ldots]_D$ is the disorder average. We then obtain the following Hamiltonian for the spiral in presence of disorder,

$$H = \frac{1}{2}\int d^2\mathbf{x} p_{k\mu}(\partial_\mu \mathbf{n}_k)^2 + \int d^2\mathbf{x}\ p_k \partial_\mu \mathbf{n}_k \cdot \mathbf{Q}_\mu \times \mathbf{n}_k, \tag{3.10}$$

where the ordered part of the dipole field cancels the second term in Eq. (3.8). Thus,

$$p_{k\mu}\partial_\mu \mathbf{n}_k \cdot [\mathbf{B}_\mu]_D \times \mathbf{n}_k + s_\mu \mathbf{n}_1 \cdot \partial_\mu \mathbf{n}_2 = 0. \tag{3.11}$$

As $\mathbf{q}_S \propto \mathbf{s}$, this equation relates the incommensurability linearly to the density of ordered dipoles. The remaining part of the dipole field, $\mathbf{Q}_\mu$, is a quenched variable with zero mean and we assume Gaussian short ranged statistics,

$$\left[Q^a_\mu(\mathbf{x})Q^b_\nu(\mathbf{y})\right]_D = \lambda\delta(\mathbf{x}-\mathbf{y})\ \delta_{ab}\ \delta_{\mu\nu}. \tag{3.12}$$

In absence of disorder, the Hamiltonian defined by Eq. (3.10) has the desired $O(3) \times O(2)/O(2)$ symmetry. The $O(3)$ symmetry is associated with the spin indices a of the

n_k^a, while the $O(2)$ symmetry is associated with the lattice indices k and arises because $p_{1\mu} = p_{2\mu}$. Hence, the equality $p_{1\mu} = p_{2\mu}$ is directly related and enforced by the symmetries of the spiral. Note that if all $p_{k\mu}$ are identical, the lattice symmetry is enhanced to $O(3)$. We further see now, that the model reduces to the collinear model Eq. (3.1) in the case $p_{1,2} = 0$ with $p_3 = \rho_s/T$, $\mathbf{n}_3 = \mathbf{n}$ and $\mathbf{f}_\mu = \mathbf{Q}_\mu \times \mathbf{n}$. Unfortunately it is not possible to reach the collinear limit by sending $\mathbf{q}_S \to 0$. The reason is that the parameters $p_{k\mu}$ are, within the approximation used in their derivation, independent of the size of the unit cell of the spiral, i.e. in the limit $\mathbf{q}_S \to 0$, the unit cell size diverges while the parameters $p_{k\mu}$ remain unaffected.

The model defined by Eq. (3.10) is in fact far more general than its derivation might suggest. In absence of disorder it is applicable to other types of frustrated spin systems with a non-collinear groundstate, such as e. g. the Heisenberg model on a triangular lattice [34, 36, 32]. It is conceivable, that certain types of randomness in such lattices may be well described by the disorder coupling employed here. More importantly, the model Eq. (3.10) can be viewed as a general model to investigate diluted spin glasses, in which a spin system is frustrated by a small number of impurities. There have been investigations of similar models of spin glasses in the past, most notably by Hertz [35], but in these investigations non-collinear correlations were not accounted for. The motivation for studying such gauge glass models is the hope of finding a spin glass fixed point. However, as non-collinear correlations are known to be essential in spin glasses (see, e. g. [37]), there is little hope in finding the correct fixed point in a treatment which ignores them. Our approach has the appeal that it can interpolate between collinear and non-collinear states and thus offers the possibility to study the transition from an ordered collinear magnet to a disordered non-collinear one continuously.

3.2.4 Renormalization

We will now investigate the renormalization of the model under a change of scale, with the objective to understand the influence of the dipoles on the correlation length of the model. For carrying out the RG calculation, it is of advantage to use a $SU(2)$ representation of the model [36] (see also App. A.1). We therefore write

$$n_k^a = \frac{1}{2}\mathrm{tr}\left[\sigma^a g \sigma^k g^{-1}\right] \tag{3.13}$$

where σ^a are Pauli matrices and $g \in SU(2)$. We further introduce the fields [38]

$$A_\mu^a = \frac{1}{2i}\mathrm{tr}\left[\sigma^a g^{-1}\partial_\mu g\right], \tag{3.14}$$

which are related to the first spatial derivatives of $\mathbf{n}_k$ through $\partial_\mu n_k^a = 2\epsilon_{ijk} A_\mu^i n_j^a$. Eq. (3.10) then aquires the form,

$$H = \frac{1}{t_\mu}\int d^2\mathbf{x}\left[\mathbf{A}_\mu^2 + b A_\mu^{z\,2}\right] +$$

$$+2\int d^2\mathbf{x}\; p_{k\mu}\; \epsilon_{ijk}\; \epsilon_{abc}\; A^i_\mu\; n^a_j\; n^c_k\; Q^b_\mu\; . \tag{3.15}$$

where $t_\mu^{-1} = 2(p_{1\mu} + p_{3\mu})$ and $b = (p_{1\mu} - p_{3\mu})/(p_{1\mu} + p_{3\mu})$. At the point $b = 0$ the symmetry is enhanced to $O(3) \times O(3)/O(3) \simeq O(4)/O(3)$ while at $b = -1$ the model is collinear. For spirals, we have initially $b = 1$.

We first discuss the dimensional scaling behavior of the model (3.10, 3.15). We assign the dimension -1 to each spatial dimension (such that ∂_μ has dimension 1). It then follows that the $\mathbf{A}_\mu$ fields, which each contain one derivative of the dimensionless fields $\mathbf{n}_k$, have a scaling dimension of 1. The scaling dimension of the first term in Eqs. (3.10, 3.15) is then $2-2 = 0$, where the -2 comes from the spatial integral (for the d-dimensional case, this term would have a scaling dimension $2 - d$, hence $d = 2$ is the lower critical dimension). Thus, this term is marginal and an RG analysis is required to study the scaling of the t_μ, b parameters. From this simple scaling analysis it is also evident that local terms containing more than two $\mathbf{A}_\mu$ terms have positive dimensions and are thus irrelevant in the sense that they scale to zero in the long wavelength regime. Hence, such terms, while they are generated in the perturbative expansion we discuss below, need not be considered.

As was pointed out in [27], for the disorder choice (3.12) the model defined by Eq. (3.1) has a lower critical dimension of two and is thus renormalizable in two dimensions, as can be shown with a general Imry-Ma type argument. The same argument can be used for the present model. The disorder coupling in Eq. (3.10) can be rewritten in momentum space as a random field coupling of the form

$$\int \frac{d^2\mathbf{q}}{(2\pi)^2} \quad \mathbf{n}_k(-\mathbf{q}) \cdot \mathbf{h}_k(\mathbf{q}); \qquad \mathbf{h}_k(\mathbf{q}) = ip_{k\mu}q_\mu \int d^2\mathbf{x}\; (\mathbf{Q}_\mu \times \mathbf{n}_k) e^{i\mathbf{q}\cdot\mathbf{x}} \tag{3.16}$$

where the random fields $\mathbf{h}_k(\mathbf{q})$ have disorder correlations with a momentum dependence $\left[h^a_k(\mathbf{q}) h^{a'}_{k'}(\mathbf{q}')\right]_D \propto \delta(\mathbf{q} - \mathbf{q}')|\mathbf{q}|^\Theta$ with $\Theta = 2$. According to general arguments by Imry and Ma [39], in models with continuous symmetries random fields will destroy long range order as long as $d < 4 - \Theta$. This implies that in our case $d = 2$ is the lower critical dimension [27] and a renormalization group analysis of both the stiffness and the disorder coupling is required.

The perturbative expansion of the model suffers from both infrared (IR) and ultraviolet (UV) divergences. We need not worry about the UV divergences as they will be cut off by the lattice of the original microscopic model. To control infrared divergences, we need to study the renormalization of the model as we go to larger and larger length scales. We therefore successively change the scale of the model, i.e. we look at how the parameters of the model change if we change the lattice cutoff by a small factor Λ. This requires an integration of the fast modes of the problem with a subsequent rescaling of fields and integration measures.

We now derive the one-loop RG equations. For this, we split the original $SU(2)$ field g, into slow and fast modes, $g = \tilde{g}\exp(i\ \varphi^a\sigma^a)$ and trace out the fast modes φ^a which have fluctuations in the range $[\Lambda^{-1}, 1]$, where we set the original UV cutoff equal to 1. For the

one-loop calculation, we need an expansion of Eq. (3.15) up to second order in φ^a (higher order terms will only contribute at higher loop order of the RG). For the fields $\mathbf{n}_k$ and $\mathbf{A}_\mu$ the expansion reads (see App. A.2 for more details)

$$A_\mu^i = \tilde{A}_\mu^i + \partial_\mu \varphi^i + \epsilon_{ijk}\varphi^j \partial_\mu \varphi^k + 2\epsilon_{ijk}\varphi^j \tilde{A}_\mu^k - 2\tilde{A}_\mu^i \, \boldsymbol{\varphi}^2 + 2\tilde{\mathbf{A}}_\mu \cdot \boldsymbol{\varphi} \; \varphi^i + \mathcal{O}(\varphi^3), \tag{3.17}$$

$$n_i^a = \tilde{n}_i^a + 2\epsilon_{ijk}\varphi^j \tilde{n}_k^a + \varphi^j \varphi^k R_{jk}^{ai} + \mathcal{O}(\varphi^3), \tag{3.18}$$

where

$$R_{jk}^{ai} = \frac{1}{2} \; \mathrm{tr} \left\{ \sigma^a \tilde{g} \left(\sigma^j \sigma^i \sigma^k - \frac{1}{2}\sigma^j \sigma^k \sigma^i - \frac{1}{2}\sigma^i \sigma^j \sigma^k \right) \tilde{g}^{-1} \right\}. \tag{3.19}$$

The expansion of the energy functional (3.15) reads

$$H = \frac{1}{t_\mu} \int d^2\mathbf{x} \left[\tilde{\mathbf{A}}_\mu^2 + b \left(\tilde{A}_\mu^z \right)^2 \right] + H_{c0} + H_\varphi + H_p \tag{3.20}$$

with

$$H_{c0} = 2 \int d^2\mathbf{x} p_{k\mu} \epsilon_{ijk} \; \epsilon_{abc} \; \tilde{A}_\mu^i \tilde{n}_j^a \tilde{n}_k^c Q_\mu^b, \tag{3.21}$$

$$H_p = H_1 + H_2 + H_3 + H_4 + H_{c1} + H_{c2} + H_{c3} + H_{c4}. \tag{3.22}$$

The first two terms in the expansion of H have exactly the same form as the original functional (3.15), but are now functionals of the slow fields. H_φ is quadratic in φ and has the form

$$H_\varphi = \frac{1}{t_\mu} \int d^2\mathbf{x} \left[(\partial_\mu \boldsymbol{\varphi})^2 + b \left(\partial_\mu \varphi^z \right)^2 \right] \tag{3.23}$$

$H_1 \ldots H_4$ are generated by the first term in Eq. (3.15) and are given by

$$H_1 = 2t_\mu^{-1} \int d^2\mathbf{x} \; \tilde{A}_\mu^i \partial_\mu \varphi^j \varphi^k \epsilon_{ijk} \left(1 - b\delta_{iz} + 2b\delta_{jz} \right), \tag{3.24}$$

$$H_2 = 2t_\mu^{-1} \int d^2\mathbf{x} \; \partial_\mu \varphi^i \tilde{A}_\mu^i \left(1 + b\delta_{iz} \right), \tag{3.25}$$

$$H_3 = 4bt_\mu^{-1} \int d^2\mathbf{x} \; \epsilon_{zjk} \tilde{A}_\mu^z \varphi^j \tilde{A}_\mu^k, \tag{3.26}$$

$$H_4 = 4bt_\mu^{-1} \int d^2\mathbf{x} \; \left[\left(\epsilon_{zjk} \varphi^j \tilde{A}_\mu^k \right)^2 - \left(\tilde{A}_\mu^z \right)^2 \boldsymbol{\varphi}^2 + \tilde{A}_\mu^z \varphi^z \tilde{\mathbf{A}}_\mu \cdot \boldsymbol{\varphi} \right]. \tag{3.27}$$

The coupling term in Eq. (3.15) produces the $H_{c1} \ldots H_{c4}$ terms,

$$H_{c1} = 4 \int d^2\mathbf{x} \; p_{k\mu} \epsilon_{ijk} \epsilon_{abc} \left[\epsilon_{klm} \tilde{n}_j^a \tilde{n}_m^c \tilde{A}_\mu^i + \epsilon_{jlm} \tilde{n}_k^c \tilde{n}_m^a \tilde{A}_\mu^i + \epsilon_{ilm} \tilde{n}_j^a \tilde{n}_k^c \tilde{A}_\mu^m \right] \varphi^l Q_\mu^b, \tag{3.28}$$

$$H_{c2} = 2 \int d^2\mathbf{x} \; p_{k\mu} \epsilon_{ijk} \epsilon_{abc} \partial_\mu \varphi^i \tilde{n}_j^a \tilde{n}_k^c Q_\mu^b, \tag{3.29}$$

$$\begin{aligned} H_{c3} = 2 \int d^2\mathbf{x} \; p_{k\mu} \epsilon_{ijk} \epsilon_{abc} \Big[& \tilde{A}_\mu^i \left(\tilde{n}_j^a R_{lm}^{ck} + \tilde{n}_k^c R_{lm}^{aj} \right) \varphi^l \varphi^m + 2\tilde{n}_j^a \tilde{n}_k^c \left(\tilde{\mathbf{A}}_\mu \cdot \boldsymbol{\varphi} \; \varphi^i - \tilde{A}_\mu^i \boldsymbol{\varphi}^2 \right) \\ & + 4 \left(\tilde{A}_\mu^i \epsilon_{jlm} \epsilon_{kpq} \tilde{n}_m^a \tilde{n}_q^c + \tilde{A}_\mu^m \epsilon_{ilm} \epsilon_{kpq} \tilde{n}_q^c \tilde{n}_j^a + \tilde{A}_\mu^m \epsilon_{ilm} \epsilon_{jpq} \tilde{n}_q^a \tilde{n}_k^c \right) \varphi^p \varphi^l \Big] Q_\mu^b, \end{aligned} \tag{3.30}$$

$$\begin{aligned} H_{c4} = 2 \int d^2\mathbf{x} \; p_{k\mu} \epsilon_{ijk} \epsilon_{abc} \Big[& 2 \left(\epsilon_{klm} \tilde{n}_j^a \tilde{n}_m^c + \epsilon_{jlm} \tilde{n}_m^a \tilde{n}_k^c \right) \partial_\mu \varphi^i \varphi^l \\ & + \epsilon_{ilm} \partial_\mu \varphi^m \varphi^l \tilde{n}_j^a \tilde{n}_k^c \Big] Q_\mu^b. \end{aligned} \tag{3.31}$$

The integration over the fast φ fields is performed with

$$\int \mathcal{D}[\varphi^i] \exp(-H_\varphi) \exp(-H_p) \;=\; e^{-\mathcal{F}} \int \mathcal{D}[\varphi^i] \exp(-H_\varphi) \tag{3.32}$$

where $\mathcal{F}$ is obtained from a cumulant expansion

$$-\mathcal{F} \;=\; \ln \frac{\int \mathcal{D}[\varphi^i] \exp(-H_\varphi) \exp(-H_p)}{\int \mathcal{D}[\varphi^i] \exp(-H_\varphi)} = \sum_{n=1}^{\infty} \frac{(-1)^n}{n!} \left\langle H_p^n \right\rangle_{\varphi c} \tag{3.33}$$

and $\langle \ldots \rangle_{\varphi c}$ indicates that only connected diagrams are to be considered, i.e. only averages which can not be written as a product of averages enter.

Renormalization of the spin stiffness

We ignore the (small) anisotropy of the t_μ parameter and simply use the isotropic mean $t_s = \sqrt{t_1 t_2}$ in the RG analysis below. We collect all terms in the perturbative expansion which are bilinear in $\tilde{A}^i_\mu$. After performing the disorder average of $\mathcal{F}$, the renormalized stiffnesses of the $\tilde{A}^i_\mu$ fields is found to be (see App. A.4.1)

$$\frac{1}{\tilde{t}_s} \;=\; \frac{1}{t_s} - \left[\frac{2(1-b)}{t_s} + \frac{(2-b+b^2)\lambda}{t_s^2} \right] C^x(\mathbf{0}), \tag{3.34}$$

$$\frac{\tilde{b}}{\tilde{t}_s} \;=\; \frac{b}{t_s} - \left[\frac{2b(3+b)}{t_s} + \frac{b(5+b)\lambda}{t_s^2} \right] C^x(\mathbf{0}). \tag{3.35}$$

With $\ell = \ln \Lambda$ and

$$C^x(\mathbf{0}) = \frac{t_s}{4\pi} \ln \Lambda \tag{3.36}$$

one then finds the RG equations

$$\frac{\partial}{\partial \ell} \frac{1}{t_s} \;=\; -\frac{1-b}{2\pi} - \frac{(2-b+b^2)\lambda}{4\pi t_s}, \tag{3.37}$$

$$\frac{\partial}{\partial \ell} \frac{b}{t_s} \;=\; -\frac{(3+b)b}{2\pi} - \frac{(5+b)b\lambda}{4\pi t_s}. \tag{3.38}$$

This yields

$$\frac{\partial}{\partial \ell} t_s \;=\; \frac{1-b}{2\pi} t_s^2 + \frac{2-b+b^2}{4\pi} \lambda t_s, \tag{3.39}$$

$$\frac{\partial}{\partial \ell} b \;=\; -\frac{b(1+b)}{\pi} t_s - \frac{b(1+b)(3-b)}{4\pi} \lambda. \tag{3.40}$$

For $\lambda = 0$, these equations describe the RG of a clean spiral [36], while for the collinear point $b = -1$, the equations reproduce the RG of the stiffness for disordered collinear models [27]. From Eq. (3.40) it is seen that there are two fixed points for b (the asymptotic freedom of the model prevents a true fixed point in 2D as t_s always diverges). The collinear point $b = -1$ is unstable whereas $b = 0$ is stable, irrespective of the disorder. The RG flow of t_s and b is shown in Fig. 3.6 for $\lambda = 0$. The flow does not change qualitatively for finite λ as long as $\lambda \ll t_s$. Hence, the coupling to weak disorder does not lead to any new fixed points, although the disorder renormalizes the stiffness.

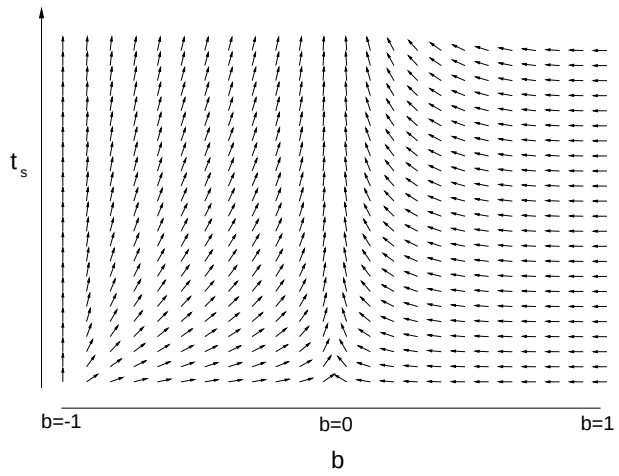

Figure 3.6: RG flow of t_s and b for $\lambda = 0$. For any $b > -1$, the flow is towards $b = 0$.

Renormalization of disorder coupling

As we discuss below, the renormalization of λ is given by terms proportional to λt_s and λ^2. As the disorder enters the renormalization of t_s only in the combination λt_s (see Eq. (3.39)), we can neglect the renormalization of λ altogether for $t_s \gg \lambda$, i. e. at high temperatures (we have $t_s \propto T/J$). However, for low temperatures the renormalization of λ must be taken into account. To calculate the renormalization of the disorder we follow the approach used in [27]. In this approach, the renormalized disorder variance is defined by the variance of all terms in the perturbative expansion which couple to the quenched disorder fields and are linear in $\tilde{\mathbf{A}}_\mu$. Note however that there exists no symmetry argument which guarantees that the funtional form of the disorder coupling remains unchanged under the RG. It is thus possible that new disorder terms are generated so that a simple renormalization of λ is not sufficient. This is indeed the situation we encounter for general $b \neq 0$ and discuss in more detail below, where we find the generation of new coupling terms at order λ^2. To find the complete renormalization of the model one would have to include all generated new terms into the original model, which is a rather laborious process which we did not pursue. Nonetheless, as we have just shown above, there are only two possible fixed points even in absence of disorder, $b = 0$ and $b = -1$. Rather than trying to categorize all possible disorder couplings, we therefore focus on a discussion of the RG of the disorder near these two possible fixed points and discuss their stability under the flow.

We begin with the collinear case, $b = -1$. In this case, the renormalized variance of the terms linear in $\tilde{A}^i_\mu$ is given by (see App. A.4.2, Eq. (A.23))

$$\frac{\lambda}{t_s^2}\int d^2\mathbf{x}\left\{\left[\left(\tilde{A}^x_\mu\right)^2+\left(\tilde{A}^y_\mu\right)^2\right]\left(1-\frac{2}{\pi}t_s\ln\Lambda-\frac{1}{2\pi}\lambda\ln\Lambda\right)+\left(\tilde{A}^z_\mu\right)^2\frac{1}{2\pi}\lambda\ln\Lambda\right\}. \tag{3.41}$$

What is evident from this result is that the renormalized disorder coupling is no longer of the original form $p_k \partial_\mu \mathbf{n}_k \cdot \mathbf{Q}_\mu \times \mathbf{n}_k$. Such a coupling has a variance which includes a prefactor of $(1+b)^2$ of $\left(\tilde{A}^z_\mu\right)^2$. According to Eq. (3.40), $b=-1$ is not changed under the influence of the original disorder coupling. A renormalization which retains the form of the original coupling can then not lead to a renormalized disorder variance with a finite prefactor of $\left(\tilde{A}^z_\mu\right)^2$ at $b=-1$. Such a term is however present in Eq. (3.41) we conclude that a new type of disorder coupling is generated at $b=-1$. This is perhaps easier to see in Fourier space, where the original disorder coupling can be written as a correlated random field coupling $\mathbf{n}_k(-\mathbf{q}) \cdot \mathbf{h}_k(\mathbf{q})$, see Eq. (3.16). For the original minimal coupling one has $\mathbf{h}_k(\mathbf{q}) \propto p_k$ and thus, in the collinear limit $b=-1$ (or $p_1=0$), only $\mathbf{n}_3$ is affected by this coupling. We can then interpret the finite prefactor of the $\left(A^z_\mu\right)^2$ term in the disorder variance as the generation of correlated fields which couple also to $\mathbf{n}_{1,2}$ even at $b=-1$. It is evident that such a coupling will drive the system away from $b=-1$ and thus destroy the collinear fixed point. Thus, even if the original AF order is collinear (i.e. in absence of dipole ordering), the disorder drives the system to a non-collinear state. An analysis which presupposes collinear order is thus not valid in the presence of dipoles and cannot describe the low temperature regime correctly. Physically, one would also expect the appearance of non-collinearity. The random canting of spins leads to a random local deviation of the spins from the ordering axis and thus destroys the remaining $O(2)$ spin symmetry of the collinear model.

To make contact with the RG result obtained from the collinear model in [27], we note that we can reproduce the result Cherepanov *et al.* obtained for the disorder renormalization if we ignore non-collinear modes. We can then define the renormalization of λ just by the terms which are present in a purely collinear theory, i.e. by the $\left[\left(\tilde{A}^x_\mu\right)^2 + \left(\tilde{A}^y_\mu\right)^2\right]$ term in Eq. (3.41). Then

$$\frac{\partial}{\partial \ell}\frac{\lambda}{t_s^2} = -\frac{2\lambda}{\pi t_s} - \frac{\lambda^2}{2\pi t_s^2}, \tag{3.42}$$

which, using Eq. (3.39) leads to

$$\frac{\partial}{\partial \ell}\lambda = \frac{3}{2\pi}\lambda^2. \tag{3.43}$$

This, together with Eq. (3.39) are the RG equations found in [27] (note that our stiffness t_s differs from the stiffness t used in [27] by a factor two). We emphasize that this result is not correct as it ignores the role of non-collinearity in the problem.

We now turn to the point $b=0$, the only remaining possible fixed point of the model. At this highest symmetry point we find that no new coupling terms are generated. The variance of the renormalized disorder coupling takes the form

$$\frac{\lambda}{t_s^2}\int d^2\mathbf{x}\left\{\tilde{\mathbf{A}}^2_\mu\left(1-\frac{4t_s+3\lambda}{4\pi}\ln\Lambda\right)\right\}. \tag{3.44}$$

Thus,

$$\frac{\partial}{\partial \ell}\frac{\lambda}{t_s^2} = -\frac{1}{\pi}\frac{\lambda}{t_s} - \frac{3}{4\pi}\frac{\lambda^2}{t_s^2} \tag{3.45}$$

which yields the RG equation, valid for $b = 0$ but any initial ratio of λ/t_s,

$$\frac{\partial}{\partial \ell}\lambda = \frac{\lambda^2}{4\pi}. \tag{3.46}$$

Using Eq. (3.39), we can simplify this through $z = t_s + \lambda/2$ to get

$$\frac{\partial}{\partial \ell} z = \frac{1}{2\pi} z^2. \tag{3.47}$$

So for $b = 0$ the presence of disorder leads to an additive renormalization of the stiffness, $t_s \to t_s + \lambda/2$. In presence of any amount of disorder, the IC correlation length ξ at $T = 0$ is finite, as can be inferred from an integration of the RG equation with $b = 0$, yielding $\xi \propto \exp(C\,(t_{s0} + \lambda_0/2)^{-1})$ with some cutoff dependent constant C. Thus, even at $T = 0$, $\xi \propto \exp(2C\lambda_0^{-1})$ is finite. While the disorder scales to strong coupling, the relative disorder strength with respect to the stiffness, λ/t_s, always scales to zero so that at long wavelengths the disorder becomes less relevant. This is surprisingly different to the situation with $b = -1$ fixed [27], where the ratio λ/t_s was found to diverge below a certain initial value of λ_0/t_{s0} which was interpreted as the scaling towards a new disorder dominated regime. Thus, if one correctly takes into account the non-collinearity, this disorder dominated phase disappears. The absence of a a sharp cross over from a weak disorder to a strong disorder regime is certainly surprising, especially as the experiments clearly observe a transition into a spin glass phase at a finite temperature [13]. The finite temperature transition may be related to the presence of inter-layer coupling. We argue below, however, that topological defects can alter the RG behavior considerably and may be a more natural explanation for the appearance of a strong disorder regime.

3.2.5 Topological defects: saddle point treatment

The RG results presented above do not take into account topological defects [40] of the spiral as only spin waves excitations enter the calculation. As is well known from XY spin models, topological defects can play an important role and drive finite temperature transitions [41]. The neglect of topological defects has been a source of criticism towards the NLσM approach to frustrated magnets, which gives controversial results for $\epsilon = 1, 2$ in an ϵ expansion around $D = 2 + \epsilon$ dimensions [42]. For two dimensional systems, the NLσM results were however found to be in very good agreement with numerical simulations as long as the temperatures were sufficiently low [43]. Only at higher temperatures, deviations from the NLσM predictions for the temperature dependence of the correlation length was observed. The discrepancy at higher temperatures has been attributed to the appearance

of isolated topological defects. In the numerical simulations the high temperature region showed some resemblance to the high temperature region of XY-models [43] which indicates that this region is characterized by free defects. However, at present a good understanding of the influence of such defects in non-collinear systems is still lacking [42].

The topological defects of spirals have their origin in the chiral degeneracy of the spiral, i.e. the spiral can turn clock- or anti-clock wise [42]. Hence, at a topological defect, the spiral changes its chirality. As the chirality can only take two possible values, the defects can be characterized as Z_2 defects, implying that a state with two defects is topologically equivalent to a defect free state. For the calculation of the RG equations used above, we have used an $SU(2)$ presentation which is in fact topologically trivial. The physically destinct chirality states should correctly be described by a $SO(3)$ theory in which pointlike Z_2 defects are present. As $SO(3) = SU(2)/Z_2$, topologically non-trivial solutions cannot be described by $SU(2)$ matrices $g(\mathbf{x})$ which are single valued functions of space. Nonetheless, we can describe defects also within the $SU(2)$ formulation, if we use double valued fields g which undergo a π phase shift along loops which enclose the defect.

It is then straightforward to find topological defect solutions of the saddle point equations of a clean spiral [40]. The saddle point equations can be obtained from the perturbative expansion of the energy density, Eqs. (3.20, 3.24-3.27). One finds that extremal solutions must satisfy for each $j = x,y,z$ the equations

$$(1 + b\delta_{jz})\, \partial_\mu A^j_\mu = 2b\epsilon_{zjk} A^z_\mu A^k_\mu, \tag{3.48}$$

where j is not summed over. For $b > -1$ one can find solutions of the form [40]

$$g_s(\mathbf{x}) = \exp\left(\frac{i}{2} m^a \sigma^a \Psi(\mathbf{x})\right), \tag{3.49}$$

where $\mathbf{m}$ is a space independent unit vector and $\Psi(\mathbf{x})$ a scalar function. With this Ansatz, one has $A^i_\mu(\mathbf{x}) = \frac{1}{2} m^i \partial_\mu \Psi(\mathbf{x})$ and thus, upon insertion into Eq. (3.48), one finds for $\mathbf{m}$ and Ψ the equations (j is agained not summed over)

$$(1 + b\delta_{jz})\, m^j \partial^2_\mu \Psi(\mathbf{x}) = b\epsilon_{zjk} m^z m^k \left(\partial_\mu \Psi(\mathbf{x})\right)^2. \tag{3.50}$$

The weight of the configuration described by g_s is given by (we set $t_\mu = t_s$)

$$H\left[g_s\right] = \frac{1}{t_s} \int d^2\mathbf{x}\ \left[\mathbf{A}^2_\mu + b\left(A^z_\mu\right)^2\right] = \frac{1}{4t_s}\left[1 + b\left(m^z\right)^2\right] \int d^2\mathbf{x}\ \left(\partial_\mu \Psi\right)^2. \tag{3.51}$$

We see that for $b < 0$, the energy is minimized for $\left(m^z\right)^2 = 1$ whereas for $b > 0$ the vector $\mathbf{m}$ is preferably orientated within the x-y plane with $m^z = 0$. For both cases, Eqs. (3.50) reduce to the two dimensional Laplace equation $\nabla^2 \Psi(\mathbf{x}) = 0$. This equation allows for topological defect solutions with $\Psi(x, y) = \arctan(y/x)$. In the left sides of Figs. 3.7 and 3.8 the spin distribution around isolated defects is shown for both $b < 0$ and $b > 0$. Using Eq. (3.51) one

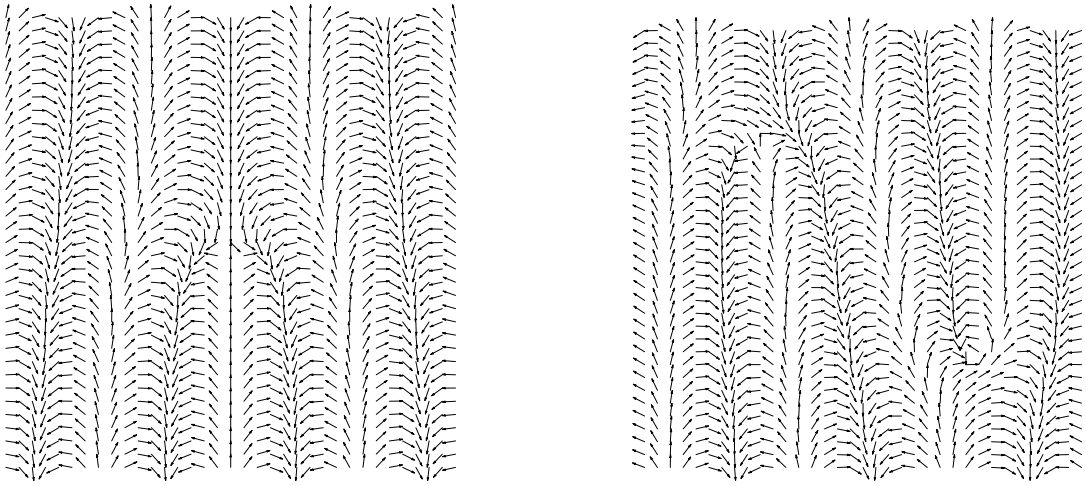

Figure 3.7: Single topological defect (left) and topological defect pair (right) of a spiral with $b \leq 0$ (small scale AF fluctuations are not shown).

finds that the energy of a topological defect solution $\Psi(x, y)$ diverges logarithmically with the linear system size R,

$$\beta E = \frac{1 + (m^z)^2 b}{2t_s} \pi \ln R. \tag{3.52}$$

Because of this logarithmic divergence of the energy, isolated defects are not present in absence of disorder and at sufficiently low temperatures. It can also be shown [44], that a bound state of defect pairs, described by $g = g_{s1} g_{s2}$ with $g_{s1,2} = \exp\left[\frac{i}{2}\mathbf{m}_{1,2} \cdot \boldsymbol{\sigma} \arctan\left(\frac{y-y_{1,2}}{x-x_{1,2}}\right)\right]$, has a finite energy if $\mathbf{m}_1 + \mathbf{m}_2 = 0$. Therefore, while isolated defects may be absent, defect pairs will be present at any finite temperature. This situation is reminiscent of the one encountered in the XY model where at low temperatures also only defect pairs are present. These pairs unbind at the critical Kosterlitz-Thouless temperature and above this temperature free defects can be found. Such an unbinding of defects is also plausible and expected in the present model. The topological defects of the spiral differ however in important aspects from those of the XY model. Spiral defects have a Z_2 charge while XY defects have Z charges. More importantly, as the present model possesses asymptotic freedom, it has a finite correlation length ξ at any finite temperature even in absence of free defects. This implies that the logarithmic divergence in Eq. (3.52) appears only up to a scale $R < \xi$. It is therefore unclear how a defect-unbinding would affect the system. A transition from a phase with algebraically decaying spin correlations to a phase which shows an exponential decay, as occurs in XY models, is clearly ruled out. Finally, while in XY models topological defects can be relatively easily incorporated into the analysis because they can be decoupled from the spin waves, this is not the case for frustrated Heisenberg models. If fluctuations around the saddle point solution are taken into account, the defects of spirals couple to the spin

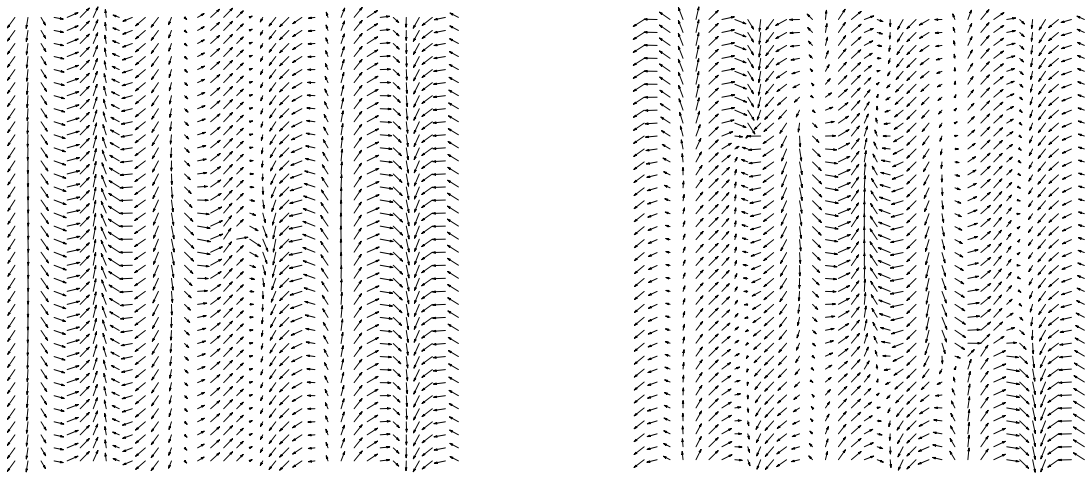

Figure 3.8: Single topological defect (left) and topological defect pair (right) of a spiral with $b \geq 0$ (small scale AF fluctuations are not shown).

waves already at second order in an expansion in the fluctuations. These difficulties have to date prevented a complete understanding of the defect unbinding in frustrated systems.

A comparison to XY models is nonetheless quite illuminating. The kind of disorder coupling we have used for the spiral phase is closely related in spirit to XY models with randomly fluctuating phases, where the disorder is also introduced in the form of a fluctuating gauge [45]. If one ignores vortices, the influence of the disorder was shown to amount to a simple renormalization of the spin stiffness, at all orders in a perturbative treatment of the disorder coupling [46, 45] and no disordering transition as a function of the disorder strength is found. However, once topological defects are included in the analysis, the coupling of vortices to the random gauge field can lead to a disordered phase even at $T = 0$. Such a disorder driven transition is caused by the creation of unpaired defects if the fluctuations of the gauge field are stronger than some critical value [45, 47]. It is interesting that the critical disorder strength beyond which such defects appear can be estimated quite accurately when one calculates the free energy of an isolated defect in presence of disorder [45, 48]. It turns out that a similar analysis of a single defect in a spiral in presence of disorder can be carried out with some modifications, at least at the level of saddle point solutions. Within this approximation, the free energy of an isolated spiral defect is given by

$$\beta F = \frac{1 + (m^z)^2 b}{2t_s} \pi \ln R - [\ln Z_d]_D \,, \tag{3.53}$$

where the second term contains the corrections due to the disorder coupling,

$$Z_d = \int d^2\mathbf{y} \exp\left(-2 \int d^2\mathbf{x}\; p_k\; \epsilon_{ijk}\; \epsilon_{abc}\; A^i_\mu\; n^a_j\; n^c_k\; Q^b_\mu\right) \tag{3.54}$$

with $\mathbf{A}_\mu$, $\mathbf{n}_k$ obtained from Eqs. (3.13), (3.14) and (3.49). With use of the replica trick $[\ln Z_d]_D = \lim_{N\to 0} \frac{1}{N} \ln \left[Z_d^N\right]_D$, we have, assuming $b < 0$,

$$\left[Z_d^N\right]_D = \int d^2\mathbf{y}_1 \ldots d^2\mathbf{y}_N \exp\left(2\lambda p_1^2 \sum_{n,n'=1}^{N} \int d^2\mathbf{x} \partial_\mu \Psi_n \partial_\mu \Psi_{n'}\right); \tag{3.55}$$

with $\Psi_n(\mathbf{x}) = \Psi(\mathbf{x} - \mathbf{y}_n)$. We write

$$\int d^2\mathbf{x} \partial_\mu \Psi_n \partial_\mu \Psi_{n'} = -\frac{1}{2}\Delta_{nn'} + V^2, \tag{3.56}$$

with $V^2 \simeq 2\pi \ln R$ and $\Delta_{nn'} \simeq 4\pi \ln|\mathbf{y}_n - \mathbf{y}_{n'}|$ [47]. For large separations $|\mathbf{y}_n - \mathbf{y}_{n'}|$ we approximate $\Delta_{nn'} \simeq 4\pi \ln R$ while for small distances $\Delta_{nn'}$ is negligible. To find the highest weight configuration, the replicas are grouped together in N/m sets containing each m replicas, with small distances between replicas within a set and large distance for replicas in different sets. $\left[Z_d^N\right]_D$ then scales with R as

$$\left[Z_d^N\right]_D \sim R^{4\lambda\pi p_1^2 N^2 + \max_m\left(2\frac{N}{m} - 4\pi\lambda p_1^2 N(N-m)\right)}. \tag{3.57}$$

In the limit $N \to 0$, maximization is replaced by minimization with respect to m in the range $0 \le m \le 1$, so

$$\beta F = \left[2p_1\pi - \min_{0\le m\le 1}\left(2/m + 4\lambda p_1^2 \pi m\right)\right] \ln R\ . \tag{3.58}$$

For $2\lambda p_1^2 \pi < 1$ one finds $\beta F = 2[p_1\pi(1 - 2\lambda p_1) - 1] \ln R$ so that for $p_1\pi(1 - 2\lambda p_1) \le 1$ free defects are favorable. This is the phase boundary for thermal creation of defects. At low temperatures, $2\lambda p_1^2 \pi > 1$, one obtains $\beta F = 2\pi p_1(1 - \sqrt{8\lambda/\pi}) \ln R$ and a critical disorder strength $\lambda_c = \pi/8$ beyond which the disorder favors isolated defects even at $T = 0$. Similar considerations for the case $b \ge 0$ lead to the same critical disorder strength and the condition $\pi(p_1 + p_3)[1 - \lambda(p_1 + p_3)] \le 2$ for thermal creation of free defects.

Let us first discuss the results for the disorder free case $\lambda = 0$. The situation is summarized in Fig. 3.9, which shows the line separating the regime where free vortices exist from the regime in which all defects are bound. Notice that the unbinding temperature goes linearly to zero in the limit $b \to -1$. At $b = -1$, free defects are present at any finite temperature. This is expected, as at $b = -1$ and finite t_s, the topological defects we discuss here lose their meaning as the stiffness for rotations around the collinear ordering axis disappears and the model becomes a $O(3)/O(2)$ model which has no finite temperature transition. Whether or not free defects are present exactly at the point $b = -1$, $t_s = 0$ depends on how this point is approached. To see this, we note that the symmetry of the model in the limit $p_3 \to \infty$ but finite p_1 reduces to an XY symmetry as fluctuations of the $\mathbf{n}_3$ vector get suppressed which forces all fluctuations of the orthonormal pair $\mathbf{n}_{1,2}$ to lie within a plane. Therefore one obtains an XY model with stiffness p_1. In terms of the b, t_s parameters, this limit is

approached as $t_s \to 0$ and $b \to -1$ with finite $(1+b)/t_s = 4p_1$. Thus, depending on whether one approaches the point $b = t_s = 0$ with a slope larger or smaller than the critical one given by $(1+b)/t_s = 4/\pi$, one arrives at the disordered phase or the ordered phase of the XY model. This behavior is correctly reproduced by the free energy argument. The validity of the critical curve $(1+b)/t_s = 4/\pi$ also for finite $1+b > 0$, as predicted by the free energy argument, is quite plausible, as topological defect solutions also survive in this limit. Below this line, the RG Eqs. (3.39, 3.40) hold and the system should scale towards the point $b = 0$. We can only speculate however what happens above that line. At least for some finite regime near $b = -1$ the unbinding transition would presumably drive p_1 to zero, as it does in the XY model, and affect the renormalization of p_3 only weakly. Thus, the appearance of free defects will probably modify the RG equations at high temperatures in such a way that the system will flow back to the collinear point $b = -1$ as long as $1+b$ remains small enough. For larger b the nature of the RG is unclear. Numerical simulations on triangular Heisenberg models [49, 50] have found however clear evidence for a defect unbinding transition. As the triangular Heisenberg model is believed to have initially $b = 1$ [36], it is likely that an unbinding transition indeed occurs for every initial value of b. As no RG equations are available which can describe the transition, the form of the correlation length near this transition is unknown. It was however argued [40], that the temperature dependence of the correlation length should cross over from the NLσM behavior to an XY behavior when the defects unbind. Numerical results seem to support such a scenario [43].

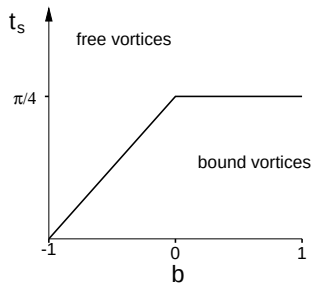

Figure 3.9: The critical line for the thermal unbinding of topological defects is shown in b, t_s space.

Let us now turn to the case with disorder. Disorder will lead to the formation of free defects if $\lambda > \pi/8$. According to the free energy argument above, this critical disorder strength is independent of the stiffnesses p_k and is thus also valid in the XY limit discussed above. Thus, if disorder is strong enough, free topological defects will exist already at $T = 0$, invalidating our NLσM analysis and producing very short low-temperature correlation lengths for the spiral. Again, we cannot make any definite statements on the RG or the correlation length behavior in this regime. However, similar to the thermal unbinding scenario, one

might again expect a crossover to XY behavior. If this is the case, then one would expect the correlation length at $T = 0$ to behave like $\xi \propto \exp(B/\sqrt{\lambda - \lambda_c})$ (with some constant B) near the critical disorder strength [45]. This form of the correlation length has a divergence of ξ at $\lambda = \lambda_c$ which is correct for the XY model but cannot be correct for the spiral because, as discussed above, even without vortices, the coupling of any finite amount of disorder to the spins will lead to a finite correlation length. The correct dependence of the correlation length at $T = 0$ on the disorder is expected to be an interpolation between the NLσM result and the XY behavior.

Certainly, the free energy argument is not expected to work as well in the present model as it does for XY models. The parameters λ and t_s flow to strong coupling and thus the predictions of the free energy argument also become scale dependent. In other words, while at some small scale the system might look stable against the creation of free defects, at some larger scale the system will become unstable according to the free energy argument. There does not seem to be a simple answer as to which scale is the correct one for applying the argument. Note that such problems do not arise in the XY model where the stiffness remains unchanged under the RG as long as vortices are ignored. In view of the divergence of the λ and t_s parameters in the NLσM, one possible scenario would be that free defects will always be present at sufficiently large length scales. Numerical results do however not support such a scenario and rather point to the existence of a finite critical temperature [50]. Below we shall apply the free energy argument with the bare parameters, i.e. at the smallest possible scale, which, if anything, would overestimate the stability of the system against free defect formation.

3.3 Comparison with experiments

Let us now compare our results with experimental data on the SG phase of $La_{2-x}Sr_xCuO_4$. Neutron scattering data [14] have revealed an incommensurability of the spins which scales roughly linearly with x, see Fig. 2.4. Within the dipole model this is easily explained. The linear scaling is reproduced within the dipole model if the fraction of the dipoles which are ordered is doping independent. Only at very small x is a small deviation from the linear dependence observed, pointing to a slight decrease of the ordered fraction. This might be explained with the increase of the average separation between dipoles at small x and a resulting diminished tendency of the dipoles to align.

The same experimental data also shows a strong one dimensional character of the IC modulation, i.e. the incommensurability is observed only in one lattice direction and thus breaks the symmetry of the square lattice. Again, this is expected for a spiral, and as mentioned in the introduction, this symmetry breaking is expected to show long range order because the dipoles prefer a discrete set of lattice orientations.

To judge, whether or not topological defects play a role in the LSCO SG phase, we need

an estimate of λ. We can use as a lower bound for λ the result obtained from the collinear analysis [27] where a disorder parameter equivalent to ours, but defined on the much smaller scale of the AF unit cell, was used. From a fit of the x dependence of the correlation length at $x < 0.02$ and large temperatures $T > T_N$, one obtaines $\lambda \simeq 20x$. In this regime of x, the low temperature phase has long range AF order and a collinear analysis is well justified. We assume that the linear dependence of the disorder parameter on x, $\lambda \simeq 20x$, also holds in the SG regime. This view is supported by measurements, which found that the width of the distribution of internal magnetic fields (i.e. local staggered moments) increases simply linearly with doping, with no detectable change on crossing the AF/SG phase boundary [11], see also Fig. 2.3. It is remarkable that with our above estimate for the critical disorder strength $\lambda_c = \pi/8$ we find a critical doping concentration $x_c \sim 0.02$. Considering that $\lambda \simeq 20x$ is a conservative lower bound of λ at the long length scales relevant to spirals, we conclude that in the entire SG phase, free topological defects will be present already at $T = 0$, leading to a strongly disordered spiral phase. Experiments have in fact shown that the correlation lengths in the SG regime are extremely short and of the same order as the periodicity of the IC modulation [14]. In Fig. 3.10 the neutron scattering data of a sample with $x = 0.024$ is shown. While this is in accordance with the expected presence

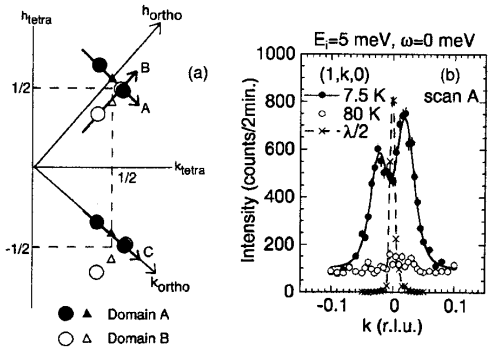

Figure 3.10: Neutron scattering data showing the short ranged IC spin structure of $La_{1.976}Sr_{0.024}CuO_4$ (from reference [14]).

of topological defects, the correlation lengths are so short that the condition $\xi \gg |\mathbf{q}_s|^{-1}$ is not fulfilled. The regime where spiral correlations become dominant is therefore barely reached, and the RG scaling predictions cannot be well tested. From our discussion of the topological defects we would expect that at $T = 0$ the IC correlation length roughly follows $\xi \sim \exp(B/\sqrt{20x - \lambda_c})$. Further, we expect the spin fluctuations in the disordered regime to be of XY-type. There are indeed experimental indications of XY fluctuations at low temperatures in the SG regime [51], although these may also be related to the presence of a small spin anisotropy.

Thus, qualitatively the experimental data supports a description of the SG phase as a strongly disordered spiral state, but both the extremely short correlation lengths and our limited understanding of topological defects prevent a more quantitative comparison.

We point out, that our suggestion, that the incommensurability of the spins is related to ordered dipolar frustration centers can be directly tested experimentally on co-doped samples $La_{2-x}Sr_xZn_zCu_{1-z}O_4$. Zn replaces Cu in the CuO_2 planes and effectively removes one spin. Zn doping leads therefore to a dilution of the AF but does not introduce frustration. Dilution is not very effective in destroying the AF order and pure Zn doping (with $x = 0$) leads to a destruction of long range order only for concentrations in excess of 20% [52]. Surprisingly, for very small Sr concentration $x \leq 0.02$ it was found that co-doping with Zn can increase T_N [53]. This is remarkable as both kinds of impurities lead to a reduction of T_N in singly doped samples. A possible explanation for this behavior was suggested by Korenblit *et al.* [54]. While Zn couples only weakly to the spin degrees of freedom in an ordered state, if placed near a Sr donor, it disturbs the symmetry around the Sr atom and can modify the nature of the localized hole state considerably. This can lead to a reduction or even complete destruction of the frustration induced by the hole. Thus, the effective density of dipoles will be renormalized to $x \to x(1 - \gamma z)$ where γ must be calculated from a microscopic theory (experiments indicate that γ is of order 2 [54]). Thus, co-doping with Zn will have two effects: First, it lowers the amount of frustration in the sample and thus increases the correlation length [54, 53]. But if the incommensurability observed in the SG phase is indeed related to the density of ordered dipoles, then Zn doping will also lower the total amount of ordered dipoles and thus lead to a decrease of the incommensurability by a factor $1 - \gamma z$. This effect should be observable in neutron scattering experiments.

Chapter 4

Striped phases

Already quite soon after the discovery of high temperature superconductivity in the cuprates, mean field investigations of two dimensional Hubbard models indicated the somewhat exotic possibility of so called striped phases as the ground state of hole doped copper oxide layers [55, 56, 57, 58]. In these striped phases the charges (holes) form one dimensional lines which act as anti-phase domain walls to the nearly undoped antiferromagnetic (AF) environment. As stressed by several authors [55, 58, 59], these domain walls can be viewed as two dimensional versions of the solitonic modes known from the one dimensional Su-Schrieffer-Heeger Hamiltonian [60] and the striped phase resembles a soliton lattice. A schematic picture of both a diagonal and a vertical stripe is shown in Fig. 4.1.

Contrary to the weakly doped regime discussed in the previous chapter which we argue is dominated by the properties of isolated holes, a striped phase represents a highly collective hole state which should only be relevant at higher doping concentrations. This, as discussed below, is supported by experiments, which found e. g. in $La_{2-x}Sr_xCuO_4$ signatures of stripes only for $x > 0.05$ and unambiguous evidence only at $x = 1/8$. After reviewing some key experimental data and theoretical results on striped phases in Sec. 4.1, we develop a phenomenological description of stripes based on a quantum string picture, which will allow us to investigate the stability of the striped phase against disorder potentials, produced by the quenched distribution of ionized donors, and lattice potentials, both of which were found experimentally to have a strong influence on the striped phase. This is the subject of Sec. 4.2, where we further also discuss the interplay between stripe and spin fluctuations. In Sec. 4.3 we analyse a possible depinning of disordered stripes by external fields. We estimate the depinning barrier, discuss the creep for sub-critical fields and briefly compare our predictions with transport data obtained from the SG phase of $La_{2-x}Sr_xCuO_4$. Finally, in Sec. 4.4, we extend the quantum string model to allow for longitudinal charge and spin excitations along the stripe, in order to study the influence of transverse stripe fluctuations on the possible phases of the longitudinal degrees of freedom of a stripe with a finite electron filling. This is an important problem to address, both because stripe fluctuations have been argued to

be an essential requirement for the appearance of superconductivity and because the stripes believed to exist in cuprates have a finite on-stripe charge and spin density which allows for longitudinal fluctuations along the stripe.

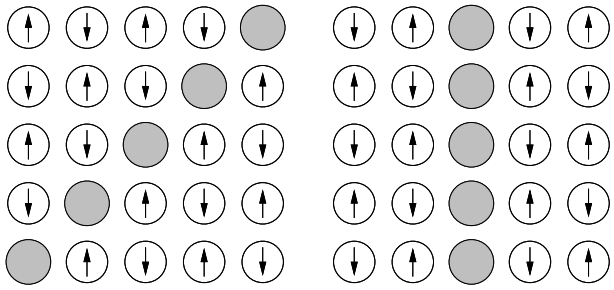

Figure 4.1: Schematic representation of a diagonal (left) and vertical (right) stripe.

4.1 Introduction to the striped phase

There is by now strong experimental evidence for the presence of striped phases in nickelate materials and also some cuprate materials, but neither on the mechanism behind stripe formation nor on the physical properties of striped phases has a consensus been established. A possible scenario for the formation of stripes is frustrated phase separation, an idea described and developed mainly by Emery and Kivelson (for a review see [59]). In this approach, it is assumed that a hole doped Mott insulator has a tendency to phase separate into two phases, a hole rich and a hole depleted phase [61]. An immobile charged background of dopants would however prevent macroscopic phase separation because of the associated large electrostatic energies. Rather, a frustrated phase separated state forms, in which phase separation occurs only at mesoscopic scales. In a simplified model calculation it was shown that competition between long range repulsive Coulomb interactions and short range attraction between holes can indeed lead to the formation of stripes [62]. There have since been many efforts to investigate the phase separation instability in t-J and Hubbard models. Whether or not the instability to phase separation exists for a realistic choice of parameters is however still hotly debated [63, 64]. If an instability towards phase separation is indeed present, one would expect to observe it in systems with mobile dopants. Interstitial oxygen dopants are relatively mobile, at least down to temperatures of about 200-300 K. The fact that phase separation has been repeatedly observed in oxygen doped nickelates [65] and cuprates [66] lends therefore strong support to the idea of frustrated phase separation.

The view that long range Coulomb forces are required to stabilize striped phases has however been challenged by numerical studies of the t-J model by White and Scalapino

[67, 63] in which striped phases were discovered in absence of long ranged interaction. Thus, the tendency towards stripe formation may be inherent already in the short ranged physics of the t-J model. This point of view has also found support in numerical studies by Martins *et al.* [68].

While most theoretical works on stripe formation concentrated on the renormalized classical regime of spins with locally well defined AF correlations, recently the problem of stripe formation has been looked at from the quantum disordered side, where the spins are disordered due to strong quantum fluctuations. In this approach the combined effect of long range Coulomb repulsion of the holes and an instability of quantum disordered spins to the formation of spin Peierls states [69, 70, 71] led to charged stripes [72, 73]. At least within the mean field approach used in these works, Coulomb repulsion is essential to stabilize stripes.

Certainly, the occurrence of IC spin order by itself does not imply the existence of a striped phase. Various other theoretical models also lead to similar incommensurabilities for the spins, but do not predict the appearance of charge density modulations. One of the first models to predict IC spin states was proposed by Shraiman and Siggia, who found an instability of weakly hole doped t-J models to the formation of a spiral phase [4]. This instability is based on the assumption that the quasiparticle associated with a hole moving in an AF produces a long ranged dipolar distortion of the AF. While the spin order in the superconducting region of the cuprates does not seem to be spiral [74], it is likely that a mechanism similar to that described by Shraiman and Siggia is responsible for IC correlations in the spin glass phase of $La_{2-x}Sr_xCuO_4$ [75, 13, 31], as discussed in the previous chapter. Another possibility for doping induced IC spin fluctuations is based on more conventional Fermi-nesting effects [76].

4.1.1 Stripes in nickelates

Static striped phases similar to those predicted by mean field theories [77] were first clearly observed in doped nickelates $La_{2-x}Sr_xNiO_{4+\delta}$ [78, 79, 80]. Nickelates are very similar in structure to the cuprates, however their electronic degrees of freedom are more complicated. In contrast to the cuprates, undoped nickelates have high spin 1 with considerable admixture of the Ni $3d_{3z^2-1}$ orbital [81]. Upon doping, spin 1 states are replaced by spin 1/2. A description of this compound within a simple one band model is not possible and three band models are required [77]. Nickelates remain insulators even if strongly doped which probably is related to the presence of a strong electron phonon coupling which is far more pronounced in nickelates than in cuprates. This strong coupling leads to a strong polaronic character [77] and a self trapping of charges.

Oxygen doped nickelates show a very rich phase diagram. Only certain doping levels represent stable phases and at an arbitrary doping level phase separation into an oxygen and hole deficient phase and several stacked phases with 2D or 3D ordering of the oxygen

interstitials is observed. The stacked phases show stripe order in the NiO_2 planes with a periodicity locked to a value commensurate with the oxygen ordering. A good summary of the experiments and further references can be found in [82]. At low temperature, the striped phases encountered in the nickelates approach a periodicity which corresponds to an on-stripe hole density of around 1, which agrees quite well with predictions of Hartree Fock calculations [77]. However, the stripe periodicity shows a marked step like temperature dependence with several lock in plateaus at commensurate values [82]. The stripes are oriented along the diagonal of the Ni square lattice, an alignment which is favored by the lattice distortions of the polaronic hole state [77, 83]. The spin and charge correlation lengths of the striped phases in oxygen doped samples are quite large and for the oxygen concentration $\delta = 2/15$, the striped phase even has perfect long range order [82]. Doping with Sr has the advantage that any hole density can be studied as phase separation is frustrated by the quenched distribution of Sr dopants. This introduces however also a considerable amount of disorder into the sample which competes with the pinning potential of the underlying lattice. Long ranged ordered striped phases were therefore never observed.

While the precise mechanism of stripe formation in nickelates is not clear, there are strong indications that phonon coupling plays an important role. The large charge gap of about 250 meV which was observed in $La_{5/3}Sr_{1/3}NiO_4$ [84] is one order of magnitude larger than the effective spin exchange as inferred from Raman scattering data [85] but comparable to some oxygen breathing phonon modes. This, together with the commensurability effects of the striped phase mentioned above, suggest that lattice coupling is an important ingredient to stripe formation.

4.1.2 Cuprates

A static striped phase in a cuprate material was first observed in neutron scattering measurements on co-doped $La_{1.48}Nd_{0.4}Sr_{0.12}CuO_4$ by Tranquada *et al.*[16]. The striped phase observed in $La_{1.48}Nd_{0.4}Sr_{0.12}CuO_4$ differs from those observed in nickelates. First, the lattice orientation is vertical as opposed to diagonal as in the nickelates. Secondly, the periodicity of the stripe array in the cuprate material is roughly a factor two larger for comparable hole concentrations. This points to a on-stripe charge density of roughly 1/4, i.e. on average only every second site on the stripe is occupied by a hole, see Fig. 4.2. $La_{1.6-x}Nd_{0.4}Sr_xCuO_4$ has a strongly suppressed superconducting transition temperature at the special doping concentration $x = 1/8$ where the stripe order is best developed and stripe order seems to compete with the SC state [86]. The preference of the system towards a stripe order near 1/8th hole doping is believed to be caused by commensurate pinning of stripes by the underlying lattice. Such a commensurate pinning is especially pronounced in this system as the Nd co-doped compounds undergo a transition to a low temperature tetragonal phase (LTT) in which the oxygen octahedra are periodically tilted which should help to pin one dimensional

structures like stripes. Fig. 4.3 shows neutron scattering data of the 1/8 compound, the IC magnetic order is clearly visible at low temperatures. However, while the 1/8 anomaly is most pronounced in the LTT Lanthanum based cuprates, it has also been observed in a variety of other cuprates and is most likely common to all cuprate materials [87]. Electrical resistivity measurements indicate that the 60K plateau of the superconducting transition temperature T_c, characteristic of the Y-123 compound, depends neither on the oxygen content in $Y_{1-x}Ca_xBa_2Cu_3O_{7-y}$ nor on the onset of the LTT phase, but is driven by an in plane hole concentration $n \sim 1/8$ [88].

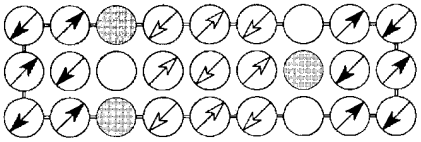

Figure 4.2: A possible stripe pattern consistent with neutron scattering data on $La_{1.48}Nd_{0.4}Sr_{0.12}CuO_4$, from [89]. The combination of white and shaded empty circles is used to indicate that on average, only every second site of the stripe is occupied by a hole.

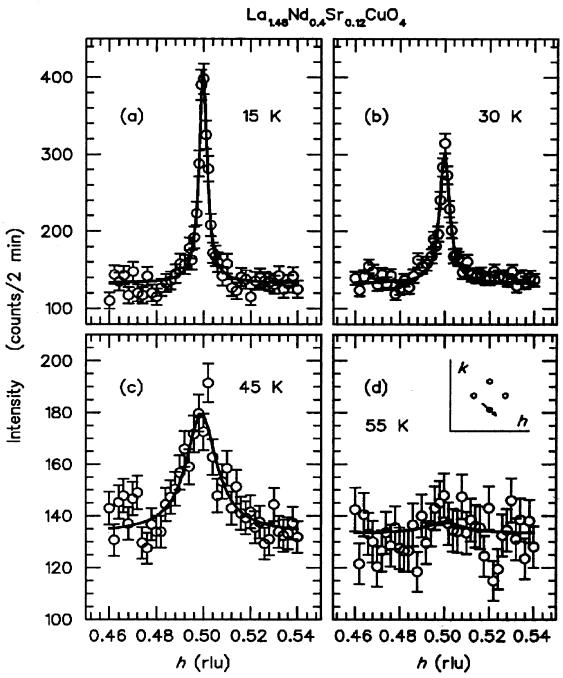

Figure 4.3: Neutron scattering data showing IC magnetic correlations in the 1/8th compound, from [90].

It was known for some time that the dynamic spin response of $La_{2-x}Sr_xCuO_4$ is IC [91, 92], i.e. the finite frequency spin susceptibility has its maxima at the characteristic in-plane wave

vectors $(\frac{1}{2} \pm \delta, \frac{1}{2})$, $(\frac{1}{2}, \frac{1}{2} \pm \delta)$ (in units of $2\pi a^{-1}$ where a is the copper lattice spacing and δ is the incommensurability). The incommensurability of underdoped $La_{2-x}Sr_xCuO_4$ was found to be linear in x, linking the periodicity of the striped phase found at 1/8 continuously with the dynamic fluctuations for more weakly doped compounds. Further, the superconducting transition temperature of $La_{2-x}Sr_xCuO_4$ was also found to scale simply linearly with the incommensurability of the spin fluctuations [15] (see Fig. 2.4), which suggests that the IC fluctuations may play a central role in the mechanism of superconductivity. This point of view is supported by the nearly critical nature of the IC spin fluctuations of $La_{2-x}Sr_xCuO_4$ at optimal doping, which indicates the proximity of a fixed point which may be associated with a striped phase [93].

The similarity between the dynamic IC spin fluctuations observed in the SC phase of $La_{2-x}Sr_xCuO_4$ and the static spin order seen in the LTT material was interpreted as evidence of either thermal or quantum fluctuations of stripes in the superconducting compound [94]. As static stripe order in the LTT cuprates coincides with a suppression of superconductivity, it was speculated that stripe fluctuations are a necessary condition for superconductivity whereas non-fluctuating stripes would instead lead to an insulating stripe crystal, a frozen charge- and spin wave density state [95]. Experimental results [15] indeed show that the dynamic IC spin fluctuations in $La_{2-x}Sr_xCuO_4$ disappear near the critical doping $x \sim 0.05$ where superconductivity also disappears.

4.1.3 Disorder and Stripes

Several experiments have revealed disorder to be relevant in stripe materials, both in cuprates [90, 96, 97, 98] and in nickelates [99, 100, 82, 80]. An obvious source of disorder in these materials are ionized dopants like Sr which are located in the planes neighboring to the NiO_2 or CuO_2 planes. A comparison with oxygen doped samples, which have an annealed rather than a quenched dopant distribution, allow for an investigation of the role of disorder. In Sr doped nickelates, the observed correlation lengths associated with the IC order are always short ranged [101, 80], in contrast to some oxygen doped samples, where apparently long ranged order was observed [82]. In contrast, the dynamic spin fluctuations observed in $La_{2-x}Sr_xCuO_{4+\delta}$ are insensitive to the type of doping [93, 102].

The importance of disorder has been observed most clearly in the spin sector. Local probes such as NMR [96, 103], NQR [99], μ-SR [11, 97] have revealed anomalously slow relaxation times for the spins, reminiscent of spin glass behavior, in co-doped lanthanum based cuprates with $x \sim 1/8$. The width of the broad distribution of relaxation times was almost identical to the one observed in the very weak doping regime $x < 0.05$ [103]. The similarity between the weakly doped region and the point $x = 1/8$ extends also to the static spin correlations observed in neutron scattering. While the spin correlation length is very large for $x = 1/8$, it clearly saturates at a finite value at low temperatures, rather than

approaching an ordered state at $T = 0$ [90], see Fig. 4.4. This behavior is reminiscent of the spin glass regime, where the spin correlation length also saturates, albeit at a much smaller length [51], and suggests a similar disordering mechanism in these two doping regimes.

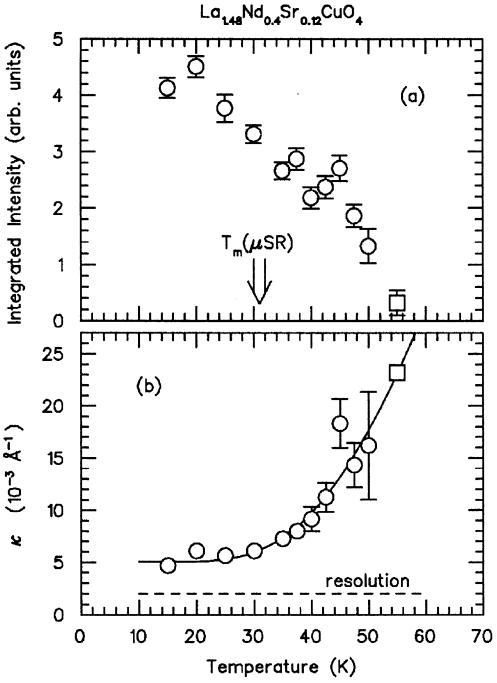

Figure 4.4: Top: the integrated intensity of the IC magnetic scattering can be interpreted as an order parameter of the striped phase. Bottom: inverse correlation length of the magnetic scattering of the $x = 1/8$ compound. The correlation length is clearly seen to saturate at low temperatures (from [90]).

4.2 Phenomenological analysis of stripes

Theoretical investigations of the striped phase have so far been largely phenomenological, owing to the complexity of the problem. We pursue this strategy here also, so as to understand some general aspects about the influence of disorder and lattice potentials on the striped phase and to avoid the uncertainties associated with the precise microscopic structure of the stripes. A phenomenological treatment similar to the one we use in this section has been pioneered in [94, 104, 105], where the influence of disorder was however not addressed.

4.2.1 Stripes as quantum strings

To begin with, let us consider a stripe filled with holes, so that there are neither charge nor spin excitations along the stripes. The only excitations of such a stripe are its transversal

fluctuations. To investigate the dynamics of the stripe, it is then possible to use a first quantized formulation of the problem. The model we assume is a directed string of holes (enumerated by the integer n) on a square lattice with lattice constant a. We further allow only hopping of holes in the transverse direction. To account for the stripe stiffness, we include a parabolic potential of strength K which couples adjacent holes in the stripe. The model is then quite simple and in fact we are just investigating the dynamics of an isolated domain wall on a lattice. A stripe (or domain wall) state can be represented as a superposition of states

$$|\mathbf{u}\rangle = |\ldots u_{n-1} u_n u_{n+1} \ldots\rangle \tag{4.1}$$

where u_n is the transverse position of the nth hole of the stripe. Because the stripe is on a lattice, the u_n are integer multiples of the lattice constant a. We introduce a single site transverse hopping of the holes and a parabolic potential for transverse displacements of the stripe. The Hamiltonian for the stripe dynamics can then be written in the basis above as

$$\hat{H}_S = -t \sum_n \left(\hat{\tau}_n^+ + \hat{\tau}_n^- \right) + \frac{K}{2a^2} \sum_n \left(\hat{u}_{n+1} - \hat{u}_n \right)^2 \tag{4.2}$$

where t is the hopping parameter and the K term penalizes deviations of the line from a straight configuration. The translational operators $\hat{\tau}_n^{\pm}$ are defined by their action on the states (4.1), $\hat{\tau}_n^{\pm} |\mathbf{u}\rangle = |\mathbf{u} \pm \mathbf{e}_n\rangle$ where $e_n^m = \delta_n^m$. The $\hat{\tau}_n^{\pm}$ operators can be written in terms of momentum operator $\hat{p}_n$ with commutators $[\hat{u}_n, \hat{p}_m] = i\delta_{nm}$ (we use units with $\hbar = k_B = 1$) as $\hat{\tau}_n^{\pm} = \exp(\pm i \hat{p}_n a)$ and Eq. (4.2) then takes the form

$$\hat{H}_S = -2t \sum_n \cos\left(\hat{p}_n a\right) + \frac{K}{2a^2} \sum_n \left(\hat{u}_{n+1} - \hat{u}_n \right)^2 \tag{4.3}$$

In the limit $t \gg K$ we can expand the cosine in Eq. (4.3) to second order and it is easy to show then that the excitations of the stripe are simple acoustic waves with dispersion $\omega = ak\sqrt{2tK}$ for $|ka| \ll 1$. These are just the excitations of a harmonic quantum string and the lattice is thus unimportant in the long wavelength limit. We shall call this the free phase of the string. In the free phase, the system is equivalent to a continuum Gaussian field theory with the action

$$S_0[\phi(y,\tau)] = \frac{1}{2\pi\mu} \int_0^\beta d\tau \int dy \left[\frac{1}{c} \left(\partial_\tau \phi \right)^2 + c \left(\partial_y \phi \right)^2 \right]. \tag{4.4}$$

where $\phi(y,\tau)$ is now a field defined on a continuum, $c = a\sqrt{2tK}$ is the velocity of the acoustic excitations and $\mu = \sqrt{2t/K}$ is a parameter which controls the strength of the quantum fluctuations. To make closer contact with the lattice model defined in Eq. (4.2) we reintroduce the lattice via a cosine potential which favors values $\phi(y)$ which are multiples of $\sqrt{\pi}$ (we have rescaled the space direction for convenience), so that the action becomes

$$S = S_0 + \frac{g}{a} \int d\tau \int dy \cos(2\sqrt{\pi}\phi). \tag{4.5}$$

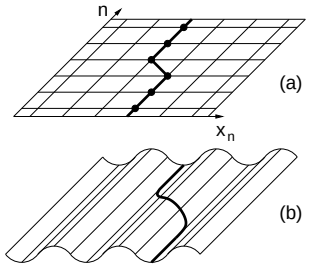

Figure 4.5: Two stripe models: a) discrete string model; b) sine-Gordon model defined on a continuum.

In the limit $g \to \infty$ this model becomes again a discrete model. Fig. 4.5 shows the relation between the lattice and continuum model. The action obtained is now simply of the sine-Gordon type which has been thoroughly studied in the literature (see e.g. [106, 107]). This system undergoes a zero temperature roughening transition of the Kosterlitz-Thouless (KT) type, which separates the free phase with the massless excitations discussed above from the lattice pinned (or flat) phase in which all excitations are gapped. In the language of the quantum string, this is simply a transition from a flat string in which transversal fluctuations of the string become suppressed at large wavelength to a freely fluctuating string which is characterized by logarithmical wandering, i.e. the expectation value of $(\phi(y)-\phi(0))^2$ diverges logarithmically with y. The excitations in the flat phase of the lattice model are bosonic kink/antikink pair excitations, where the size of such a kink/antikink pair diverges at the roughening transition. We will discuss the renormalization group (RG) equations below when we also discuss the influence of disorder. The quantum string model can also be mapped onto a massive Thirring model, as was shown in [108]. The critical μ at which the roughening transition occurs is $\mu_{c1} = 2/\pi$ [108, 109].

4.2.2 Influence of weak disorder

We now generalize the above simple considerations concerning the influence of the lattice potential to discuss the influence of disorder. The question is whether there is the possibility of a phase in which disorder is irrelevant. Results on classical strings in a disorder potential are not encouraging. In the absence of lattice potentials and at the classical level, the long wavelength limit of a sufficiently dilute array of stripes can be described as a membrane with anisotropic stiffnesses, where the stiffness in the direction perpendicular to the stripes is dominated by the entropic repulsion between neighboring stripes. In presence of disorder, such a membrane is pinned at all temperatures, leading to a glassy striped phase [110]. Similarly, in the presence of a weak substrate lattice potential, it was found that a weakly IC phase near a $p \times 1$ registered phase is unstable to the formation of topological defects

and hence a fluid if $p < \sqrt{8}$ [111]. As the hole stripes in the cuprates act as domain walls to the AF background, the striped phase is topologically equivalent to an IC phase near $p = 2$ which led Zaanen *et al.* [94] to the conclusion that the striped phase in the cuprates is a stripe liquid. The topological defects are easily pinned by disorder, again producing a glassy stripe.

However, the instability of the membrane to both disorder pinning and formation of topological defects is rooted in the form of the entropic repulsion of classical strings embedded in a plane. The entropic repulsion arises from a non-crossing condition of the strings and, for classical strings in a plane, decays algebraically with the distance between the strings. At low temperatures the fluctuations of the strings are no longer thermal but predominantly quantum. In this case, the effective interaction between neighboring stripes decays exponentially with the distance rather than algebraically. The reason for this is that a quantum string has logarithmic divergent fluctuations rather than the algebraic divergent fluctuations which characterize a classical string at finite temperatures.

To study the influence of disorder and lattice perturbations in the quantum regime of the striped phase, we shall focus here on the intermediate time and length scale regime, as e.g. probed in neutron scattering experiments, where the dynamics is dominated by a single stripe rather than the collective and coherent membrane physics. The neighboring stripes nonetheless play an important role as they confine the stripe wandering. That the neighboring stripes weaken the influence of the disorder can be easily understood: to take advantage of the disorder potential, the stripe has to meander, but meandering is frustrated by the neighbors. The stripe therefore cannot find the optimal path through the disorder environment. We want to make clear, however, that the very long wavelength physics will always be influenced by disorder. What we are interested in below, is the crossover from a regime in which the disorder becomes important only at wavelengths larger than the inter-stripe distance, where the dynamics of the stripe array can be described within a membrane model, to a regime where the disorder is so strong that the long wavelength membrane regime is never reached. Formulated differently, we investigate the influence of disorder fluctuations which happen at a scale smaller or equal to the inter-stripe distance.

We start again with the phenomenological model of a stripe on a lattice as in the previous section but now also include a disorder potential. The Hamiltonian is therefore given by

$$\begin{aligned} \hat{H} &= \hat{H}_S + \hat{H}_D, \\ \hat{H}_D &= \sum_n V_n(\hat{u}_n) \ . \end{aligned} \tag{4.6}$$

where $\hat{H}_S$ is defined through Eqs. (4.2, 4.3) and $\hat{H}_D$ describes the interaction of the stripe with a disorder potential. The disorder correlations are given by

$$[V_n(u)V_{n'}(u')]_D = \Delta(u - u') \ \delta_{n,n'} \tag{4.7}$$

where $[...]_D$ denotes the Gaussian average over the disorder ensemble and $\Delta(u)$ describes the correlations between displacements. Using the fact that $|u| < L$ it is convenient to expand all physical quantities in Fourier series with period L, in particular,

$$V_n(u) = \frac{1}{L}\sum_k V_{n,k} e^{i\pi k u/L} \tag{4.8}$$

and

$$\Delta(u) = \frac{1}{L}\sum_k D_k \cos(\pi k u/L) \tag{4.9}$$

where we used that $\Delta(u) = \Delta(-u)$. The probability distribution of $V_{n,k}$ is given as

$$P(V_{n,k}) = \frac{1}{\pi D_k} e^{-|V_{n,k}|^2/D_k} \tag{4.10}$$

which yields

$$[V_{n,k} V_{n',k'}]_D = \delta_{n,n'}\delta_{k,-k'} D_k \tag{4.11}$$

and therefore leads to Eq. (4.7). Thus, D_k gives the width of the distribution of the Fourier components of the disordered potential.

4.2.3 Derivation of the continuum action

We want to find a continuum formulation of the disorder average of the free energy functional and to calculate the disorder average of the logarithm of the partition function

$$Z = \mathrm{tr}\exp\left(-\beta\hat{H}\right) = \sum_{\{\mathbf{u}\}} \left\langle \mathbf{u}\right| \exp(-\beta\hat{H}) \left|\mathbf{u}\right\rangle, \tag{4.12}$$

For the calculation of the average of $[\ln Z]_D$ we employ the replica trick which relies on the introduction of N replicas of the original system and the identity

$$[\ln Z]_D = \lim_{N\to 0} \frac{\left[Z^N\right]_D - 1}{N} \tag{4.13}$$

The disorder average is usually easy to perform for integer N, but taking the limit $N \to 0$ is non-trivial. However, in the RG treatment we carry out below the replicas are merely a convenience in keeping track of the correct diagrams and for the RG we are not concerned with the mathematical not well defined limit $N \to 0$.

We use standard techniques to convert Z into a path integral form. With $\epsilon = \beta/M$ we write

$$\left\langle \mathbf{u}\right| e^{-\beta\hat{H}} \left|\mathbf{u}\right\rangle = \left\langle \mathbf{u}\right| \left[\exp(-\epsilon\hat{H})\right]^M \left|\mathbf{u}\right\rangle = \sum_{\{\mathbf{u}_1 \ldots \mathbf{u}_{M-1}\}} \langle \mathbf{u}| e^{-\epsilon\hat{H}} |\mathbf{u}_{M-1}\rangle \ldots \langle \mathbf{u}_1| e^{-\epsilon\hat{H}} |\mathbf{u}\rangle. \tag{4.14}$$

where now $\mathbf{u}_m = \mathbf{u}(\tau = \epsilon m)$ are τ-dependent. We rewrite the expectation values as

$$\begin{aligned}\langle \mathbf{u}_m | e^{-\epsilon \hat{H}} | \mathbf{u}_{m-1} \rangle &\simeq \int \prod_n \frac{dp_{nm}}{2\pi} \langle \mathbf{u}_m | \mathbf{p}_m \rangle \langle \mathbf{p}_m | : e^{-\epsilon \hat{H}} : | \mathbf{u}_{m-1} \rangle \\ &= \int \prod_n \frac{dp_{nm}}{2\pi} \prod_n \exp\left[i p_{nm} \Delta_\tau u_{nm} + 2t\epsilon \cos(p_{nm} a) \right. \\ &\qquad \left. - \frac{\epsilon K}{2a^2} \left(\Delta_y u_{nm-1}\right)^2 - \epsilon V(u_{nm-1}) \right].\end{aligned} \tag{4.15}$$

where we introduced $\Delta_y u_{nm} = u_{n+1,m} - u_{nm}$ and $\Delta_\tau u_{nm} = u_{nm} - u_{nm-1}$. Using the Villain approximation, $\exp(\alpha \cos\phi) \simeq \sum_q \exp(-q^2/(2\alpha) + iq\phi)$ we can rewrite Eq. (4.15) as

$$\int \prod_n \frac{dp_{nm}}{2\pi} \sum_{\{q_{nm}\}} \prod_n \exp\left[i p_{nm} (\Delta_\tau u_{nm-1} + a q_{nm}) - \frac{q_{nm}^2}{4t\epsilon} - \frac{\epsilon K}{2a^2} \left(\Delta_y u_{nm-1}\right)^2 - \epsilon V(u_{nm-1}) \right].$$

Integration over the momentum variables shows that only configurations with $\Delta_\tau u_{nm-1} + a q_{nm} = 0$ contribute and we obtain

$$\langle \mathbf{u}_m | e^{-\epsilon \hat{H}} | \mathbf{u}_{m-1} \rangle = \exp\left[- \sum_n \left(\frac{1}{4t\epsilon a^2} \left(\Delta_\tau u_{nm-1}\right)^2 + \frac{\epsilon K}{2a^2} \left(\Delta_y u_{nm-1}\right)^2 + \epsilon V(u_{nm-1}) \right) \right].$$

Hence, the partition function can be written as

$$Z \simeq \sum_{\{u_{nm}\}} \exp\left[- \sum_{m=0}^{M-1} \sum_n \left(\frac{1}{4t\epsilon a^2} \left(\Delta_\tau u_{nm}\right)^2 + \frac{\epsilon K}{2a^2} \left(\Delta_y u_{nm}\right)^2 + \epsilon V(u_{nm}) \right) \right] . \tag{4.16}$$

Introducing $i = 1, \ldots, N$ replicas, performing the disorder average and taking the continuum limit $\epsilon, a \to 0$, we find

$$\left[Z^N \right]_D = \int \prod_i \mathcal{D}[u^i(x,\tau)] e^{-\tilde{S}^r} \tag{4.17}$$

with

$$\begin{aligned}\tilde{S}^r &= \sum_i \tilde{S}_0[u^i(y,\tau)] + \frac{g}{a} \sum_i \int_0^\beta d\tau \int dy \ \cos\left(\frac{2\pi u^i(y,\tau)}{a} \right) \\ &\quad - \frac{1}{2a} \sum_{i,i'} \int dy \int_0^\beta d\tau d\tau' \ \Delta\left(u^i(y,\tau) - u^{i'}(y,\tau') \right).\end{aligned} \tag{4.18}$$

We here introduced the parameter g which denotes the strength of the lattice potential. The action $\tilde{S}_0$ is given by

$$\tilde{S}_0[u(y,\tau)] = \int_0^\beta d\tau \int dy \left(\frac{1}{4ta^3} \left[\partial_\tau u(y,\tau)\right]^2 + \frac{K}{2a} \left[\partial_y u(y,\tau)\right]^2 \right) \tag{4.19}$$

Introducing the dimensionless fields $\phi^i = \sqrt{\pi}u^i/a$ we arrive at our final form of the replicated action,

$$\begin{aligned} S^r &= \sum_i S_0[\phi^i] + \frac{g}{a}\sum_i \int_0^\beta d\tau \int dy \ \cos\left(2\sqrt{\pi}\phi^i\right) \\ &\quad - \sum_k \frac{D_k}{2aL}\sum_{i,i'}\int dy \int_0^\beta d\tau d\tau' \ \cos\left(2\sqrt{\pi}\delta k\left(\phi^i(y,\tau) - \phi^{i'}(y,\tau')\right)\right) \end{aligned} \tag{4.20}$$

where $\delta = a/(2L)$ is essentially the incommensurability (or stripe density) and

$$S_0[\phi] = \frac{1}{2\pi\mu}\int_0^\beta d\tau \int dy \left(\frac{1}{c}\left(\partial_\tau\phi\right)^2 + c\left(\partial_y\phi\right)^2\right). \tag{4.21}$$

The velocity $c = a\sqrt{2tK}$ and the dimensionless parameter $\mu = \sqrt{2t/K}$ completely determine the action S_0 and hence the dynamics of the free stripe.

4.2.4 Renormalization of the model

We will now perform a perturbative RG analysis of the model defined by Eq. (4.20) to obtain the scaling of its parameters. The action defined through Eq. (4.20) is in fact similar to those describing one dimensional bosonic [112] and fermionic [113] models with disorder and we can use similar techniques for analysing its properties.

To understand the possible phases of the system, we consider both the lattice and the disorder, i.e. g and D_k as small parameters and treat them perturbatively. We will further only keep the most relevant disorder contribution $D = D_1$. It is straightforward to generalize the results obtained below to the case with all D_k present and we will comment on this briefly. However, the D_k for $k > 1$ terms are only relevant deep inside the disordered regime which cannot be studied within the present perturbative treatment. We carry out an RG analysis to find the flow of D and g and obtain the phase diagram. In deriving the RG equations, we closely follow the method developed by Giamarchi and Schulz [113], which is based on a Coulomb gas representation of the problem and on a perturbative calculation of the correlator $\left\langle \exp\left(i\sqrt{2}\left[\phi^{i_1}(y_1,\tau_1) - \phi^{i_2}(y_2,\tau_2)\right]\right)\right\rangle$ to lowest non-vanishing order in g and D, where we denote the average over the full partitation function by $\langle \ldots \rangle$. For the free stripe we find

$$\left\langle e^{i\sqrt{2}\left(\phi^{i_1}(y_1,\tau_1) - \phi^{i_2}(y_2,\tau_2)\right)}\right\rangle_0 = \delta_{i_1 i_2} e^{-F(y_1-y_2,\tau_1-\tau_2)} \tag{4.22}$$

where $\langle \ldots \rangle_0$ is the average taken only with the gaussian part S_0 and F is given by

$$F(y,\tau) = \frac{\mu}{2}\ln\left(\frac{y^2 + c^2\tau^2}{a^2}\right) + \kappa\cos(2\theta). \tag{4.23}$$

The parameter κ measures the anisotropy of the y- and $c\tau$-direction. Initially, $\kappa = 0$ but a finite κ, reflecting a renormalization of the velocity c, is generated in the renormalization

procedure. To lowest order, only the expectation values diagonal in the replica indices contribute and therefore the replica index i can be dropped below. The angle between $(y, \tau c)$ and the y-axis is denoted by θ. To second order in g and first order in D, the correlator is

$$\begin{aligned}\frac{Z}{Z_0}\left\langle e^{i\sqrt{2}(\phi_1-\phi_2)}\right\rangle \simeq\ & e^{-F(y_1-y_2,\tau_1-\tau_2)} \\ &+\frac{g^2}{8a^2}\sum_{\epsilon_3,\epsilon_4=\pm 1}\int d\tau_3 d\tau_4 dy_3 dy_4 \left\langle e^{i\sqrt{2}\phi_1-i\sqrt{2}\phi_2+i2\epsilon_3\sqrt{\pi}\phi_3+i2\epsilon_4\sqrt{\pi}\phi_4}\right\rangle_0 \\ &+\frac{D}{4aL}\sum_{\epsilon=\pm 1}\int d\tau_3 d\tau_4 dy_3 dy_4 \delta(y_3-y_4)\left\langle e^{i\sqrt{2}\phi_1-i\sqrt{2}\phi_2+i2\epsilon\sqrt{\pi}\delta\phi_3-i2\epsilon\sqrt{\pi}\delta\phi_4}\right\rangle_0\end{aligned} \tag{4.24}$$

where we used the shorthand notation $\phi_j = \phi(y_j, \tau_j)$, Z is the full partition function and Z_0 the partition function of the gaussian model. The above expectation values are simple to evaluate and after some algebra (see App. (B.1) and App. (B.2)) one finds

$$\left\langle e^{i\sqrt{2}(\phi(y_1,\tau_1)-\phi(y_2,\tau_2))}\right\rangle \simeq \exp\left(-\frac{\tilde{\mu}}{2}\ln\left(\frac{(y_1-y_2)^2+c^2(\tau_1-\tau_2)^2}{a^2}\right)-\tilde{\kappa}\cos(2\theta)\right) \tag{4.25}$$

with

$$\begin{aligned}\tilde{\mu} &= \mu - \frac{1}{2}\mathcal{D}\mu^2\int_{y>a}\frac{dy}{a}\left(\frac{y}{a}\right)^{2-2\pi\mu\delta^2} - \frac{1}{2}\mathcal{G}^2\mu^2\int_{y>a}\frac{dy}{a}\left(\frac{y}{a}\right)^{3-2\pi\mu} \\ \tilde{\kappa} &= \kappa + \frac{1}{4}\mathcal{D}\mu^2\int_{y>a}\frac{dy}{a}\left(\frac{y}{a}\right)^{2-2\pi\mu\delta^2}\end{aligned} \tag{4.26}$$

where $\mathcal{D} = 4\pi^2 D\delta^2 a^2/(c^2 L)$ and $\mathcal{G} = \pi g a/c$. The renormalization group equations are now obtained following the method of Jose *et al.* [114]. We find under the rescaling $a' = \lambda a$, $\lambda = e^\ell$ the flow equations (for details see App. (B.3))

$$\frac{d}{d\ell}\mathcal{D} = (3-2\pi\mu\delta^2)\mathcal{D} \tag{4.27}$$

$$\frac{d}{d\ell}\mathcal{G} = (2-\pi\mu)y \tag{4.28}$$

$$\frac{d}{d\ell}\mu = -\frac{1}{2}\mu^2(\mathcal{G}^2+\mathcal{D}) \tag{4.29}$$

$$\frac{d}{d\ell}\kappa = \frac{1}{4}\mathcal{D}\mu^2. \tag{4.30}$$

(If we were to include all disorder correlations D_k, Eq. (4.27) would become $\partial_\ell \mathcal{D}_k = (3 - 2\pi\mu k^2\delta^2)\mathcal{D}$ with $\mathcal{D}_k = 4\pi^2 D_k\delta^2 a^2/(c^2 L)$, whereas in Eq. (4.29) and Eq. (4.30), $\mathcal{D}$ would be replaced by $\sum_k \mathcal{D}_k$).

The validity of these equations is limited to intermediate length and time scales, at large scales the network of stripes must be considered and the problem becomes considerably more involved. However, we will show below that the physics obtained from Eqs. (4.27-4.30) is already quite rich and gives important clues about the relevance of disorder and lattice

perturbations. We can estimate the range of validity of our approach as follows. If we assume short ranged interactions among neighboring stripes, the scale at which stripe-stripe interaction becomes important can be estimated by looking for the scale at which the average transversal fluctuations of the free stripe equal the average inter stripe distance L. The mean square transversal wandering of the free stripe is given by

$$\Delta u(y,\tau) \simeq \frac{a}{\pi}\sqrt{\mu \ln \frac{y^2+c^2\tau^2}{a^2}} \ .$$

This immediately yields $y_c = \tau_c c \simeq a \exp[\pi^2/(8\ \delta^2\mu)]$. Therefore, on time and length scales smaller than y_c, τ_c, the physics is dominated by single stripe dynamics while for larger scales the interaction must be taken into account. Note that the crossover scales y_c,τ_c are exponentially large in the inverse stripe density and thus the physics we describe is relevant at a fairly large scale.

With no disorder ($\mathcal{D} = 0$), the set of Eqs. (4.28, 4.29) reduces to the conventional KT form describing the roughening transition of the stripe at $\mu_{c1} = 2/\pi$ [108]. For $\mu < \mu_{c1}$, $\mathcal{G}$ diverges, signalling a pinning of the stripe by the underlying lattice. The stripe is flat on large length scales has infinite stiffness and its excitations are massive. For $\mu > \mu_{c1}$, the lattice potential is irrelevant and the system flows towards a gaussian fixed point with renormalized μ^*, c^*. This fixed point is characterized by massless excitations and a logarithmic transversal wandering of the stripe because of quantum fluctuations.

The RG equations can be solved analytically for $\mathcal{D} = 0$ in the vicinity of the transition. For this, we introduce $\epsilon_{\mathcal{G}} = 2-\pi\mu$. To linear order in $\epsilon_{\mathcal{G}}$ we then obtain from Eqs. (4.28, 4.29)

$$\frac{\partial}{\partial \ell}\epsilon_{\mathcal{G}} \simeq \frac{2}{\pi}\mathcal{G}^2, \tag{4.31}$$

$$\frac{\partial}{\partial \ell}\mathcal{G}^2 \simeq 2\epsilon_{\mathcal{G}}\mathcal{G}. \tag{4.32}$$

It follows, that

$$\frac{\partial}{\partial \ell}\left(\epsilon_{\mathcal{G}}^2 - \frac{2}{\pi}\mathcal{G}^2\right) = 0 \tag{4.33}$$

i.e. $\epsilon_{\mathcal{G}}^2 - 2\mathcal{G}^2/\pi = C_{\mathcal{G}}$ is a constant under the RG flow. The RG equation for $\epsilon_{\mathcal{G}}$ can then be written as $\partial_\ell \epsilon_{\mathcal{G}} = \epsilon_{\mathcal{G}}^2 - C_{\mathcal{G}}$. The critical line in the $\epsilon_{\mathcal{G}}$-$\mathcal{G}$ plane separating the RG flow with diverging $\mathcal{G}$ from the region where $\mathcal{G}$ scales to zero is located at $C_{\mathcal{G}} = 0$. This yields a critical value of μ for the roughening transition [115],

$$\mu_{c1} = 2/\pi + 2^{1/2}\pi^{-3/2}\mathcal{G}. \tag{4.34}$$

Thus, a finite $\mathcal{G}$ leads to a shift of the critical value of μ linear in $\mathcal{G}$. A simple integration of the RG leads further to a pinning length L_{p1} above which the string becomes flat which scales as $L_{p1} \propto \exp[A/\sqrt{\mu_{c1}-\mu}]$ (A is a constant).

In the presence of disorder there is another instability, which for $\mathcal{G}$,$\mathcal{D} \simeq 0$ is located at $\mu_{c2} = 3/(2\pi\delta^2)$, see Eq. (4.27). At μ_{c2}, $\mathcal{D}$ becomes relevant. If $\mu < \mu_{c2}$, $\mathcal{D}$ flows to infinity and the stripe is in a disordered (pinned) state. Again, we integrate the RG analytically in the neighborhood of μ_{c2}, for the case of a vanishing lattice potential ($\mathcal{G} \simeq 0$). To linear order in $\epsilon_{\mathcal{D}} = 3 - 2\pi\delta^2$, Eqs. (4.27, 4.29) become

$$\frac{\partial}{\partial \ell}\mathcal{D} = \epsilon_{\mathcal{D}}\mathcal{D}, \tag{4.35}$$

$$\frac{\partial}{\partial \ell}\mu^{-1} = \frac{1}{2}\mathcal{D}, \tag{4.36}$$

or

$$\frac{\partial}{\partial \ell}\epsilon_{\mathcal{D}} = \frac{1}{2}\left(\epsilon_{\mathcal{D}}^2 + C_{\mathcal{D}}\right), \tag{4.37}$$

and $C_{\mathcal{D}} = \mathcal{D} - 2\pi\delta^2\epsilon_{\mathcal{D}}^2/9$ is constant under the RG. The critical line of the RG in the $\mathcal{D}$-$\epsilon_{\mathcal{D}}$ space, separating the disorder pinned from the free stripe, is given by $C_{\mathcal{D}} = 0$ which yields

$$\mu_{c2} = \frac{3}{2\pi\delta^2} + \frac{3\mathcal{D}^{1/2}}{(2\pi\delta^2)^{3/2}} \tag{4.38}$$

We can define a localization or collective pinning length L_{p2} of the stripe as the length scale where the renormalized disorder strength has reached a value of order one. The asymptotic dependence of L_{p2} on the disorder strength near the critical region (and $\mathcal{G} = 0$) is then found to be given by $L_p \propto \exp[-B\delta/\sqrt{\mathcal{D}_0 - \mathcal{D}_c}]$ where $\mathcal{D}_0$ is the bare and $\mathcal{D}_c$ the critical disorder strength and B is a constant. Even though the transverse excitations of the disorder pinned stripe are localized, the density of states remains unaffected by the disorder. Moreover, contrary to the lattice pinned stripe, the stiffness of the disorder pinned stripe is finite: adding a small linear tilt to the fields $\phi^i \to \phi^i + \delta\phi\, y$ leaves the disorder term in the action Eq. (4.20) unchanged and the gaussian part of the action is modified only at order $(\delta\phi)^2$. Hence, the change of the free energy per unit length is zero and the kink free energy vanishes [112].

The diagram in Fig. 4.6 shows the stability regions of the stripe in the δ-μ plane, for $\mathcal{D}, \mathcal{G} \simeq 0$. There are three distinct regimes: the freely fluctuating gaussian stripe ("free"), if neither disorder nor lattice perturbations are relevant, the disordered stripe, if disorder is relevant, and the flat stripe if the lattice is relevant and disorder is not [116]. The disordered stripe, which exists if disorder is relevant, can be further distinguished whether or not the lattice pinning is a relevant perturbation. Even though disorder always wins in the long wavelength limit, the stripe is locally flat if the lattice potential is relevant ("loc. flat") and if $L_{p1} < L_{p2}$. In the locally flat phase the sharp band edge of the massive excitations which exist in the flat phase are washed out by the disorder and Lifshitz-like tails extend down to zero energy. No true gap survives but the lattice pinning reduces the low energy spectral

weight and gives rise to a pseudogap. At $L_{p1} \approx L_{p2}$ the pseudogap disappears and a crossover to the disordered phase takes place.

In Fig. 4.6 we have plotted the different crossover lines as a function of δ and μ. Note that δ is proportional to the doping as long as the on-stripe charge density remains constant (which, for LSCO, is the case for small x up to $\sim \frac{1}{8}$ [15]).

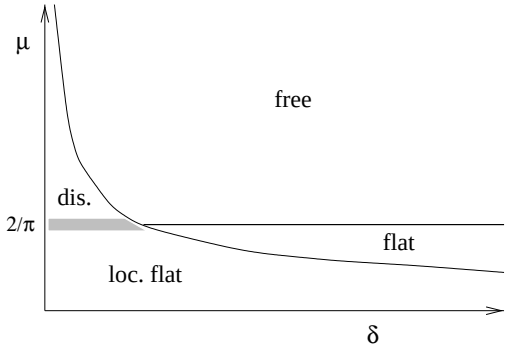

Figure 4.6: Phase diagram of the stripe as a function of $\delta = a/(2L)$ and $\mu = \sqrt{2t/K}$.

4.2.5 Comparing the RG results with experiments

From our analysis, it follows that dynamical fluctuating stripe order occurs only in a situation in which both disorder and lattice potentials are irrelevant, implying that the dynamical striped phase believed to be present in $La_{2-x}Sr_xCuO_4$ must be insensitive to disorder. Indeed, the IC spin fluctuations in this compound at near optical doping [93] are strikingly similar to those found in $La_2Cu_2O_{4+\delta}$ [102], which is relatively free of disorder because of the annealed character of the interstitial oxygen dopants. Although this shows that weak disorder is unimportant near optimal doping, at lower doping we expect from Fig. 4.6 a critical doping x_c below which the disorder will become relevant. Hence, below x_c the stripes will become pinned, which leads to a strong broadening of the IC spin fluctuations. We interpret the observed broadening of the IC peaks near $x \sim 0.05$ [15, 117], the superconductor-spin glass phase boundary, as evidence of stripe pinning, which possibly leads to a destruction of stripes in the spin glass phase.

In oxygen doped nickelates [65, 79, 82], the IC peak widths are always much narrower than in the Sr doped ones, [80, 101]. Thus, disorder is relevant and, hence, $\mu < \mu_{c2}$ for the nickelates. Furthermore, both Sr and O doped nickelates show strong commensuration effects [82]. The stability of a commensurate state depends on the competition between the effective stripe interactions and the strength of the lattice potential. To compare these two effects, one must integrate over the independent stripe fluctuations which exist up to the cutoff scale y_c. If $\mu < \mu_{c1}$, the effective lattice coupling is strong and very wide commensurate plateaus as a function of either doping or temperature are expected. This is the situation in

the nickelates. A similar commensuration effect is observable also in the cuprates; however, because $\mu > \mu_{c1}$, the renormalized lattice coupling strength at the scale y_c is exponentially suppressed and only a very narrow commensurate plateau exists. The striped phase is then nearly always in a floating phase IC with the lattice. This is consistent with the very weak Bragg peaks which are observable in $La_{2-x}Sr_xCuO_4$ only at $x = 1/8$ [18], and the static striped phase of $La_{1.6-x}Nd_{0.4}Sr_xCuO_4$ which is most pronounced again at $x = 1/8$ [16], whereas at other compositions the IC Bragg peaks are much weaker and broader [86].

4.2.6 Influence of stripe dynamics on spin correlations

The symmetries of a striped phase are rather different from those of a homogeneous magnet and share some properties with spiral phases which we discussed in the first chapter of this thesis. Both spiral and striped phases break not only the spin symmetry but also the translational lattice symmetry. The difference is that the spin order in a striped phase is collinear. The breaking of the translational symmetry is responsible for the presence of optical modes at the AF wave vector, as we discuss in this section within the context of stripes. Therefore, the dispersion of the IC peaks which we calculate is not particular to stripes but rather a manifestation of broken translational and spin symmetry. Thus, any ordered IC state would give rise to similar results. In the approach taken below, the two symmetries are treated separately, the broken spin symmetry being associated with the AF regions and the broken translational symmetry being associated with the dynamics of the charged stripes.

To discuss how stripe fluctuations affect the experimentally observable spin fluctuations (see also [109]), we take a simplified view on the dynamics of the stripe array, where we now account also for weak inter-stripe interactions. As mentioned above, these interactions are only relevant in the very long wavelength limit. We ignore here first disorder and lattice potentials. Approximating the effective stripe-stripe coupling by a harmonic potential, the action of the stripe array can then be written as

$$\begin{aligned} S &= \frac{1}{2\pi\mu}\sum_m \int_0^\beta d\tau \int dy \left[\frac{1}{c}\left(\partial_\tau \phi_m\right)^2 + c\left(\partial_y \phi_m\right)^2\right] \\ &\quad + \frac{Uc}{2\pi a^2}\sum_m \int_0^\beta d\tau \int dy \left[\phi_m - \phi_{m+1}\right]^2 . \end{aligned} \tag{4.39}$$

where U is dimensionless and quantifies the strength of the inter-stripe coupling. The integer m numerates the stripes and should not be confused with the replica index i used in Eq. (4.20). The corresponding propagator for the fields ϕ_m is then given by the inverse of the kernel in Eq. (4.39),

$$\Gamma_m(y,\tau) = \frac{\pi\mu L c}{\beta}\sum_{\omega_n}\int \frac{d^2\mathbf{k}}{(2\pi)^2}\frac{e^{ik_x mL + ik_y y - i\omega_n \tau}}{\omega_n^2 + c^2 k_y^2 + 2\frac{Uc^2\mu}{a^2}(1-\cos k_x L)} \tag{4.40}$$

with UV cutoffs $\Lambda_y = \pi/a$ and $\Lambda_x = \pi/L$. The Matsubara frequencies are given by $\omega_n = 2\pi n/\beta$. The propagator is massless around $k_{x,y} = 0$ but the modes at the Brillouin boundary $k_x = \pi/L$ show a gap $2c\sqrt{U\mu}/a$. Should lattice potentials be relevant, an additional mass would appear in the propagator. We now address the question, how the fluctuations of the stripes affect the spin correlations of the cuprates. In the striped phase, the charged stripes act as domain walls which separate undoped regions with opposite (probably short ranged) staggered magnetic order. We therefore write the staggered spin density as a product of the form $\mathbf{M}(\mathbf{r},\tau) = \mathbf{M}_{AF}(\mathbf{r},\tau)M_S(\mathbf{r},\tau)$ where $\mathbf{M}_{AF}$ describes the staggered spin density of the confined undoped regions and M_S is a function which changes sign at the position of the domain walls. We can write M_S as [118]

$$\begin{aligned} M_S(x,y,\tau) &= \sum_m (-1)^m \Theta_\xi(x - mL - a\phi_m(y,\tau)/\sqrt{\pi}) \\ &= \int \frac{dq}{2\pi}\left[\sum_m (-1)^m e^{iq(x-mL-a\phi_m(y,\tau)/\sqrt{\pi})}\Theta_\xi(q)\right] \end{aligned} \tag{4.41}$$

where $\Theta_\xi(x) = \int^x d\alpha \delta_\xi(\alpha)$ and $\delta_\xi(x) = \exp[-x^2/(2\xi^2)]/(\sqrt{2\pi}\xi)$ is a broadened delta function of width ξ. As the stripes are separated in space from the spins in the undoped region, it is a reasonable assumption that the dynamics of M_S and $\mathbf{M}_{AF}$ decouple [119] so that

$$\langle \mathbf{M}(\mathbf{r},\tau)\mathbf{M}(\mathbf{0},0)\rangle \simeq \langle \mathbf{M}_{AF}(\mathbf{r},\tau)\mathbf{M}_{AF}(\mathbf{0},0)\rangle \left\langle M_S(\mathbf{r},\tau)M_S(\mathbf{0},0)\right\rangle \tag{4.42}$$

It is then easy to show that we can write

$$\begin{aligned} \langle M_S(\mathbf{r},\tau)M_S(\mathbf{0},0)\rangle &\simeq \frac{4}{L}\int \frac{dq}{2\pi}\sum_m (-1)^m e^{iq(mL+x)} \left\langle e^{-iqa[\phi_m(y,\tau)-\phi_0(0,0)]/\sqrt{\pi}}\right\rangle \times \\ &\times \Theta_\xi(q)\Theta_\xi(-q), \end{aligned}$$

where $\Theta_\xi(q) = \exp(-q^2\xi^2/2)/(iq+\epsilon)$ is the Fourier transform of the broadened Heavyside step function. Taking the average with the action Eq. (4.39) gives

$$\begin{aligned} \left\langle e^{-iqa[\phi_m(y,\tau)-\phi_0(0,0)]/\sqrt{\pi}}\right\rangle &= e^{-q^2a^2[\Gamma_0(0,0)-\Gamma_m(y,\tau)]/\pi} \\ &\simeq \exp\left(-q^2a^2\Gamma_0/\pi\right)\left(1 + q^2a^2\Gamma_m(y,\tau)/\pi\right) . \end{aligned}$$

The last decomposition is only possible at $T = 0$ (for $T \neq 0$, Γ_0 diverges because of the Mermin-Wagner theorem). The exponential pre-factor in the last line is the quantum analog of the Debye-Waller factor, with $\Gamma_0 \simeq \pi\mu^{3/4}/(4U^{1/4})$. Hence, we see that strong quantum fluctuations of the stripes and weak stripe-stripe coupling (large μ and small U) suppress $\langle M_S M_S\rangle$. We can now decompose the Fourier transform of $\langle M_S M_S\rangle$ into an elastic and an inelastic part to find

$$\langle M_S M_S\rangle_{el}(\mathbf{k},\omega) \propto \delta(\omega)\delta(k_y)\delta(k_x \pm \pi/L)\exp\left[-\frac{\pi^2}{L^2}\left(\xi^2 + \frac{a^2}{\pi}\Gamma_0\right)\right] \tag{4.43}$$

$$\langle M_S M_S\rangle_{inel}(\mathbf{k},\omega) \propto \Gamma_{k_x\pm\pi/L}(k_y,\omega)\exp\left[-k_x^2\left(\xi^2 + \frac{a^2}{\pi}\Gamma_0\right)\right] \tag{4.44}$$

where $\Gamma_{k_x}(k_y, \omega)$ is the Fourier transform of $\Gamma_m(y, \tau)$. Using Eq. (4.40), we see that the inelastic part (i. e. $\Gamma_{k_x \pm \pi/L}(k_y, \omega)$) has gapless (acoustic) modes around $k_x = \pm\pi/L$, and gapped (optical) modes at $k_x = 0$ (both with $k_y = 0$). Because of the convolution with $\langle \mathbf{M}_{AF} \mathbf{M}_{AF} \rangle$, as implied by Eq. (4.42), the wave vector $\mathbf{k}$ is measured with respect to the commensurate AF positions $(\pm\pi/a, \pm\pi/a)$.

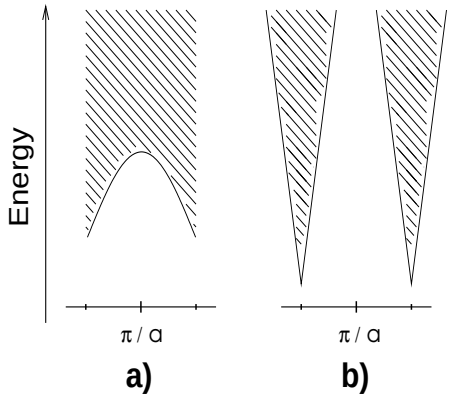

Figure 4.7: Evolution of the IC signal with energy. At low energies, the modes disperse away from the IC position $k_x = \frac{\pi}{a} \pm \frac{\pi}{L}$ (position indicated by marks next to the π/a position). The shaded region shows the continuum of excitations. a) Situation with freely fluctuating stripes; b) Situation with commensurate and non-fluctuating stripes.

The acoustic modes, which are excited at low energies, will therefore give rise to IC scattering in neutron scattering experiments. However, increasing the energy will result in peaks that disperse away from the IC positions and finally the optical modes will be excited which are located at the commensurate positions. Therefore, starting from low energies, one would first see IC peaks which, with increasing energies, merge into a broad commensurate peak. Our simple picture describes qualitatively the experimentally observed evolution of the IC peaks in $La_{2-x}Sr_xCuO_4$ [120, 121]. In [94], a merging of the IC peaks has been explained as a result of *single* stripe dispersion. In our view, the single stripe dynamics contribute to the continuum of excitations but the lower bound of the continuum is determined by the inter-stripe coupling. Further, as can be seen from Eq. (4.44), the dispersion away from the IC position is not symmetric around the IC positions, because signals at large values of k_x are exponentially suppressed both by the finite thickness of the domain walls and the quantum fluctuations of the stripes. Such an asymmetry has also been observed experimentally [120, 121]. We have sketched the evolution with energy schematically in Fig. 4.7a, where we assumed very soft stripe fluctuations such that Eq. (4.44) determines entirely the dispersion of the signal. In the figure it can be seen how the IC scattering evolves into the commensurate scattering at higher energies. As the signal at the commensurate position corresponds to optical modes of the stripe array, one would only expect a resonance

at the commensurate position if the stripe fluctuations are highly coherent. Recently, the continuous evolution of the IC fluctuations into commensurate ones was indeed observed [122], the experimentally determined dispersion is shown in Fig. 4.8. We note that the resonance at the commensurate AF wave vector was only observed in the superconducting state. As the optical excitations are directly related to the translational symmetry breaking, this indicates that the stripe array is more ordered in the superconducting phase. Thus, it seems that stripe fluctuations are coherent in the superconducting phase but incoherent once the superconductivity is destroyed. Signatures of a transition from coherent to incoherent stripe fluctuations at the superconducting phase transition were recently also inferred in [123].

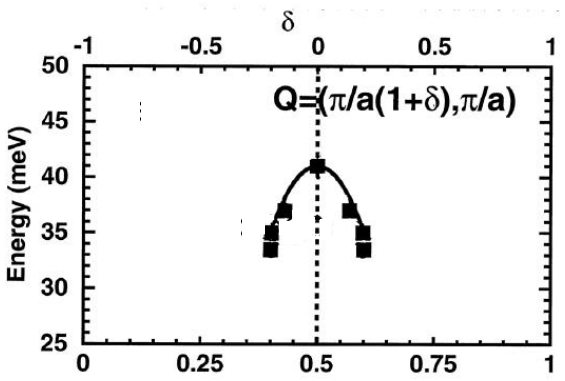

Figure 4.8: Black squares indicate the dispersion of the IC peaks as observed in $YBCO_{6.85}$, from Bourges *et al.* [122].

A finite spin correlation length in the AF regions would add a gap to the spectrum, which would result in a shift of the spectra in Fig. 4.7 to higher energies. The absence of any signal at very low energy transfers in the neutron scattering experiments thus indicates a finite coherence length of the spin order in the AF regions. For commensurately pinned stripes the stripe fluctuations are suppressed, but long ranged AF order gives rise to dispersion at low energies through spin waves. The absence of soft stripe fluctuations leads to a hardening of the IC modes and an energy evolution as drawn qualitatively in Fig. 4.7b. Such an energy dependence of the peak width has been measured in $La_2NiO_{4.133}$ [17]. We note, that at high energies, a merging of the IC modes at the commensurate position should occur however also in this system, as the translational symmetry is still broken. Such a merging should be observable experimentally.

4.3 Stripe dynamics in the strongly disordered regime

While both the lattice pinned and free phase of the stripe are expected to have fairly well developed dynamic or static stripe correlations, in the disorder pinned phase, the correlation

length of the stripe array is expected to be very short so that a detection of stripes in scattering experiments could be difficult or even impossible if stripe correlation lengths become shorter than the average stripe spacing. The crossover to the disordered stripe described above happens when the disorder becomes relevant already at scales where the inter-stripe interaction plays no role. Thus our disorder pinned phase describes individually pinned stripes and in a further investigation of this phase below it is legitimate to focus on a single and isolated stripe in a disorder potential [124].

Under sufficiently strong external electrical fields, it will be possible for the stripe to overcome the pinning potential and move freely. An interesting question relevant to experiments is how large such a field would be. We shall attempt in this section an estimate on the order of magnitude of such a depinning field and also discuss qualitatively the creep of pinned stripes for fields smaller than the depinning field.

For $La_{2-x}Sr_xCuO_4$, the most likely regime where a picture of strongly disordered stripes might apply is the spin glass regime and our analysis allows for a qualitative comparison of the transport measurements in this regime with the predictions obtained below for a disordered stripe glass in which the transport is assumed to be dominated by stripe creep. We shall concentrate here on the case of a classical string and determine its collective pinning lengths, the depinning field and the creep of the stripe for subcritical fields. A discussion of the creep of stripe accounting for quantum fluctuations can be found in [125].

4.3.1 Depinning transition under an external electric field

For strongly disordered stripes, commensuration effects are negligible and thus we neglect here the lattice pinning completely and use the continuum formulation. The free energy describing an infinite elastic string along the y-direction, which tends to move due to the action of an externally applied electrical field E competing against the pinning barrier V_{pin} is then in the classical limit

$$\mathcal{F}[u(y)] = \int_{-\infty}^{\infty} dy \left[\frac{K}{2a} \left(\frac{\partial u}{\partial y} \right)^2 - V_{pin} - \frac{eEu}{a} \right]. \tag{4.45}$$

The next step is to obtain an estimate for the pinning potential V_{pin}. Let us assume that the pinning mechanism is produced by the ionized acceptors which sit on a plane parallel to and close to the CuO_2-plane. An impurity with two dimensional coordinates $\mathbf{r}'$ produces the Coulomb potential $G(\mathbf{r}' - \mathbf{r})$ at the position $\mathbf{r}$ in the CuO_2-plane - we ignore the finite separation between the donor and the CuO_2-plane - with

$$G(\mathbf{r}' - \mathbf{r}) \simeq \frac{e^2}{\epsilon |\mathbf{r}' - \mathbf{r}|} \quad . \tag{4.46}$$

The total potential felt at position $\mathbf{r}$ on the CuO_2 planes can then be written as

$$V_{pin}(\mathbf{r}) = \frac{1}{a^2} \int d^2\mathbf{r}' \mathcal{N}(\mathbf{r}') G(\mathbf{r}' - \mathbf{r}), \tag{4.47}$$

where $\mathcal{N}(\mathbf{r}')$ is the number of impurities (zero or one) at the position $\mathbf{r}'$, e is the elementary unit of charge and ϵ is here the (static) dielectric constant. Hence, $\mathcal{N}(\mathbf{r}) = (\mathcal{N}(\mathbf{r}))^2$. Let us denote the average number of impurities per lattice site $[\mathcal{N}(\mathbf{r})]_D = x$, where $[\ldots]_D$ represents again the average over the disordered impurity ensemble and $0 < x < 1$. If the impurity distribution is uncorrelated, we can write the density-density correlator as

$$\rho_0(\mathbf{r}, \mathbf{r}') = [\mathcal{N}(\mathbf{r})\mathcal{N}(\mathbf{r}')]_D - [\mathcal{N}(\mathbf{r})]_D [\mathcal{N}(\mathbf{r}')]_D = x(1-x)\delta(\mathbf{r} - \mathbf{r}'). \tag{4.48}$$

Its Fourier-transform is a constant for any value of the wave vector $\mathbf{k}$, $\rho_0(\mathbf{k}) = x(1-x) = const.$ This correlator describes long-wavelength fluctuations with any k, including the small ones. Although the small-k fluctuations are allowed by the statistics of the completely disordered state, in reality they are strongly suppressed by the long-range Coulomb interaction of the impurities. Hence, the real correlator should be suppressed for small k at some scale $k < \lambda_{\rm co}$. This cut-off can be introduced by the following choice of the correlation function:

$$\rho(\mathbf{k}) = \frac{x(1-x)}{1 + \lambda_{\rm co}^2/k^2}. \tag{4.49}$$

Since the only length scale in the system of the impurities is the average distance between two neighbour impurities $u = ax^{-1/2}$, the $\lambda_{\rm co}$ parameter should be estimated as $\lambda_{\rm co} \sim 1/u$. Furthermore, the two-point correlator of the impurity potential is given by

$$\begin{aligned} \mathcal{K}(\mathbf{r}) &= [V_{pin}(\mathbf{r})V_{pin}(0)]_D - [V_{pin}(\mathbf{r})]_D [V_{pin}(0)]_D \\ &= \frac{1}{a^4} \int d^2\mathbf{r}' \; d^2\mathbf{r}'' G(\mathbf{r}'') G(\mathbf{r}' - \mathbf{r}) \rho(\mathbf{r}', \mathbf{r}''). \end{aligned}$$

The Fourier transform of $\mathcal{K}(\mathbf{r})$ reads

$$\mathcal{K}(\mathbf{k}) = (x - x^2) \left(\frac{e^2}{\epsilon a}\right)^2 \frac{4\pi^2}{(k^2 + \lambda_{\rm co}^2)a^2}, \tag{4.50}$$

where $G(\mathbf{k}) = 2\pi e^2/(\epsilon k)$ is the 2D Fourier-transform of the Coulomb potential $G(\mathbf{r})$. Rewriting then the correlator of the potential in real space we find

$$\mathcal{K}(\mathbf{r}) = 2\pi \left(\frac{e^2}{\epsilon}\right)^2 (x - x^2) K_0(\lambda_{\rm co} r), \tag{4.51}$$

where $K_0(\lambda_{\rm co} r)$ is the modified Bessel function.

Let us now define $\varepsilon_{pin} = \int dy V_{pin}$. If the stripe interacting with the random pinning potential is stiff, the average pinning energy $[\varepsilon_{pin}(L)]_D$ of a segment of length L is zero. The fluctuations of the pinning energy, however, remain finite,

$$\left[\varepsilon_{pin}^2\right]_D = \frac{1}{a^2} \int_0^L dy dy' \mathcal{K}(0, y - y') \simeq \gamma L \tag{4.52}$$

with

$$\gamma = \frac{2\pi^2 \varepsilon_c^2 \sqrt{x}}{a}. \tag{4.53}$$

Here, $\varepsilon_c = e^2/\epsilon a$ denotes the Coulomb energy scale. The sublinear growth of $\left[\varepsilon_{pin}^2(L)\right]_D^{1/2}$ is due to the competition between individual pinning centers. To investigate the competition between the pinning and elastic energies, we use the dynamic approach to this problem which was introduced by Larkin and Ovchinnikov [126] in the "Collective Pinning Theory" (CPT) for describing the dynamics of weakly pinned vortex-lines in the high temperature superconductors. This approach was also applied in connection with the pinning problem in charge-density-wave systems [127, 128]. The results of the CPT can be summarized as follows [129]: Eq. (4.52) would imply that a stiff stripe is never pinned, since the pinning force grows only sublinearly, whereas the electric driving force increases linearly with length. This arguments ignores however the finite elasticity of the stripe and its competition with the disorder fluctuations. Due to the elasticity, the stripe can accommodate to the potential on some "collective pinning length" L_{cp}. Then, each segment L_{cp} of the stripe is pinned independently and the driving force is balanced. This length L_{cp} can be estimated from dimensional arguments. The evaluation of the free energy for a segment of length L with dimensional estimates provides

$$\mathcal{F}[u, L] \sim \frac{K u^2}{aL} - \sqrt{\gamma L} - \frac{eEuL}{a}. \tag{4.54}$$

The collective pinning length of the stripe is then obtained from minimizing $\mathcal{F}[u, L]/L$ with respect to L at zero bias field [129],

$$\frac{\delta \mathcal{F}/L}{\delta L}\Big|_{L_{cp}} = 0, \qquad L_{cp} \simeq \left(\frac{K u^2}{a\sqrt{\gamma}}\right)^{2/3}. \tag{4.55}$$

The characteristic value of the displacement u is given by the average distance between the impurities, hence $u \sim \lambda_{\rm co}^{-1} \sim a/\sqrt{x}$. Using Eq. (4.53) we find

$$L_{cp} \simeq a x^{-5/6} \left(\frac{K}{\varepsilon_c}\right)^{2/3}. \tag{4.56}$$

Experimentally, it is difficult to measure the collective length L_{cp}. However, the threshold electric field E_c corresponding to the vanishing of the barrier is a quantity which can be more easily experimentally determined. The critical threshold field E_c beyond which the stripe is free to move through the sample is obtained from comparing the energy of the driving field with the pinning energy $eEuL_{cp} \simeq \sqrt{\gamma L_{cp}}$. This yields

$$E_c = \frac{a}{eu}\sqrt{\frac{\gamma}{L_{cp}}} \sim \frac{x^{7/6}\varepsilon_c}{ea}\left(\frac{\varepsilon_c}{K}\right)^{1/3}. \tag{4.57}$$

For typical high-T_c materials, such as $La_{2-x}Sr_xCuO_4$, $J \approx 0.1$ eV, $a \approx 4$ Å and the static dielectric constant $\epsilon = \epsilon_0 \approx 30$ [130]. Hence, one can estimate the elastic energy $K \sim J \approx 0.1$ eV and the Coulomb energy $\varepsilon_c = e^2/(\epsilon a) \approx 0.1$ eV. For a doping concentration in the insulating phase, for instance, for $x \simeq 10^{-2}$, we obtain the collective pinning length $L_{cp} \approx 10^2$ Å and the critical electrical field $E_c \approx 10^4$ V/cm. This field is rather strong and it is unclear whether a stripe depinning could be clearly detected in an experiment. The biggest obstacle for a detection of stripe depinning is the large depinning energy which in our simple estimate is of the same order of magnitude as J. Clearly, at this fundamental energy scale there might be many different types of processes in the cuprates, which may complicate an unambiguous detection of stripe depinning in an experiment. While the depinning field $E_c \approx 10^4$ V/cm is quite large, the stripes can also move for subcritical fields, either through thermal activation for the case of classical stripes or, at very low temperatures such that quantum processes become important, through tunneling. The subcritical creep may offer a simpler route for finding signatures of stripes and below we therefore investigate the nature of the creep.

4.3.2 Stripe relaxation processes

We have estimated the threshold field E_c corresponding to a depinning of stripes. The next step is to discuss the relaxation for a stripe subject to a subcritical field $E < E_c$. In this case, the stripe is in a metastable configuration and has to overcome a finite pinning barrier to move. This barrier can be overcome either via thermal processes in the classical limit or via quantum tunneling. Here, we will focus on the classical creep.

Classical limit

At high temperatures, the dominant relaxation process is classical and driven by thermal activation. In this case the decay rate Γ_t of the metastable configuration is given by an Arrhenius law, $\Gamma_t \sim \exp(-U/T)$. To calculate the activation energy U we only need to evaluate the free energy $\mathcal{F}$ at the saddle point configuration u_s, $U = \mathcal{F}[u_s]$. Dynamical terms in the free energy can be neglected as these only contribute to the prefactor multiplying the exponential function. The activation energy U depends on the externally applied field E but it scales with the collective energy pinning energy U_c which is a quantity independent from E and can again be obtained from dimensional estimates. Substituting the expression for the collective pinning length L_{cp}, Eq. (4.56), into the free energy Eq. (4.54) setting $E = 0$ yields

$$U_c \simeq \sqrt{\gamma L_{cp}} \simeq x^{-1/6} \left(K\varepsilon_c^2\right)^{1/3} \tag{4.58}$$

For the case of $La_{2-x}Sr_xCuO_4$ a rough estimate for $x \sim 10^{-2}$, as used also above, we estimate the pinning energy barrier to be at the order of 10^3 K with a doping dependence $U_c \propto x^{-1/6}$.

Again, this is a rather high energy scale comparable to J.

Having obtained both the characteristic energy scale U_c and the collective pinning length scale L_{cp} of the problem, we now need to look at the scaling for lengths $L > L_{cp}$. A central parameter for this is the wandering exponent of the stripe, defined through

$$\left[\left\langle (u(L) - u(0))^2 \right\rangle\right]_D \sim u_c^2 \left(\frac{L}{L_{cp}}\right)^{2\zeta}, \qquad L > L_{cp}, \tag{4.59}$$

where, for us, $u_c \sim \lambda_{co}^{-1}$ and $[\langle \ldots \rangle]_D$ denotes the full thermal and disorder average. For the present case of a classical string in a disordered plane the wandering exponent $\zeta = 2/3$ was found by exact calculations [131, 132]. The typical energy barrier $\mathcal{U}$ seen by the stripe in absence of external fields then follows from the scaling of the free energy Eq. (4.54) with $E = 0$. As the elastic energy exactly balances the pinning energy, we can determine the scaling of the free energy from the scaling of the elastic term and find

$$\mathcal{U} \sim U_c \left(\frac{L}{L_{cp}}\right)^{2\zeta-1}. \tag{4.60}$$

Similarly, for $E \ll E_c$ we obtain the scaling of the free energy in presence of a small external field,

$$\mathcal{F}(L) \sim U_c \left(\frac{L}{L_{cp}}\right)^{2\zeta-1} - \frac{eEL_{cp}u_c}{a} \left(\frac{L}{L_{cp}}\right)^{\zeta+1}. \tag{4.61}$$

The problem now has been reduced to a nucleation process [133]. If a nucleus with length L larger than some optimal length L_{opt} is formed, the nucleus will grow until the whole stripe has relaxed into the new neighboring minimum. On the other hand, if the activated segment is smaller than the optimal one, the nucleus will shrink and collapse to zero. The optimal nucleus is found by extremizing the full free energy, $\partial_L \mathcal{F}(L)|_{L=L_{opt}} = 0$ and we obtain

$$L_{opt}(E) \sim L_{cp} \left(\frac{E_c}{E}\right)^{1/(2-\zeta)}. \tag{4.62}$$

Inserting Eq. (4.62) back into the free energy Eq. (4.61) we find that the average barrier for creep increases algebraically for decreasing bias field,

$$U(E) \sim U_c \left(\frac{E_c}{E}\right)^{\mu} \tag{4.63}$$

with $\mu = (2\zeta - 1)/(2 - \zeta) = 1/4$. This behavior defines a glassy state, with diverging barriers in the limit of vanishingly small applied electric fields.

The other interesting limit is the one with applied fields smaller but close to the critical one, i.e. $0 < E_c - E \ll E_c$. This case is more difficult to treat because for nearly critical external bias the system is far removed from equilibrium. At present the creep of randomly pinned strings in this regime is not understood. In order to gain some insights into the

problem, we shall assume here a spatially uniform potential barrier height for the stripe, i.e. we neglect fluctuations in the local depinning field strength around the mean value E_c. This allows to obtain results which cast some light also on the creep in presence of disorder. To treat the limit of applied fields close to the critical one, we therefore approximate the overall potential arising from the pinning and the bias electric field by an effective potential which describes a metastable configuration. The simplest form of a metastable potential which has the property that the metastable state vanishes at $E = E_c$ is of the form

$$V_{\mathit{eff}} = V_E \left[\left(\frac{u}{u_E} \right)^2 - \left(\frac{u}{u_E} \right)^3 \right] \tag{4.64}$$

with $V_E \sim V_c(1 - E/E_c)^{3/2}$ and $u_E \sim u_c\,(1 - E/E_c)^{1/2}$. The critical potential barrier is given by $V_c = eE_c u_c/a$ and the critical displacement of the stripe (which is a function of the external bias E) is given by u_E. Again, we now have to analyse a nucleation process and find the critical size of the nucleus beyond which the nucleus will expand. For the energy of a distortion u_E over a length L_E we then find the energy

$$\mathcal{E}(u_E, L_E) \sim \left[\frac{K}{2} \left(\frac{u_E}{L_E} \right)^2 + V_{\mathit{eff}}\,(u_E) \right] L_E. \tag{4.65}$$

The competition is now again between the potential energy which scales like $u^3 \propto (1 - E/E_c)^{3/2}$ and the elastic energy which scales like $K(u_E/L_E)^2 \propto (1 - E/E_c)$. The length L_{ES} of the saddle point nucleus therefore scales like

$$L_{ES} \sim u_c \sqrt{\frac{K}{V_c}} \left(1 - \frac{E}{E_c} \right)^{-1/4} \sim L_{cp} \left(1 - \frac{E}{E_c} \right)^{-1/4}. \tag{4.66}$$

From Eq. (4.65) we then obtain for the energy barrier

$$U(E) \sim u_c V_c \left(\frac{K}{V_c} \right)^{1/2} \left(1 - \frac{E}{E_c} \right)^{\alpha} \sim U_c \left(1 - \frac{E}{E_c} \right)^{\alpha}, \tag{4.67}$$

where, in absence of disorder, $\alpha = 5/4$. For the random pinning one might expect that the energy barrier for thermal activation still obeys a power law of the type above but with a different exponent α. However, the exponent α is not known for the case of random pinning. More severely, the validity of a power law relation of type (4.67) has not been rigorously proven and the assumption that the effective energy barrier scales with the average critical depinning field may well be wrong.

Let us now compare briefly our results with experimental data on the transport in the SG regime. The transport data of $La_{2-x}Sr_xCuO_4$ for $0.02 < x < 0.05$ is characterized at the lowest measured temperatures by a temperature dependence of the resistivity which follows $\rho \propto \exp(\sqrt{T^*/T})$, with a characteristic temperature $T^* \sim 50$K [51]. This temperature dependence is characteristic for 3D variable range hopping. In contrast, for a system with a transport dominated by stripe creep one would expect a temperature evolution $\rho \propto \frac{U_c}{T} \exp(U_c/T)$,

with approximately $U_c \sim 10^3$K. This temperature evolution of the resistivity is not observed and therefore the low temperature transport in $La_{2-x}Sr_xCuO_4$ is not dominated by classical creep of charged stripes. We thus conclude that either stripes are not present in the spin glass regime, or, if they are, the transport is not dominated by collective stripe motion but rather by hopping of individual charge carriers between stripes. As discussed in detail in the first section of this thesis, the magnetic data from the spin glass regime is well described by a model in which the charge distribution is completely quenched. This strongly suggests the absence of stripes for $x < 0.05$.

4.4 Coupling of transverse and longitudinal fluctuations

While we have so far focused on the dynamics of a completely charge depleted stripe (a chain of holes), experiments on cuprates point to a finite electron filling of the stripes. Thus, stripe excitations may involve also longitudinal charge and spin fluctuations. As an exact treatment of the dynamics of a filled stripe seems impossible, we need to develop some approximate scheme. For a completely flat stripe, with all transverse fluctuations completely frozen, the excitations of the stripe are just those of a one dimensional interacting electron model. Such models can be well studied and described with bosonization techniques. Similarly, a completely empty stripe has only transverse modes and we have already discussed some aspects of these in previous sections. The approach we shall follow in this section is that we assume a weak coupling between the transverse and longitudinal modes. Using well known perturbative techniques we will then investigate the possible phases of the filled stripe with special attention to the experimentally most relevant case of a quarter filled stripe. Our analysis shows that a weak coupling of the transverse and longitudinal modes does not lead to a strong superconducting instability but rather may lead to a charge density wave (CDW) instability exactly at quarter filling. For charge densities close to 1/4, the excitations have solitonic character. We begin with a description of the transverse modes using a spin-1 language and review its properties following closely the framework laid out by Schulz [134]. The discussion of the transverse modes is rather detailed and also serves as a brief introduction to the basic concepts of bosonization techniques. We then introduce the coupling to the longitudinal modes and study the combined model with bosonization techniques.

4.4.1 Transverse modes as a spin model

Our starting point for the transverse modes is again the simple chain of holes model introduced previously in Eq. (4.3),

$$\hat{H}_S = -2t \sum_n \cos\left(\hat{p}_n a\right) + \frac{K}{2a^2} \sum_n \left(\hat{u}_{n+1} - \hat{u}_n\right)^2 \tag{4.68}$$

Applying the unitary transformation $\hat{\varphi}_n = \sum_{m<n} \hat{p}_m$, $\hat{\pi}_n = \hat{u}_n - \hat{u}_{n+1}$, we can rewrite this as

$$H_S = -2t \sum_n \cos\left(\hat{\varphi}_{n+1} - \hat{\varphi}_n\right) + \sum_n \frac{K}{2a^2} \hat{\pi}_n^2 \tag{4.69}$$

If we restrict transversal fluctuations to $\hat{u}_{n+1} - \hat{u}_n = \pm 1, 0$, we can rewrite the Hamiltonian in spin 1 language, using $S_n^z = \hat{\pi}_n$ and $S_n^{\pm} = \sqrt{2}\exp(\pm i\hat{\varphi}_n)$,

$$\hat{H}_{S1} = \sum_n \left[-t \left(S_n^x S_{n+1}^x + S_n^y S_{n+1}^y \right) - J_z S_n^z S_{n+1}^z + d(S_n^z)^2 \right], \tag{4.70}$$

where $d \sim K$ is renormalized by the $\mathbf{S}_n^2 = 1$ constraint and we included a further $S_n^z S_{n+1}^z$ interaction characterized by the parameter J_z (we omit here an additional $\left(S_n^z S_{n+1}^z\right)^2$ "curvature" term whose effect is discussed in [104]). There is a vast amount of literature on this spin-1 Hamiltonian and while exact solutions are only known for some special parameters, the zero temperature phase diagram seems well understood. A possible approach to study this Hamiltonian is to replace the spin-1 operator by a sum of two spin 1/2 operators, $\mathbf{S}_n = \boldsymbol{\tau}_a(n) + \boldsymbol{\tau}_b(n)$. The spin 1/2 operators allow for a Jordan-Wigner transformation into a system of interacting fermions. The obvious drawback of the use of spin 1/2 operators is the introduction of a local singlet (with $\mathbf{S}_n^2 = 0$) which is absent in the original model. This leads to some problems as we will discuss later. Using a Jordan Wigner transformation, one can transform the spin 1/2 operators to Fermi operators,

$$\tau_a^+(n) = a_n^\dagger \exp\left[i\pi \sum_{m=1}^{n-1} a_m^\dagger a_m\right] \ , \quad \tau_a^z(n) = a_n^\dagger a_n - \frac{1}{2} \tag{4.71}$$

with $\{a_n, a_m^\dagger\} = \delta_{nm}$ and an analogous transformation for $\tau_b^+(n)$ to Fermi operators b_n. The filling factor of the Fermions is directly related to the z-component of the total spin of the spin chain, $S^z = \sum_{n=1}^N S_n^z = N_F^a + N_F^b - N$ with $N_F^a = \sum_n a_n^\dagger a_n$ and analogous equation for N_F^b, so that for $S^z = 0$ (a straight string) we have $N_F^a + N_F^b = N$. For symmetry reasons and also to correctly describe the roughening transition (which in this fermion description is driven by Umklapp scattering) we need to choose $k_F^a = k_F^b$. Thus, the filling factor is exactly 1/2 and the Fermi surface is at $k_F = \pm\pi/2$. The Hamiltonian (4.70) can then be written as

$$H_{S1} \simeq H + H' \tag{4.72}$$

where H can be expressed in terms of the a_n, b_n operators,

$$\begin{aligned} H &= \sum_n \Big[-\frac{t}{2}\left(a_n^\dagger a_{n+1} + a_{n+1}^\dagger a_n\right) + J_z\left(a_n^\dagger a_n - \frac{1}{2}\right)\left(a_{n+1}^\dagger a_{n+1} - \frac{1}{2}\right) \\ &+ J_z\left(a_n^\dagger a_n - \frac{1}{2}\right)\left(b_{n+1}^\dagger b_{n+1} - \frac{1}{2}\right) + d\left(a_n^\dagger a_n - \frac{1}{2}\right)\left(b_n^\dagger b_n - \frac{1}{2}\right) + a \leftrightarrow b \Big] \end{aligned} \tag{4.73}$$

and H', which cannot be simply expressed in terms of a_n, b_n, has the form

$$H' = -\frac{t}{2}\sum_n \left[\tau_a^+(n)\tau_b^-(n+1) + \tau_a^-(n)\tau_b^+(n+1) + \tau_a \leftrightarrow \tau_b\right] \tag{4.74}$$

The Hamiltonian H now is a standard one dimensional interacting Fermi model which can be transformed into bosonic language with well established methods. For this, one linearizes the dispersion of the non-interacting Fermions around $k_F = \pm\pi/2$ and writes the lattice operators a_n, b_n in terms of continuum Fermi operators for left and right moving particles,

$$a_n \simeq e^{-ik_F n}\psi_{a,L}(r_n) + e^{ik_F n}\psi_{a,R}(r_n) \tag{4.75}$$

and an identical transformation for the b_n operators. Then, H can be written in terms of bosonic density operators $\tilde{\rho}_{L/R,a/b}(q) = \sum_k \psi^\dagger_{L/R,a/b}(k+q)\psi_{L/R,a/b}(k)$ as

$$\begin{aligned} H &= \frac{\pi t}{\mathcal{L}} \sum_{k\neq 0,L/R} \left\{ \left(1 - \frac{2J_z}{\pi t}\right) \left[\tilde{\rho}_{R/L,a}(k)\tilde{\rho}_{R/L,a}(-k) + \tilde{\rho}_{R/L,b}(k)\tilde{\rho}_{R/L,b}(-k)\right] \right. \\ &+ \frac{d-J_z}{\pi t}\left[\tilde{\rho}_{R/L,a}(k)\tilde{\rho}_{R/L,b}(-k) + \tilde{\rho}_{R/L,b}(k)\tilde{\rho}_{R/L,a}(-k)\right] \\ &- \frac{2J_z}{\pi t}\left[\tilde{\rho}_{R/L,a}(k)\tilde{\rho}_{L/R,a}(-k) + \tilde{\rho}_{R/L,b}(k)\tilde{\rho}_{L/R,b}(-k)\right] \\ &\left. + \frac{d-J_z}{\pi t}\left[\tilde{\rho}_{R/L,a}(k)\tilde{\rho}_{L/R,b}(-k) + \tilde{\rho}_{R/L,b}(k)\tilde{\rho}_{L/R,a}(-k)\right] \right\}, \end{aligned} \tag{4.76}$$

where $\mathcal{L}$ is the length of the string. Introducing the linear combinations $\tilde{\rho}_{L/R,\pm} = (\tilde{\rho}_{L/R,a} \pm \tilde{\rho}_{L/R,b})/\sqrt{2}$ one can rewrite this in the form

$$\begin{aligned} H &= \frac{\pi t}{\mathcal{L}} \sum_{k\neq 0,L/R} \left\{ \left(1 - \frac{3J_z - d}{\pi t}\right) \tilde{\rho}_{L/R,+}(k)\tilde{\rho}_{L/R,+}(-k) \right. \\ &+ \left(1 - \frac{J_z + d}{\pi t}\right) \tilde{\rho}_{L/R,-}(k)\tilde{\rho}_{L/R,-}(-k) \\ &\left. - \frac{3J_z - d}{\pi t}\tilde{\rho}_{L/R,+}(k)\tilde{\rho}_{R/L,+}(-k) - \frac{J_z + d}{\pi t}\tilde{\rho}_{L/R,-}(k)\tilde{\rho}_{R/L,-}(-k) \right\} \end{aligned} \tag{4.77}$$

Following Schulz [134], we introduce bosonic phase fields

$$\Psi_{a/b}(x) = -\frac{i\pi}{\mathcal{L}} \sum_{k\neq 0} \frac{1}{k}\left[\tilde{\rho}_{R,a/b} + \tilde{\rho}_{L,a/b}\right] e^{-\alpha|k|/2 - ikx}, \tag{4.78}$$

$$\chi_{a/b}(x) = \frac{1}{\mathcal{L}} \sum_{k\neq 0} \left[\tilde{\rho}_{R,a/b} - \tilde{\rho}_{L,a/b}\right] e^{-\alpha|k|/2 - ikx}, \tag{4.79}$$

where α is a necessary high energy cutoff which can be thought of as a lattice cutoff. The fields satisfy bosonic commutation relations $\left[\Psi_{a/b}(x), \chi_{a/b}(y)\right] = i\delta(x-y)$ while fields with different a/b indices commute. The $\Psi_{a/b}$ are related to density fluctuations of the a,b fermions through

$$\partial_x \Psi_{a/b}(x) = -\pi\left(\tilde{\rho}_{R,a/b}(x) + \tilde{\rho}_{L,a/b}(x) - \frac{1}{2}\right); \tag{4.80}$$

Introducing $\Psi_\pm = (\Psi_a \pm \Psi_b)/\sqrt{2}$ and $\chi_\pm = (\chi_a \pm \chi_b)/\sqrt{2}$, the full Hamiltonian H_{S1} can then finally be written as $H_{S1} = H_+ + H_-$ with

$$\begin{aligned} H_+ &= \frac{u_+}{2\pi}\int dx \left[K_+\pi^2\chi_+^2 + K_+^{-1}\left(\partial_x\Psi_+\right)^2\right] + \frac{\mu_1}{\pi^2\alpha^2}\int dx \cos\left[\sqrt{8}\Psi_+\right]; \\ H_- &= \frac{u_-}{2\pi}\int dx \left[K_-\pi^2\chi_-^2 + K_-^{-1}\left(\partial_x\Psi_-\right)^2\right] + \frac{\mu_2}{\pi^2\alpha^2}\int dx \cos\left[\sqrt{8}\Psi_-\right] \\ &+ \frac{\mu_3}{\pi^2\alpha^2}\int dx \cos\left[\sqrt{2}\Theta_-\right]. \end{aligned} \tag{4.81}$$

Here, $\Theta_-(x) = \pi \int^x dx' \chi_-(x')\ u_\pm$ are the velocities of the acoustic excitations of the model, with $u_+ \simeq t\sqrt{1+2(d-3J_z)/(\pi t)}$ and $u_- \simeq t\sqrt{1-2(d+J_z)/(\pi t)}$. The dimensionless parameters $K_\pm$ are given by $K_+ = [1+2(d-3J_z)/(\pi t)]^{-1/2}$ and $K_- = [1-2(d+J_z)/(\pi t)]^{-1/2}$. The coupling constants for the nonlinear terms are approximately given by $\mu_1 = \mu_2 = J_z + d$ and $\mu = -t$. While the μ_1 and μ_2 terms are familiar from interacting Fermi models and represent back- and forward scattering contributions respectively, the μ_3 term originates from the non-local Fermi coupling hidden in H' and is a so-called disorder operator. The form of the μ_3 term as written in Eq. (4.81) is obtained from H' via the bosonization identity [134]

$$\psi_{a/b,R} = \frac{1}{\sqrt{2\pi\alpha}} e^{-i\Psi_{a/b}+i\Theta_{a/b}} \quad \text{and} \quad \psi_{a/b,L} = \frac{1}{\sqrt{2\pi\alpha}} e^{i\Psi_{a/b}+i\Theta_{a/b}} \tag{4.82}$$

where $\Theta_{a/b}(x) = \pi \int^x dx' \chi_{a/b}(x')$. With the use of Eqs. (4.75, 4.80, 4.82) one finds

$$\exp\left[i\pi \sum_{m=1}^{n} a_m^\dagger a_m\right] \sim \exp\left[ik_F x - i\Psi_a(x=n)\right] \tag{4.83}$$

where we have omitted an unimportant $i\Psi_a(x=1)$ term in the exponent on the right hand side. We thus have

$$\begin{aligned} \tau_a^+(n)\tau_b^-(n+1) &= a_n^\dagger \exp\left[i\pi \sum_{m=1}^{n-1} a_m^\dagger a_m\right] \exp\left[-i\pi \sum_{j=1}^{n} b_j^\dagger b_j\right] b_{n+1} \\ &\sim \frac{1}{2\pi\alpha}\left[e^{ik_F x - i\Psi_a - i\Theta_a} + e^{-ik_F x + i\Psi_a - i\Theta_a}\right] e^{ik_F x - i\Psi_a} e^{-ik_F x + i\Psi_b} \times \\ &\quad \times \left[e^{-ik_F x + i\Psi_b + i\Theta_b} + e^{ik_F x - i\Psi_b + i\Theta_b}\right]. \end{aligned} \tag{4.84}$$

Similar expressions can be found analogously for the other terms in H'. The most relevant operator resulting from H' is $\cos(\Theta_a - \Theta_b) = \cos\left(\sqrt{2}\Theta_-\right)$ which is the only one included in Eq. (4.81). There are other operators which mix the (+) and (−) sectors but their scaling dimension is such that they are never dominant. The decoupling of the (+) and (−) sector in Eq. (4.81) is thus only approximate but should hold in the long wavelength regime.

To analyse the possible phases of the model defined through Eq. (4.81), it is convenient to treat the non-linear terms as perturbations and look at their scaling behavior. We shall refer to the (+) sector as the roughening sector and the (−) sector as the restructuring sector for reason which will become evident below. The scaling dimensions of the non-linear perturbations can be easily determined. As was shown in [135], for some constant A,B

$$\dim[\cos(A\Psi_\pm + B\Theta_\pm)] = \frac{A^2 K_\pm + B^2 K_\pm^{-1}}{4}, \tag{4.85}$$

where $\dim[\mathcal{O}]$ denotes the scaling dimension of the operator $\mathcal{O}$. If the scaling dimension is smaller than two, the operator is relevant. It follows, that the μ_1 term is relevant for

$d > 3J_z$. The transition at $d = 3J_z$ is the roughening transition of the string, which can be seen calculating the large n behavior of

$$G_u(n) = \left\langle (u_0 - u_n)^2 \right\rangle = \sum_{i,j=0}^{n-1} \left\langle S_i^z S_j^z \right\rangle_0 . \tag{4.86}$$

The bosonized form of S_n^z is

$$S^z(x) \simeq -\frac{\sqrt{2}}{\pi}\partial_x \Psi_+ + \frac{2}{\pi\alpha} e^{i\pi x} \cos(\sqrt{2}\Psi_+) \cos(\sqrt{2}\Psi_-), \tag{4.87}$$

Denoting by $\langle \ldots \rangle_0$ the average performed with the gaussian part of Eq. (4.81) we find the equal time correlation function

$$G_z(x) = \langle S^z(0) S^z(x) \rangle_0 \simeq \frac{2K_+}{\pi^2}\frac{1}{x^2} + C_z e^{i\pi x} |x|^{-2K_+ - 2K_-} \tag{4.88}$$

which consists of a smooth and an oscillating part (C_z is a constant). The smooth part gives rise to a logarithmic divergence of $G_u(n)$ for $K_+ \neq 0$ as is easily verified using Eq. (4.86). However, for $d > 3J_z$ the μ_1 operator is relevant and K_+ scales to zero, killing the logarithmic divergence of $G_u(n)$. Hence, the transition at $d = 3J_z$ is the roughening transition.

The analysis of the restructuring sector is more complicated. The μ_2 operator is relevant for $d + J_z < 0$ and the μ_3 operator is relevant for $d + J_z > -15\pi t/2$ [134]. Thus, the gaussian fixed point is never stable and the restructuring sector always flows to strong coupling. This implies that a perturbative approach starting from the gaussian model cannot be trusted. However, it was pointed out by den Nijs [136, 134] that the $(-)$ sector has an Ising symmetry. It has a form identical to the continuum limit of a classical 2D XY model $H_{xy} = \sum_{\langle ij \rangle} \cos(\phi_i - \phi_j)$ with a 2-fold (Ising) symmetry breaking term of the form $\cos 2\phi_i$. We therefore expect a transition in the $(-)$ sector of the Ising type. We can roughly locate the critical line of the transition as the line where the scaling dimensions of the two non-linear operators in the $(-)$ Hamiltonian are equal, which yields $d + J_z \sim -3t\pi/2$.

To analyse the properties of the phases we investigate the behavior of the equal time correlation function $G_\perp(n) = \langle S^+(n) S^-(0) \rangle$. Using bosonization, one finds

$$\begin{aligned} S^+(n) &= \tau_a^+(n) + \tau_b^+(n) \\ &\sim \sqrt{\frac{2}{\pi\alpha}} e^{-\frac{i}{\sqrt{2}}\Theta_+} \left\{ \cos\left[\frac{\Theta_-}{\sqrt{2}}\right] + (-1)^n e^{-i\sqrt{2}\Psi_+} \cos\left[\frac{\Theta_-}{\sqrt{2}} + \sqrt{2}\Psi_-\right] \right\}. \end{aligned} \tag{4.89}$$

If Ψ_+ is ordered (i.e. $d > 3J_z$), then $G_\perp$ decays exponentially as Θ_+ correlations are short ranged. Similarly, if $d < 3J_z$ and $d + J_z > -3t\pi/2$, such that Ψ_- has long range order, then Θ_- correlations also are short ranged, again leading to an exponentially $G_\perp$. However, for $d < 3J_z$ and $d + J_z < -3t\pi/2$, Θ_- is ordered and $G_\perp$ decays algebraically like

$$G_\perp(x) \sim |x|^{-\frac{1}{4K_+}} \tag{4.90}$$

Combining the results from the (+) and (−) sectors, we then find five different phases. 1) a gapfull flat phase, with dominant μ_1 and μ_3 perturbations, exponentially decaying G_z and $G_\perp$ correlations and a finite limit of G_u. 2) A gapless rough phase in which only μ_3 is relevant, with an algebraic decay in the smooth part of G_z, exponentially decaying $G_\perp$ and logarithmically divergent G_u correlations. 3) A gapless bond centered (BC) rough phase. This phase is also gapless but differs from the rough phase in that it has an algebraic decay in the $G_\perp$ correlations. This phase has a local zig-zag pattern of the string (antiferromagnetic correlation with $S_z = \pm 1$ but no $S_z = 0$ states). 4) A BC flat phase with dominant μ_2 and μ_3 perturbations. Like the BC rough phase, this phase has a zig-zag pattern which now is however long ranged, as can be seen from Eq. (4.87). This phase is gapped. 5) For $3J_z - d > \pi t/2$, the present analysis cannot be applied because the diagonalization of the quartic a, b interactions through a Bogoliubov transformation breaks down, leading to an unphysical purely imaginary value of K_+. As argued by Schulz [134], this signals a transition to a ferromagnetic state, i.e. a diagonal stripe state.

Contrary to the the analysis by Schulz, which we have reviewed here, den Nijs [137] has identified not five but six different phases of the model (4.70). The additional phase found by den Nijs is a disordered flat phase (DOF), which is gapfull. This phase has, in contrast to the flat phase, a finite density of kinks and anti-kinks ($S_z = \pm 1$ states) but the G_u correlator does not show a logarithmic divergence, making this phase different from the rough phase. In the DOF phase the kinks are positionally disordered, but the kinks have an antiferromagnet order in the sense that a kink $S_z = 1$ is more likely to be followed by an anti-kink $S_z = -1$ rather than another kink, with any number of $S_z = 0$ states in between them. In spin language, the DOF phase is the valence bond phase which is responsible for the Haldane gap.

In fact, there are signs of this transition also in the abelian bosonization approach. At $d + J_z = 0$, μ_1 and μ_2 changes sign. This is unimportant for μ_2 as in this parameter regime the (−) sector is dominated by the μ_3 and not the μ_2 operator. However, if the μ_1 operator is relevant, than a sign change of μ_1 is of consequence. Typically, such a sign change is indicative of a competition between two fixed points. A similar situation occurs in a spin-1/2 chain with nearest and next-nearest interactions, where dimerized and antiferromagnetic ground states compete [138]. In the present situation, the competition is between on-site (d) and nearest neighbor interaction (J_z). A useful order parameter to distinguish between the flat and the disorder flat phases is the parity of the steps, $P = \langle \cos(\pi u_n) \rangle$, which in bosonized form becomes $P \sim \cos \sqrt{2}\,(\Psi_+(x) - \Psi_+(0))$, with $x = 0$ being the boundary of the string. If the μ_1 operator is relevant, the field Ψ_+ is pinned and a sign change in μ_1 leads to a π phase shift of $\sqrt{8}\Psi_+$. As a result, P shifts from zero to a finite value (if the boundary term is left unchanged). Therefore, while the abelian bosonization approach does not allow for a detailed study of the preroughening transition or the DOF phase, the existence of this transition can be readily inferred. The topology of the phase diagram is shown in Fig. 4.9

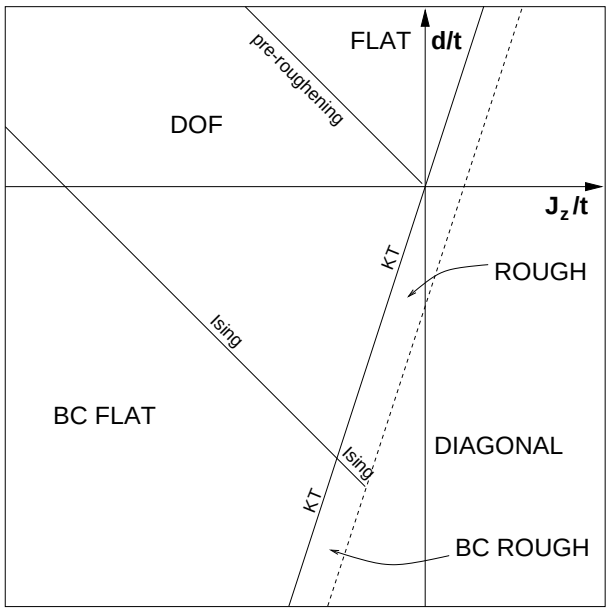

Figure 4.9: Phase diagram of spin 1 chain. It is almost identical to the phase diagram found in [134] with the exception that we distinguish between the DOF and FLAT phases.

and the nature of the different phases is depicted in Fig. 4.10.

4.4.2 Local coupling between longitudinal modes and stripe fluctuations

Having reviewed the physics of the transverse modes in detail, we now turn to the description of the complete model with both transverse and longitudinal modes. To describe the longitudinal modes along the stripe, we choose a bosonic model. Short ranged electron interactions can be described readily within such a scheme and, away from half filling, the relevant long wave length physics of the purely longitudinal model can be studied with the Hamiltonian

$$\begin{aligned} H_\rho &= \frac{u_\rho}{2\pi}\int dx\left[K_\rho\pi^2\Pi_\rho^2 + K_\rho^{-1}\left(\partial_x\Phi_\rho\right)^2\right]; \\ H_\sigma &= \frac{u_\sigma}{2\pi}\int dx\left[K_\sigma\pi^2\Pi_\sigma^2 + K_\sigma^{-1}\left(\partial_x\Phi_\sigma\right)^2\right] + \frac{g_1}{2\pi^2\alpha^2}\int dx\cos\left[\sqrt{8}\Phi_\sigma\right] \end{aligned} \tag{4.91}$$

where g_1 is the backward scattering strength. The fields $\Phi_{\rho/\sigma} = (\Phi_\uparrow \pm \Phi_\downarrow)/\sqrt{2}$, $\Pi_{\rho/\sigma} = (\Pi_\uparrow \pm \Pi_\downarrow)/\sqrt{2}$ are related to the Fermi fields of left- and right-moving particles through (see Eq. (4.82))

$$\psi_{\uparrow/\downarrow,R} = \frac{1}{\sqrt{2\pi\alpha}}e^{-i\Psi_{\uparrow/\downarrow}+i\Theta_{\uparrow/\downarrow}} \quad \text{and} \quad \psi_{\uparrow/\downarrow,L} = \frac{1}{\sqrt{2\pi\alpha}}e^{i\Psi_{\uparrow/\downarrow}+i\Theta_{\uparrow/\downarrow}} \tag{4.92}$$

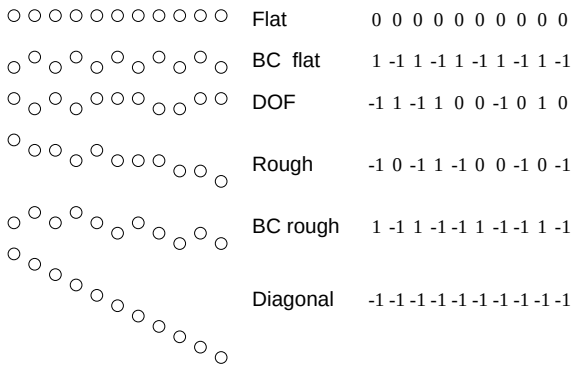

Figure 4.10: Representation of the string phases. Left shows real space picture and right shows the S^z_n values of the spin representation.

The parameters of the bosonic model dependent on the underlying lattice model. In the following, we shall assume that the underlying lattice model is the Hubbard model with repulsive on-site interactions. In that case, we have $K_\rho < 1$ and $K_\sigma > 1$. As the backward scattering term is relevant only for $K_\sigma < 1$, it is unimportant for the case studied here.

Physically, the coupling of the transverse and longitudinal modes arises from a scattering of the electrons which move along the stripe from transverse kinks. This interaction is local and we can express it in terms of the longitudinal electron density $\rho_{\uparrow/\downarrow}$ and the kink density S^2_z. We will consider only terms which couple the charge density to the kink density. Terms which couple the kinks and the spin density are irrelevant in presence of repulsive interactions and we thus omit them here. A local coupling of the electron density to the kink density can thus be written as

$$\begin{aligned} H_{c1} &= \gamma_1 \int dx \, (\rho_\uparrow + \rho_\downarrow) \, (S^z)^2 \\ H_{c2} &= \gamma_2 \int dx \rho_\uparrow \rho_\downarrow \, (S^z)^2 \end{aligned} \tag{4.93}$$

with coupling constants γ_1,γ_2. These terms can be readily bosonized. From H_{c1} one obtains the following terms,

$$\begin{aligned} H_{c1} &\sim \frac{2\gamma_1}{\pi^2} \int dx \; \partial_x \Psi_+ \; \partial_x \Phi_\rho + \lambda_1 \int dx \; \partial_x \Phi_\rho \; \cos\left(\sqrt{8}\Psi_-\right) \\ &+ \lambda_2 \int dx \; \partial_x \Phi_\rho \; \cos\left(\sqrt{8}\Psi_+\right) + \text{irrelevant terms}, \end{aligned} \tag{4.94}$$

with $\lambda_1 = \lambda_2 = \gamma_1 \left(\sqrt{2}\pi^3\alpha^2\right)^{-1}$. The first term represents scattering with $k \sim 0$ momentum transfer between the acoustic transverse and longitudinal charge modes. In general, these two modes have different velocities $u_+ \neq u_\rho$ and thus this interaction is retarded as can be seen by performing a gaussian average over one of the modes. This first term and the

gaussian parts of H_+ and H_ρ and can be jointly diagonalized, leading to a hybridization of the transverse and longitudinal modes. This leads to an instability of the system which is similar to the Wentzel-Bardeen instability in one dimensional metals coupled to phonons. However, this instability occurs only at a very large coupling $\gamma_1 \sim 4\sqrt{(\pi K_+ K_\rho)/(u_\rho u_+)}$ [139]. For small γ_1, the case considered here, the $k \sim 0$ interaction is not very efficient [140]. Also, as the hybridization is small for small γ_1, the scaling analysis below is only weakly affected by the hybridization and we thus ignore this correction here completely. The λ_1 and λ_2 terms are only important if the respective cosine terms have a finite expectation value. If they do, these terms act like a shift of the chemical potential of the electrons, as $\partial_x \Phi_\rho$ measures the deviation from the charge density of its equilibrium value. These terms compete however with terms generated by γ_2, as will be discussed below.

Bosonization of the γ_2 interaction gives the following terms,

$$\begin{aligned} H_{c2} \;\sim\; & \lambda_3 \int dx\; \partial_x \Psi_+ \cos\left(\sqrt{8}\Phi_\sigma\right) + \lambda_4 \int dx\; \cos\left(\sqrt{8}\Phi_\sigma\right) \cos\left(\sqrt{8}\Psi_+\right) \\ & + \lambda_5 \int dx\; \cos\left(\sqrt{8}\Phi_\rho - \sqrt{2}\Psi_+ + (4k_F - \pi)\, x\right) \cos\left(\sqrt{2}\Psi_-\right) + \text{irrelevant terms} \end{aligned} \tag{4.95}$$

The λ_3 and λ_4 terms result from scattering involving two a,b operators whereas λ_5 involves four a,b operators. While the first two terms describes processes with momentum transfer $k \sim 0$ between transverse and longitudinal modes, the λ_5 term results from processes with momentum transfer $4k_F$ from longitudinal to transverse modes. Only at $k_F = \pi/4$, i.e. at quarter filling of the stripe is this term important, as can be seen from the oscillatory x dependence of this term.

4.4.3 A quarter filled stripe: Possible phases

To examine the effect of the longitudinal-transversal coupling we need to examine the scaling dimensions of the λ_i operators. As mentioned above, we envision strongly repulsive interactions among the electrons on the stripe with $K_\rho < 1$ and $K_\sigma > 1$. The λ_4 operator is relevant only for $K_\sigma + K_+ < 1$ and thus unimportant. Similarly, λ_3 can be neglected as it relevant only for $K_\sigma < 1/2$. The λ_1 operator is relevant for $K_- < 1/2$, λ_2 is relevant for $K_+ < 1/2$ and the λ_5 operator is relevant for $2K_\rho + K_+ + K_- < 2$.

Let us assume, that initially $K_+ < 1$, i.e. the (+) sector is massive. In that case, the transverse modes behave at large wavelengths as if $K_+ = 0$. Then, if $2K_\rho + K_- < 2$, the λ_5 operator will become relevant at large scales. The λ_5 term pins the longitudinal charge modes to the transverse modes and induces a longitudinal charge density wave. This is most easily seen for the case that $K_- < 1/2$, i.e. in the BC flat phase, where both Ψ_+ and Ψ_- have long range order. The freezing of the transverse modes in a zig-zag pattern leads to a π periodic potential for the transverse modes and allows for Umklapp scattering of the quarter filled stripe which causes a longitudinal $4k_F$ charge density state. Thus, a relevant λ_5 term will make the Φ_ρ field massive and pin in to the frozen kink-antiking pattern of the

transverse fluctuations. Such a stripe with a frozen kink pattern and a longitudinal CDW pinned to it is depicted in Fig. 4.11a. It is interesting, that even if $K_- > 1/2$, i.e. in the DOF phase, the λ_5 term can be relevant for sufficiently strong repulsion (small K_ρ). However, if one assumes a Hubbard model for the longitudinal modes, the lower limit for K_ρ is $1/2$ so that in the flat phase, with $K_- > 1$, the λ_5 operator is always irrelevant.

If the λ_5 term is relevant, it is in direct competition with the λ_1 and λ_2 terms which favor a non-zero $\partial_x \Phi_\rho$. While an exact treatment of this competition is not possible, we can gain some insights if we assume mean field values for the transverse fields. Deep into the BC flat phase we may replace $\cos\left(\sqrt{8}\Psi_\pm\right)$ in the $\lambda_{1,2}$ terms by their finite expectation values $\left\langle \cos\left(\sqrt{8}\Psi_\pm\right)\right\rangle$ and similarly the λ_5 term may be written (after a possibly required phase shift of Φ_ρ) in the mean field approximation as

$$\lambda_5 \int dx \;\; \cos\left(\sqrt{8}\Phi_\rho\right) \left\langle \cos\left(\sqrt{2}\Psi_+\right)\right\rangle \left\langle \cos\left(\sqrt{2}\Psi_-\right)\right\rangle \tag{4.96}$$

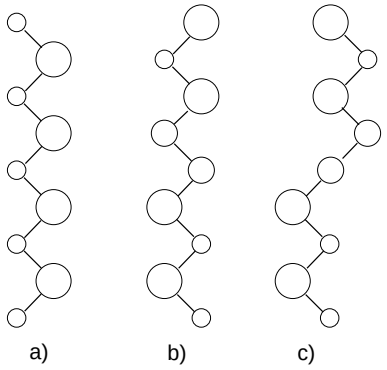

Figure 4.11: A 4 k_F CDW state in the BC flat phase. The size of the circle represents the local density of holes. a) commensurate ground state. b) CDW domain wall soliton. c) soliton state of both the transverse and longitudinal order.

In this approximation the longitudinal charge sector has a Hamiltonian which is well known from studies of commensurate-incommensurate transitions [141, 142]. Such a model can be studied within a fermion description of the model in terms of spinless holons [141, 142], in which the λ_5 Umklapp term becomes quadratic rather than quartic as in the original Fermi operators. In these models, a gapped commensurate state, which exists for small $\lambda_{1,2}$ (i.e. a small prefactor of the $\partial_x \Psi_\rho$ term) is followed by an incommensurate state at large values of $\lambda_{1,2}$ where the gap is destroyed and a small number of holons move as weakly interacting particles through the system. These holons are solitonic in character and can be interpreted within the present framework as point like domain "walls" of the π periodic charge density

wave state. Such a CDW soliton state, which involves only the transverse sector, is depicted in Fig. 4.11b. The combined nature of both transverse and longitudinal degrees of freedom allows also for another solitonic state, which represents a domain "wall" not only for the longitudinal degrees of freedom but also for the transverse ones (Fig. 4.11c).

Thus, the coupling of the transverse and longitudinal degrees of freedom does not lead to strong superconductivity or strong singlet correlations. Rather it can lead at 1/4 filling to the appearance of a charge density wave. The presence of only weakly interacting solitonic excitations in the stripe with an electron filling close to but a finite distance away from 1/4 filling would however allow for dominant pairing correlations if other type of modes of the environment are included in the analysis. An exchange of spin waves of the AF environment between such solitonic excitations would for example lead to an attractive interaction which may trigger the pairing. To summarize, the only strong divergence we found is associated with a $4k_F$ CDW formation at quarter filling. This may explain why T_c is suppressed at $x = 1/8$ in LSCO. We do not find a strong signature of pairing from a coupling between tranverse and longitudinal fluctuations. It appears that a coupling to the AF environment of the stripes is essential to obtain a pairing mechanism.

Chapter 5

Summary and outlook

In this thesis we addressed two different theoretical models of incommensurate spin states of the cuprates, with special emphasis on the influence of disorder on these phases. We first review our results on the spin glass phase, which we described as a strongly disordered spiral state, in which topological defects proliferate and render both the chirality of the spiral and the spin correlation length short ranged.

Disorder in non-collinear spin systems

In the first part of the thesis, we developed a theory for the spin glass phase of the cuprate material $La_{2-x}Sr_xCuO_4$, with $0.02 < x < 0.05$. This study was motivated by the recent observation of incommensurate spin correlations in the spin glass regime. Our theory is based on a phenomenological model in which doped holes, which are localized near the randomly distributed Sr donors, are assumed to produce a dipolar frustration of the AF texture. This model has previously been successfully applied to the AF regime $x < 0.02$ with the implicit assumption that the dipole orientation is completely random. Our model is a natural extension of these earlier theories, in which we allow for dipole orientational order. In absence of 3D AF ordering, the dipoles prefer to align which gives rise to an average spiral twist of the spin alignment. This mechanism provides a simple explanation for the observed incommensurability. An important characteristic of the spiral order is that it represents a non-collinear spin state in which the $O(3)$ spin symmetry is broken completely and the resulting symmetry group for the spiral order parameter is $O(3) \times O(2)/O(2)$. This leads to the appearance of a third Goldstone mode, in addition to the two transverse ones which also exist in collinear magnets. While the incommensurability is a measure of the average orientation of the dipoles, the short correlation length of the spin texture is caused by the fluctuation of the disorder distribution around the mean. Because of the quenched spatial distribution of dipoles, these fluctuations are inherent in the model.

1. **RG analysis of disordered non-collinear models:** To investigate the dipole model, we use a description based on an extension of the continuum NLσM. This approach is inspired both by the success of the NLσM in describing the magnetism of the undoped compound ($x = 0$) and by the long range character of the dipolar distortion which makes a continuum theory a natural choice. In our model, the order parameter of the spiral is represented by three orthonormal unit vectors $\mathbf{n}_k$, as opposed to the order parameter of a collinear theory which can be represented by just one unit vector. The dipoles couple to the order parameter via a minimal coupling scheme familiar from gauge theories, and the fluctuations of the dipole distribution are assumed to be short ranged.

   Using a renormalization group approach which accounts for spin wave like excitations we find that at high temperatures, the disorder has no strong effect apart from a renormalization of the spin stiffness. Two symmetry points remain fixed under the high temperature RG flow. The collinear $O(3)/O(2)$ symmetry is unstable and the presence of any non-collinear correlations will drive the system towards a $O(4)/O(3)$ symmetric point which is stable. This behavior of the RG is qualitatively the same as that of a clean spiral state. At low temperatures, however, the RG of the disorder must be taken into account. We find that, in general, under the RG disorder coupling terms are generated which cannot be expressed within a minimal coupling scheme and that these terms lead to a destruction of the collinear symmetry. At the fixed point with $O(4)/O(3)$ symmetry, the minimal coupling is however preserved under the RG and we find that disorder leads to a simple additive renormalization of the spin stiffness. Thus, at low temperatures, our analysis finds only one stable symmetry in presence of disorder.

2. **Importance of topological defects:** The NLσM results implicitly assume the absence of topological defects in the spin texture and thus the influence of these must be addressed within a separate framework. We investigated the stability of the spiral against the formation of topological defects which change the spiral's chirality using arguments based on the evaluation of the free energy of an isolated defect configuration. Similar arguments have been highly successfull in determining the phase boundaries of disordered XY models. The free energy was evaluated within a saddle point approximation and with the help of the replica trick. We found that isolated defects can be generated both thermally and through the coupling to disorder and computed the respective thresholds. The appearance of isolated defects leads to a breakdown of the NLσM RG equations and a further reduction of the spin correlation length, beyond that which occurs already through the renormalization of spin wave modes. Because of the non-abelian nature of the spiral symmetry group an extension of the free energy argument beyond the saddle point level is difficult to perform and it is uncertain how

higher order corrections would modify the result. As presently no theoretical frame work exists which is capable of treating defects and spin waves on an equal footing, the precise nature of the transition, which might conceivably also be a crossover, remains open. Numerical results on related models indicate however that the disordered spiral phase behaves similar to the disordered phase of XY models, and we therefore expect an XY dependence of the correlation length as a function of either disorder strength or temperature once topological defects proliferate.

We applied our results to the spin glass phase of $La_{2-x}Sr_xCuO_4$. Both the linear scaling of the incommensurability with doping and the breaking of the square lattice symmetry observed in this regime are in accordance with the presence of spiral correlations, caused by a doping independent fraction of ordered dipoles. Using previous estimates for the strength of disorder in the weak doping regime, we compute the critical doping concentration beyond which isolated defects will appear. We find $x_c \sim 0.02$, which is very close to the spin glass-AF phase boundary. As $x_c \sim 0.02$ represents a lower estimate for the critical doping concentration, we conclude that in the entire spin glass phase, such defects are present already at $T = 0$.

Phenomenological analysis of the striped phase

In the second part of the thesis, we employed a phenomenological description of the striped phase, which has been suggested to be present in the underdoped cuprate materials and has been detected in co-doped lanthanum based cuprates and also in the chemically closely related nickelates.

The aim of our analysis was foremost to understand the properties of a striped phase which is subject to both lattice and disorder potentials. Both types of distortions have experimentally been found to be relevant and both lattice and disorder pinned stripes were detected in scattering experiments. We introduced a simple model of a chain of holes, representing the anti-phase domain wall, in which the holes are allowed discrete steps in the transversal direction. Kinks in the chain are penalized by a potential which is harmonic in the relative transverse displacements of neighboring holes.

1. **RG analysis of disorder and lattice potentials:** Using the replica trick for the disorder average and subsequently performing the continuum limit, the model of a discrete stripe in a disorder potential, confined by its neighboring stripes, was mapped onto a bosonic string model with an action similar to those encountered in 1D theories of interacting particles in a random potential. This model was then investigated within a perturbative RG analysis in order to study the scaling of the lattice and disorder potential strengths. Three different regimes were identified, a freely fluctuating gaussian stripe, with gapless excitations, which is dominant at large transverse hopping

strengths and at small inter-stripe distances; a lattice pinned stripe which exists for small transverse hopping strengths; and a disorder pinned stripe which arises at large inter-stripe distances and/or weak quantum fluctuations. The lattice pinned stripe is characterized by the absence of transverse wandering and gapped excitations whereas the disorder pinned stripe has strong transversal wandering, induced by disorder, and a finite density of states at zero energy. We find the asymptotic dependence of the pinning length for both disorder and lattice pinning. Comparing our results with neutron scattering data on nickelates and cuprates, we find that quantum fluctuations are weaker in the nickelates and that this is the reason for the stronger effect of disorder pinning in nickelates. Although disorder was found to be irrelevant at higher doping concentrations, we predict the appearance of a disorder pinned phase at small doping concentrations for cuprates and argue that the broadening and subsequent destruction of the dynamic IC fluctuations on approaching $x \sim 0.05$ is a manifestation thereof.

2. **Influence of stripe fluctuations on spin dynamics:** To understand the influence of dynamical fluctuating stripes on the spin fluctuations, we introduced a simple model in which the spin fluctuations in the AF ordered domains between the charged stripes were assumed to be independent of the fluctuations of the stripes or domain walls. For the case of irrelevant disorder and lattice potentials, the propagator of a membrane of harmonically interacting stripes was used to qualitatively discuss the resulting dispersion of the incommensurate spin excitations. We found that incommensurate gapless excitations are continously linked to gapped excitations centered at the commensurate AF wave vector, as a result of the combined effect of broken spin symmetry and broken translational symmetry of the striped phase. The qualitative form of the IC dispersion agrees with the experimentally observed dispersion.

3. **Depinning of disordered stripes:** In the disordered pinned regime, a stripe depinning by externally applied fields would allow for a detection of stripes even if the stripe correlations are so short that they would be difficult to observe in scatttering experiments. We have therefore used a collective pinning scaling analysis to estimate the average pinning energy of a stripe pinned by Coulomb forces of randomly placed donors like Sr. The critical depinning field was estimated and we calculated the scaling of the average depinning barrier as a function of the applied field. The pinning energy turned out to be of the order of the AF exchange J, and the associated depinning fields are very large. We subsequently discussed the thermal stripe creep for subcritical fields. Our results were compared with transport data from the spin glass phase of cuprates and it was found that the data does not support the presence of stripes in the spin glass regime.

4. **Coupling of transverse and longitudinal stripe fluctuations:** Fluctuating stripes

have repeatedly been connected with the appearance of superconductivity in cuprates. As stripes in cuprates have a finite electron density, there is the possibility of transport of charge and spin along the stripe and these longitudinal charge and spin density fluctuations are expected to be coupled to the transverse excitations of the stripe. We investigated the coupled problem to find whether or not transverse excitations, associated with fluctuating stripes, lead to a pairing mechanism even in presence of predominantly repulsive interactions among the electrons. We therefore rewrote the Hamiltonian for the transverse modes as a spin-1 chain. To study the transverse modes, we reviewed and employed a well known approximation in which one replaces the spin-1 operators by a sum of two spin-$\frac{1}{2}$ operators which can then be treated with a Jordan-Wigner transformation and bosonization techniques. The longitudinal modes were similarly described within a bosonized form.

The interaction between the longitudinal and the transverse modes was assumed to be dominated by scattering of the longitudinal charge modes at the transverse kinks. This interaction, once translated into bosonic form, generates several different operators. The scaling of these operators was investigated and the possible phases of the combined system analyzed. At the stripe filling fraction $\frac{1}{4}$, a value believed to be relevant for cuprate materials, the most dominant instability found was towards the formation of a phase with a frozen zig-zag pattern of the transverse displacements combined with a 4 k_F charge density wave along the stripe. However, we did not find a strong instability towards a superconducting phase at 1/4 filling. For fillings close to 1/4 the charge carriers have a solitonic character and are only weakly interacting, so any kind of further attractive interactions not included in our analysis, e. g. spin wave mediated attraction, might conceivably lead to superconductivity.

Outlook

An interesting problem, which is related to but was not directly addressed in this thesis, is to understand the presence of glassy behavior in the magnetism of the $x = 1/8$ compounds [103]. There are intriguing similarities between these higher doped materials and the very weakly doped spin glass regime. Both are characterized by a broad distribution of extremely slow relaxation times and at both compositions, the correlation length saturates at finite temperature (the correlation length of the $x = 1/8$ compound is however much larger). These similarities point to the presence of random frustration also in the stripe material and a possible cause of frustration is the presence of defects in the stripe array. It is easy to see, that besides pinning of stripes, disorder can and should also lead to the creation of defects. Via the creation of defects, the stripe array can locally vary the stripe density and thus accommodate to variations in the disorder potential, see also Fig. 5.1. However, while

the creation of defects is easy to understand their density is hard to quantify.

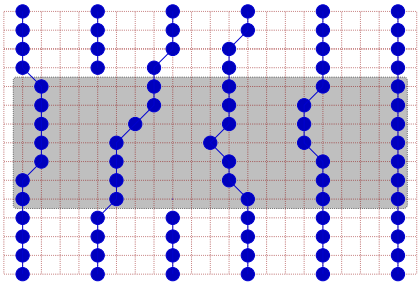

Figure 5.1: The stripe array configuration with a defect pair. The stripe density is reduced within the shaded area.

The presence of defects, i. e. forks or finite stripe segments, affects not only the charge sector but also strongly the spin sector. As an illustration, we calculate the saddle point configuration of the spin configuration of a rather simple defect structure which couples only to the spins. We consider an imperfect stripe, in which a part of the stripe is missing, i. e. rather than one infinite domain wall we have two semi-finite ones. Employing again the NLσM formalism, we have to find solutions for the non-linear saddle point equations of the local staggered magnetization $\mathbf{n}$. As shown by Polyakov [143], the $\mathbf{n}$ fields minimize the action if

$$\partial_\mu \mathbf{n} = \epsilon_{\mu\nu} \mathbf{n} \times \partial_\nu \mathbf{n}, \qquad \mathbf{n}^2 = 1, \tag{5.1}$$

where $\mu = x_1, x_2$. These equations can be transformed into a simpler form via a stereographical projection [143],

$$n^x + i n^y = \frac{2w}{1+|w|^2}, \qquad n^z = \frac{1-|w|^2}{1+|w|^2} \tag{5.2}$$

where w is a complex field. Solutions of Eq. (5.1) must then simply satisfy $\partial_z w = (\partial_1 + i\partial_2) w = 0$, i.e. must be harmonic in the appropriate domain. To find the solution to our problem we must hence simply find harmonic solutions with the appropriate boundary conditions. We imagine a domain wall extending along the x_2 axis from $-\infty$ to -1 and from 1 to ∞. The orientation of $\mathbf{n}$ at infinity is given by $\lim_{|\mathbf{x}|\to\infty} n^x(x_1, x_2) = \mathrm{sign}(x_2)$, $\lim_{|\mathbf{x}|\to\infty} n^{y,z}(x_1, x_2) = 0$ and we require that n^x changes sign at the domain wall. A solution analytic everywhere but at the domain wall which solves these boundary conditions is $w(z) = \frac{2}{\pi} \arctan(z)$ and in Fig. 5.2 the resulting spin distribution is sketched. It is evident, that the spins distribution is strongly affected.

Besides the similarity of the experimental data, a striped phase and a disordered spiral share also some common features at the theoretical level. This is perhaps most apparent when

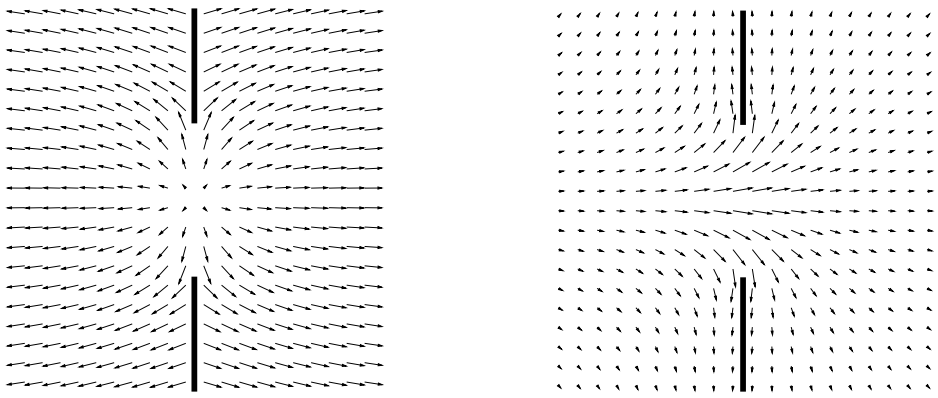

Figure 5.2: Distribution of the staggered magnetization around a domain wall defect pair. On the left, the n^x and n^y components are shown, the right picture shows the n^y and n^z components.

looking at the topological defects which in both states have a Z_2 character. Similarly, both states involve a symmetry breaking not only of the spin but also of the translational lattice symmetry. The main difference is the collinearity of the spin ordering in a striped phase. While this would suggest that the spin dynamics of a striped phase can be described within a conventional collinear $O(3)/O(2)$ model, such a model lacks Z_2 defects and also cannot describe the modes associated with stripe fluctuations. One therefore needs to construct an order parameter description of the striped phase which can overcome these deficiencies.

The description of spirals might in fact be closely related to stripes, however it is not evident that the coupling of the lattice modes and spin modes is as strong in the striped phase as it is in a spiral. With an order parameter description of the stripes at hand, an analysis of the spin wave renormalization by disorder as well as the generation and influence of topological defects could be carried out in a way similar as presented in the first part of this thesis for the spin glass phase. In view of the extremely large correlation lengths found in some stripe materials, many times larger than both the inter-stripe spacing and the spin correlation length of the spin glass phase, the results of such an analysis could be directly compared with already available experimental data.

Appendix A

RG calculation for non-collinear models

A.1 SU(2) representation

The orthonormal basis $\mathbf{n}_k$ can be related to an element g of $SU(2)$ through $g\sigma^k g^{-1} = \mathbf{n}_k \cdot \boldsymbol{\sigma}$, or

$$n_k^a = \frac{1}{2}\mathrm{tr}\left\{\sigma^a g \sigma^k g^{-1}\right\} \tag{A.1}$$

For the derivative one finds, using $\partial_\mu (g g^{-1}) = 0$,

$$\partial_\mu n_k^a = \frac{1}{2}\mathrm{tr}\left\{\sigma^a \partial_\mu g \sigma^k g^{-1} + \sigma^a g \sigma^k \partial_\mu g^{-1}\right\} = \frac{1}{2}\mathrm{tr}\left\{\sigma^k \left[g^{-1}\sigma^a g,\ g^{-1}\partial_\mu g\right]\right\}. \tag{A.2}$$

Introducing $g^{-1}\partial_\mu g = i\mathbf{A}_\mu \cdot \boldsymbol{\sigma}$ and with $[\sigma^i,\ \sigma^j] = 2i\epsilon_{ijk}\sigma^k$ one finds

$$\partial_\mu n_k^a = 2\epsilon_{ijk} A_\mu^i n_j^a. \tag{A.3}$$

Therefore, we have (with $p_{1\mu} = p_{2\mu}$)

$$\begin{aligned} p_{k\mu}\left(\partial_\mu \mathbf{n}_k\right)^2 &= 4p_{k\mu}\left(\epsilon_{ijk}A_\mu^i n_j^a\right)^2 = 4p_{k\mu}\left(\epsilon_{ijk}\right)^2\left(A_\mu^k\right)^2 \\ &= 4(p_{1\mu}+p_{3\mu})\mathbf{A}_\mu^2 + 4(p_{1\mu}-p_{3\mu})\left(A_\mu^z\right)^2 = \frac{2}{t_\mu}\left[\mathbf{A}_\mu^2 + b\left(A_\mu^z\right)^2\right], \end{aligned} \tag{A.4}$$

with $t_\mu^{-1} = 2(p_{1\mu}+p_{3\mu})$ and $bt_\mu^{-1} = 2(p_{1\mu}-p_{3\mu})$.

A.2 Expanding the energy functional in φ^i

To do the RG, we introduce $g = \tilde{g}\exp(i\boldsymbol{\varphi}\cdot\boldsymbol{\sigma})$, where φ^a are fast fields fluctuating with wavelengths $[\Lambda^{-1}, 1]$ and $\tilde{g}$ has only slow fluctuations in the range $[0, \Lambda^{-1}]$. For the 1-loop

calculation, we need to expand $\mathbf{n}_k$ and A^k_μ up to second order in φ^a. We then find

$$\begin{aligned} n^a_i &= \frac{1}{2}\mathrm{tr}\left\{\sigma^a\tilde{g}\exp\left(i\boldsymbol{\varphi}\cdot\boldsymbol{\sigma}\right)\sigma^i\exp\left(-i\boldsymbol{\varphi}\cdot\boldsymbol{\sigma}\right)\tilde{g}^{-1}\right\} \\ &= \tilde{n}^a_i + \frac{i}{2}\mathrm{tr}\left\{\sigma^a\tilde{g}\left[\boldsymbol{\varphi}\cdot\boldsymbol{\sigma},\sigma^i\right]\tilde{g}^{-1}\right\} \\ &\quad + \frac{1}{2}\mathrm{tr}\left\{\sigma^a\tilde{g}\left(\boldsymbol{\varphi}\cdot\boldsymbol{\sigma}\;\sigma^i\boldsymbol{\varphi}\cdot\boldsymbol{\sigma} - \frac{1}{2}\left(\boldsymbol{\varphi}\cdot\boldsymbol{\sigma}\right)^2\sigma^i - \frac{1}{2}\sigma^i\left(\boldsymbol{\varphi}\cdot\boldsymbol{\sigma}\right)^2\right)\tilde{g}^{-1}\right\} + \mathcal{O}(\varphi^3) \\ &= \tilde{n}^a_i + 2\epsilon_{ijk}\varphi^j\tilde{n}^a_k + \varphi^j\varphi^k R^{ai}_{jk} + \mathcal{O}(\varphi^3), \end{aligned} \tag{A.5}$$

where

$$R^{ai}_{jk} = \frac{1}{2}\,\mathrm{tr}\left\{\sigma^a\tilde{g}\left(\sigma^j\sigma^i\sigma^k - \frac{1}{2}\sigma^j\sigma^k\sigma^i - \frac{1}{2}\sigma^i\sigma^j\sigma^k\right)\tilde{g}^{-1}\right\}. \tag{A.6}$$

It turns out, that in the RG we will only need the diagonal components of R^{ai}_{jk} with $j=k$ which have the much simpler form $R^{ai}_{zz} = -2\left(\epsilon_{zqi}\right)^2\tilde{n}^a_i$ (we put here $j=k=z$ to make clear that z is not a silent index, the equation also holds for $j=x,y$). Similarly, we find

$$\begin{aligned} A^i_\mu &= \frac{1}{2i}\,\mathrm{tr}\left\{\sigma^i\exp\left(-i\boldsymbol{\varphi}\cdot\boldsymbol{\sigma}\right)\left[\partial_\mu + \tilde{g}^{-1}\partial_\mu\tilde{g}\right]\exp\left(i\boldsymbol{\varphi}\cdot\boldsymbol{\sigma}\right)\right\} \\ &= \tilde{A}^i_\mu + \frac{1}{2}\mathrm{tr}\left\{\sigma^i\left(\partial_\mu\boldsymbol{\varphi}\cdot\boldsymbol{\sigma} + \frac{1}{2i}\left[\boldsymbol{\varphi}\cdot\boldsymbol{\sigma},\partial_\mu\boldsymbol{\varphi}\cdot\boldsymbol{\sigma}\right] + i\left[\tilde{\mathbf{A}}_\mu\cdot\boldsymbol{\sigma},\boldsymbol{\varphi}\cdot\boldsymbol{\sigma}\right]\right.\right. \\ &\quad \left.\left. + \boldsymbol{\varphi}\cdot\boldsymbol{\sigma}\;\tilde{\mathbf{A}}_\mu\cdot\boldsymbol{\sigma}\;\boldsymbol{\varphi}\cdot\boldsymbol{\sigma} - \frac{1}{2}\left(\boldsymbol{\varphi}\cdot\boldsymbol{\sigma}\right)^2\tilde{\mathbf{A}}_\mu\cdot\boldsymbol{\sigma} - \frac{1}{2}\tilde{\mathbf{A}}_\mu\cdot\boldsymbol{\sigma}\left(\boldsymbol{\varphi}\cdot\boldsymbol{\sigma}\right)^2\right)\right\} + \mathcal{O}(\varphi^3) \\ &= \tilde{A}^i_\mu + \partial_\mu\varphi^i + \epsilon_{ijk}\varphi^j\partial_\mu\varphi^k + 2\epsilon_{ijk}\varphi^j\tilde{A}^k_\mu - 2\tilde{A}^i_\mu\;\boldsymbol{\varphi}^2 + 2\tilde{\mathbf{A}}_\mu\cdot\boldsymbol{\varphi}\;\varphi^i + \mathcal{O}(\varphi^3). \end{aligned} \tag{A.7}$$

A.3 Propagator of the φ^i fields

As already mentioned, there is a small spatial anisotropy in the stiffnesses $p_{k\mu}$, i.e. $p_{k1} \neq p_{k2}$. We shall keep here the spatial dependence of the stiffnesses $p_{k\mu}$ up to first order in the anisotropy, assuming that the anisotropy κ, which we define through $p_{k1}/p_{k2} = 1+\kappa$, is independent of the k index. Thus we can absorb the anisotropy into the t_μ parameter while b remains isotropic. We then define $t_s = \sqrt{t_1 t_2}$ and $t_{1,2} \simeq (1 \pm \kappa/2)t_s$. For future use, we also define the isotropic stiffnesses $p_k = \sqrt{p_{k1}p_{k2}}$. It is not clear whether the isotropy of b is preserved under the RG and we have made no attempt to write down the RG equations in presence of anisotropy. In principle, if b remains isotropic, the results obtained below allow to determine the flow of the anisotropy parameter κ under the RG. For possible future use, we will therefore keep the perturbative expansion with the anisotropy. The results used in the body of this work have however been obtained for an isotropic t_μ=t_s, i.e. $\kappa = 0$.

We need to expand the exponential $\exp(-H_P)$ and integrate out the φ^i fields. Taking the average over the φ^i fields is done with the Gaussian term H_φ, Eq. (3.23). The propagator

for the φ^i is thus quite simple and becomes, to lowest order in the anisotropy κ

$$C^i(\mathbf{x}) := \left\langle \varphi^i(\mathbf{x})\varphi^i(\mathbf{0}) \right\rangle_\varphi = \frac{t_s}{2(1+b\delta_{iz})} \int \frac{d^2\mathbf{k}}{(2\pi)^2} \quad \frac{e^{i\mathbf{k}\cdot\mathbf{x}}}{k^2}\left(1+\kappa\frac{k_1^2-k_2^2}{2k^2}\right) \times \quad (\Upsilon(k,\Lambda)-\Upsilon(k,1)). \tag{A.8}$$

The IR cutoff is provided by the function $\Upsilon(k,\Lambda)$. A sharp cutoff, $\Upsilon(k,\Lambda)=\Theta(k-\Lambda^{-1})$ has the disadvantage of producing a long ranged C^i and we therefore adopt instead $\Upsilon(k,\Lambda) = [1+(k\Lambda)^{-2}]^{-1}$, which renders C^i short ranged. In our RG calculation we will mainly need $C^i(\mathbf{0})$ which has the form

$$C^x(\mathbf{0}) = C^y(\mathbf{0}) = \frac{t_s}{4\pi}\ln\Lambda + \mathcal{O}(\kappa^2), \qquad C^z(\mathbf{0}) = \frac{1}{1+b}C^x(\mathbf{0}). \tag{A.9}$$

Another useful formula is

$$t_\mu^{-1}\int d^2\mathbf{x}\ (\partial_\mu C^x)^2 = \frac{1}{2}C^x(\mathbf{0}) + \mathcal{O}(\kappa^2). \tag{A.10}$$

A.4 Renormalization

We can immediately discard all terms of third or higher power in $\tilde{\mathbf{A}}_\mu$ as these terms are irrelevant in a RG sense. Terms second order in $\tilde{\mathbf{A}}_\mu$ renormalize t_μ and b, whereas terms linear in $\tilde{\mathbf{A}}_\mu$ are responsible for the renormalization of the disorder variance λ.

First, we note that the terms H_2, H_3 do not contribute to the renormalization, as was pointed out for the calculation of the RG for the disorder free system in [44]. This is because these terms are linear in φ while they do not involve a disorder field $\mathbf{Q}_\mu$. For an abelian theory, such terms cannot contribute because the fast φ^i fields and the slow $\tilde{\mathbf{A}}_\mu$ fields have their support in orthogonal parts of the wave vector space. Here, for the non-abelian case, this argument is not sufficient because the $\tilde{\mathbf{A}}_\mu$ fields are not linearly related to the fields g. For the present non-abelian theory this is nonetheless true, although an explicit calculation is required to see this. For example, H_2^2 does not contribute, because its contribution is built from terms of the form (we omit the upper i indices of C^i and A_μ^i here for simplicity)

$$\int d^2\mathbf{x}\int d^2\mathbf{x}'\ \tilde{A}_\mu(\mathbf{x})\tilde{A}_{\mu'}(\mathbf{x}')\partial_\mu\partial_{\mu'}C(\mathbf{x}-\mathbf{x}') \tag{A.11}$$

To evaluate this term, we change to center of mass ($\mathbf{y}$) and relative ($\mathbf{y}'$) coordinates and then perform a gradient expansion in the relative coordinate. Only the lowest order contribution is of interest, as higher order terms involve a local coupling of the type $A_\mu\,(\partial_\nu)^n\,A_{\mu'}$ with $n>0$ which are irrelevant from a scaling point of view. The lowest order term is then

$$-\int d^2\mathbf{y}\ \tilde{A}_\mu(\mathbf{y})\tilde{A}_{\mu'}(\mathbf{y})\int d^2\mathbf{y}'\partial_\mu\partial_{\mu'}C(\mathbf{y}') \tag{A.12}$$

which vanishes because the last integral is zero. In the following we will omit H_2 and H_3 from the analysis, because terms involving them do not contribute. This can be shown for each term in a way similar to the one just shown.

We want to find the RG equations up to second order in t_μ and λ. In the nth order of the cumulant expansion of $\mathcal{F}$, Eq. (3.33), we only need to consider terms which have a total number of $\boldsymbol{\varphi}$ and $\mathbf{Q}_\mu$ fields less than $2n+2$. This is because each term of order n carries a factors t_s^{-n} from the prefactors of the terms in H_p and each pair of $\boldsymbol{\varphi}$ ($\mathbf{Q}_\mu$) produces a factor t_s (λ).

We begin first with the terms renormalizing t_μ and b, where we give a detailed calculation only for the terms up to second order in H_p. The calculation of higher order terms is quite lengthy although conceptually easy and we therefore just present the results of the calculation.

A.4.1 Terms which renormalize t_μ and b

First order in H_p

There is only one term quadratic in $\tilde{\mathbf{A}}_\mu$ which contributes, H_4 (the φ^i average over H_3 is zero).

$$\begin{aligned}
-\left\langle H_4\right\rangle_{\varphi c} &= -4\frac{b}{t_\mu}\int d^2\mathbf{x}\left[\epsilon_{zjk}\epsilon_{zj'k'}\tilde{A}_\mu^k\tilde{A}_\mu^{k'}\left\langle\varphi^j\varphi^{j'}\right\rangle_\varphi - \left(\tilde{A}_\mu^z\right)^2\left\langle\varphi^l\varphi^l\right\rangle_\varphi + \tilde{A}_\mu^z\tilde{A}_\mu^l\left\langle\varphi^z\varphi^l\right\rangle_\varphi\right] \\
&= -4\frac{b}{t_\mu}\int d^2\mathbf{x}\left[(\epsilon_{zjk})^2\left(\tilde{A}_\mu^k\right)^2 C^j(\mathbf{0}) - \left(\tilde{A}_\mu^z\right)^2\sum_l C^l(\mathbf{0}) + \left(\tilde{A}_\mu^z\right)^2 C^z(\mathbf{0})\right] \\
&= -4b\ t_\mu^{-1}\int d^2\mathbf{x}\left[\tilde{\mathbf{A}}_\mu^2 - 3\left(\tilde{A}_\mu^z\right)^2\right]C^x(\mathbf{0}). \qquad \text{(A.13)}
\end{aligned}$$

Second order in H_p

Terms with odd numbers of φ^i or $\mathbf{Q}_\mu$ are zero after performing the φ^i and disorder average. There are then only two terms we need to consider, H_1^2 and H_{c1}^2 (H_{c3}^2 has a total of six φ^i and Q_μ^i fields and does not contribute and H_2 terms do not contribute as mentioned above). For H_1^2 we have

$$\begin{aligned}
\frac{1}{2}\left[\left\langle H_1^2\right\rangle_{\varphi c}\right]_D &= \frac{1}{2}\left\langle H_1^2\right\rangle_{\varphi c} \qquad \text{(A.14)} \\
&= 2t_\mu^{-1}t_{\mu'}^{-1}\int d^2\mathbf{x}\ d^2\mathbf{x}'\ \tilde{A}_\mu^i(\mathbf{x})\tilde{A}_{\mu'}^{i'}(\mathbf{x}')\epsilon_{ijk}\epsilon_{i'j'k'}\left(1-b\delta_{iz}+2b\delta_{jz}\right) \\
&\quad\times\left(1-b\delta_{i'z}+2b\delta_{j'z}\right)\left\langle\partial_\mu\varphi^j(\mathbf{x})\varphi^k(\mathbf{x})\partial_{\mu'}\varphi^{j'}(\mathbf{x}')\varphi^{k'}(\mathbf{x}')\right\rangle_\varphi
\end{aligned}$$

The four point average can be decomposed according to Wick's Theorem. Nonzero contributions arise from the contractions $\langle jk'\rangle\langle j'k\rangle$ and $\langle jj'\rangle\langle kk'\rangle$. We again employ an expansion

of H_1^2 in the relative coordinate and keep only the zeroth order term of the expansion. This yields

$$\begin{aligned}\frac{1}{2}\left\langle H_1^2\right\rangle_{\varphi c} &\simeq 2t_\mu^{-2}\int d^2\mathbf{x}\tilde{A}_\mu^i\tilde{A}_\mu^{i'}\epsilon_{ijk}\epsilon_{i'j'k'}\left(1-b\delta_{iz}+2b\delta_{jz}\right)\left(1-b\delta_{i'z}+2b\delta_{j'z}\right)\\ &\quad\times\left(\delta_{jj'}\delta_{kk'}-\delta_{kj'}\delta_{jk'}\right)\int d^2\mathbf{y}\ \partial_\mu C^j(\mathbf{y})\partial_\mu C^k(\mathbf{y})\\ &= 4t_\mu^{-2}\int d^2\mathbf{x}\left(\tilde{A}_\mu^i\right)^2\left(\epsilon_{ijk}\right)^2\left(1-b\delta_{iz}+2b\delta_{jz}\right)\left(1-b\delta_{iz}+b\delta_{jz}+b\delta_{kz}\right)\\ &\quad\times\int d^2\mathbf{y}\ \partial_\mu C^j(\mathbf{y})\partial_\mu C^k(\mathbf{y}).\end{aligned}\tag{A.15}$$

With use of Eq. (A.10), we finally find

$$\frac{1}{2}\left\langle H_1^2\right\rangle_{\varphi c}=2t_\mu^{-1}\int d^2\mathbf{x}\left[\tilde{\mathbf{A}}_\mu^2(1+b)+\left(\tilde{A}_\mu^z\right)^2 b(b-3)\right]C^x(\mathbf{0})\tag{A.16}$$

The other second order contribution is

$$\begin{aligned}\frac{1}{2}\left[\left\langle H_{c1}^2\right\rangle_{\varphi c}\right]_D &= 8\int d^2\mathbf{x}d^2\mathbf{x}' p_{k\mu}p_{k'\mu'}\epsilon_{ijk}\epsilon_{i'j'k'}\epsilon_{abc}\epsilon_{a'b'c'}\left\{\epsilon_{klm}\tilde{n}_j^a\tilde{n}_m^c\tilde{A}_\mu^i\right.\\ &\quad\left.+\epsilon_{jlm}\tilde{n}_k^c\tilde{n}_m^a\tilde{A}_\mu^i+\epsilon_{ilm}\tilde{n}_j^a\tilde{n}_k^c\tilde{A}_\mu^m\right\}\left\{\epsilon_{k'l'm'}\tilde{n}_{j'}^{a'}\tilde{n}_{m'}^{c'}\tilde{A}_{\mu'}^{i'}+\epsilon_{j'l'm'}\tilde{n}_{k'}^{c'}\tilde{n}_{m'}^{a'}\tilde{A}_{\mu'}^{i'}\right.\\ &\quad\left.+\epsilon_{i'l'm'}\tilde{n}_{j'}^{a'}\tilde{n}_{k'}^{c'}\tilde{A}_{\mu'}^{m'}\right\}\delta_{ll'}\ C^l(\mathbf{x}-\mathbf{x}')\left[Q_\mu^b(\mathbf{x})Q_{\mu'}^{b'}(\mathbf{x}')\right]_D.\end{aligned}\tag{A.17}$$

Using $\left[Q_\mu^b(\mathbf{x})Q_{\mu'}^{b'}(\mathbf{x}')\right]_D=\delta_{bb'}\ \delta_{\mu\mu'}\ \delta(\mathbf{x}-\mathbf{x}')\lambda$, $\epsilon_{abc}\epsilon_{a'bc'}=\delta_{aa'}\ \delta_{cc'}-\delta_{ac'}\delta_{ca'}$ and the orthonormality of the $\mathbf{n}_k$, we find after some algebra

$$\frac{1}{2}\left[\left\langle H_{c1}^2\right\rangle_{\varphi c}\right]_D = 2\lambda\ b^2\ t_\mu^{-2}\int d^2\mathbf{x}\left[\tilde{\mathbf{A}}_\mu^2+\left(\tilde{A}_\mu^z\right)^2\right]C^x(\mathbf{0}).\tag{A.18}$$

Higher order terms can be evaluated in much the same way as the first and second order terms, although the large number of indices makes their evaluation more tedious. We therefore refrain here from a detailed presentation of these terms and just state the results.

Third order in H_p

Terms of second order in $\tilde{\mathbf{A}}_\mu^2$ are produced by $\left(H_1+H_{c1}+H_{c3}\right)^2\left(H_{c2}+H_{c4}\right)$. However, only the terms $H_1(H_{c1}+H_{c3})(H_{c2}+H_{c4})$ have even powers of $\mathbf{Q}_\mu$. Terms with eight or more φ and $\mathbf{Q}_\mu$ fields again do not contribute to second order in λ, t_μ. Thus we are left with only $H_1H_{c1}H_{c2}$. We find

$$-\left[\langle H_1H_{c1}H_{c2}\rangle_{\varphi c}\right]_D = -2\lambda t_\mu^{-2}\ b\int d^2\mathbf{x}\left[\tilde{\mathbf{A}}_\mu^2(1+b)+\left(\tilde{A}_\mu^z\right)^2(b-3)\right]C^x(\mathbf{0}).\tag{A.19}$$

We further need to consider terms of the type $(H_{c2}+H_{c4})^2H_4$. Only $H_{c2}^2H_4$ has less than eight φ,$\mathbf{Q}_\mu$ fields and even powers of both fields. We find

$$-\frac{1}{2}\left[\left\langle H_{c2}^2H_4\right\rangle_{\varphi c}\right]_D = -2\lambda\ b\ t_s^{-1}\ t_\mu^{-1}\int d^2\mathbf{x}\left[\tilde{\mathbf{A}}_\mu^2-3\left(\tilde{A}_\mu^z\right)^2\right]C^x(\mathbf{0}).\tag{A.20}$$

Fourth order in H_p

Possible contributions arise from the terms $(H_1 + H_{c1} + H_{c3})^2(H_{c2} + H_{c4})^2$. Discarding terms with ten or more φ^i,$\mathbf{Q}_\mu$ fields, we are left with $H_{c2}^2 H_1^2$ and $H_{c2}^2 H_{c1}^2$. However, the connected part of the φ^i average of $H_{c2}^2 H_{c1}^2$ is zero (its finite disconnected parts enter the renormalization of the disorder, see below), and the only contribution is therefore

$$\frac{1}{4}\left[\left\langle H_{c2}^2 H_1^2\right\rangle_{\varphi c}\right]_D = \lambda t_s^{-1} t_\mu^{-1} \int d^2\mathbf{x}\left[\mathbf{A}_\mu^2(2+b)(1+b) + \left(\tilde{A}_\mu^z\right)^2 b\,(b-7)\right] C^x(\mathbf{0}). \quad \text{(A.21)}$$

Terms of the form $H_4(H_{c2} + H_{c4})^3$ do not contribute because their disorder average is zero.

Higher order terms in H_p do not contribute because they either involve more than four $\mathbf{Q}_\mu$ terms and are therefore of higher order than λ^2 or they do not contain finite connected parts. For example, the term $\langle H_4 H_{c2}^4\rangle_{\varphi c}$ decomposes into products of averages of $\langle H_4\rangle_{\varphi c}$ or $\langle H_4 H_{c2}^2\rangle_{\varphi c}$ and $\langle H_{c2}^2\rangle_{\varphi c}$.

A.4.2 Terms which renormalize λ

To find the renormalization of the variance of the disorder distribution, we first collect all connected terms linear in $\tilde{A}_\mu^i$. We list the contributions order by order below.

First order in H_p

Only three terms are linear in $\tilde{A}_\mu^i$, H_1, H_{c1} and H_{c3}. However, both H_1 and H_{c1} have a zero φ^i average and only $\langle H_{c3}\rangle_{\varphi c}$ contributes.

Second order in H_p

At second order there are contributions from $\langle H_{c1} H_{c2}\rangle_{\varphi c}$ and $\langle H_1 H_{c4}\rangle_{\varphi c}$. There is no contribution to second order in λ, t_μ of the disorder renormalization from $\langle H_{c3} H_{c4}\rangle_{\varphi c}$ because this term has six Q_μ^i, φ^i.

Third order in H_p

There are contributions from $\langle H_{c1} H_{c2} H_{c4}\rangle_{\varphi c}$, $\langle H_{c3} H_{c2}^2\rangle_{\varphi c}$ and $\langle H_1 H_{c2}^2\rangle_{\varphi c}$. The terms $\langle H_{c3} H_{c4}^2\rangle_{\varphi c}$ and $\langle H_1 H_{c4}^2\rangle_{\varphi c}$ do not contribute, as they contain eight or more Q_μ^i, φ^i fields.

Fourth order in H_p

Only one term contributes, $\langle H_1 H_{c2}^2 H_{c4}\rangle_{\varphi c}$. All other terms have ten or more Q_μ^i, φ^i fields or more than three $\mathbf{Q}_\mu$ fields and thus do not contribute. The same argument applies to all terms generated by higher order of H_p.

A.4.3 Calculating the renormalized disorder variance

We now must calculate the variance of all terms at the new length scale Λ^{-1} which are linear in $\tilde{A}^i_\mu$. These are the terms just found above plus H_{c0}. Thus, we need to calculate the variance of

$$-H_{c0} - \langle H_{c3}\rangle_{\varphi c} + \langle H_{c1}H_{c2}\rangle_{\varphi c} + \langle H_1 H_{c4}\rangle_{\varphi c} - \langle H_{c1}H_{c2}H_{c4}\rangle_{\varphi c} - \frac{1}{2}\left\langle H_{c2}^2 H_{c3}\right\rangle_{\varphi c}$$
$$-\frac{1}{2}\left\langle H_{c2}^2 H_1\right\rangle_{\varphi c} + \frac{1}{2}\left\langle H_1 H_{c2}^2 H_{c4}\right\rangle_{\varphi c} \tag{A.22}$$

To order λ^2, the following terms contribute to the variance.

$$\begin{aligned}
\left[H_{c0}^2\right]_D &= \lambda t_\mu^{-2}\int d^2\mathbf{x}\left\{\left[\left(\tilde{A}_\mu^x\right)^2+\left(\tilde{A}_\mu^y\right)^2\right]+\left(\tilde{A}_\mu^z\right)^2(1+b)^2\right\},\\
2\left[\langle H_{c3}\rangle_{\varphi c} H_{c0}\right]_D &= 8\lambda t_\mu^{-2}\int d^2\mathbf{x}\left\{\left[\left(\tilde{A}_\mu^x\right)^2+\left(\tilde{A}_\mu^y\right)^2\right]b\right.\\
&\qquad\left.-\left(\tilde{A}_\mu^z\right)^2 2b(1+b)\right\}C^x(\mathbf{0}),\\
-2\left[\langle H_1 H_{c4}\rangle_{\varphi c} H_{c0}\right]_D &= -4\lambda t_\mu^{-2}\int d^2\mathbf{x}\left\{\left[\left(\tilde{A}_\mu^x\right)^2+\left(\tilde{A}_\mu^y\right)^2\right](1+b)\right.\\
&\qquad\left.+\left(\tilde{A}_\mu^z\right)^2(1-b)^2(1+b)\right\}C^x(\mathbf{0}),\\
2\left[\langle H_{c1}H_{c2}H_{c4}\rangle_{\varphi c} H_{c0}\right]_D &= 2\lambda^2 t_\mu^{-3}\int d^2\mathbf{x}\left\{\left[\left(\tilde{A}_\mu^x\right)^2+\left(\tilde{A}_\mu^y\right)^2\right]b(1+b)\right.\\
&\qquad\left.+\left(\tilde{A}_\mu^z\right)^2 2b(b^2-1)\right\}C^x(\mathbf{0}),\\
\left[\left\langle H_{c2}^2 H_{c3}\right\rangle_{\varphi c} H_{c0}\right]_D &= 4\lambda^2 t_\mu^{-2}t_s^{-1}\int d^2\mathbf{x}\left\{\left[\left(\tilde{A}_\mu^x\right)^2+\left(\tilde{A}_\mu^y\right)^2\right]b\right.\\
&\qquad\left.-\left(\tilde{A}_\mu^z\right)^2 2b(1+b)\right\}C^x(\mathbf{0}),\\
-\left[\left\langle H_1 H_{c2}^2 H_{c4}\right\rangle_{\varphi c} H_{c0}\right]_D &= -2\lambda^2 t_\mu^{-2}t_s^{-1}\int d^2\mathbf{x}\left\{\left[\left(\tilde{A}_\mu^x\right)^2+\left(\tilde{A}_\mu^y\right)^2\right](1+b)(2+b)\right.\\
&\qquad\left.+\left(\tilde{A}_\mu^z\right)^2 2(1+b)(1-b)^2\right\}C^x(\mathbf{0}),\\
\left[\langle H_{c1}H_{c2}\rangle_{\varphi c}^2\right]_D &= 2\lambda^2 t_\mu^{-2}t_s^{-1}\int d^2\mathbf{x}\left\{\left[\left(\tilde{A}_\mu^x\right)^2+\left(\tilde{A}_\mu^y\right)^2\right]b^2\right.\\
&\qquad\left.+\left(\tilde{A}_\mu^z\right)^2(2+t_s t_\mu^{-1})b^2\right\}C^x(\mathbf{0}),\\
\frac{1}{4}\left[\left\langle H_1 H_{c2}^2\right\rangle_{\varphi c}^2\right]_D &= \lambda^2 t_\mu^{-1}t_s^{-2}\int d^2\mathbf{x}\left\{\left[\left(\tilde{A}_\mu^x\right)^2+\left(\tilde{A}_\mu^y\right)^2\right](1+b)^2\right.\\
&\qquad\left.+\left(\tilde{A}_\mu^z\right)^2(1-b)^2\right\}C^x(\mathbf{0}),\\
-\left[\left\langle H_1 H_{c2}^2\right\rangle_{\varphi c}\langle H_{c1}H_{c2}\rangle_{\varphi c}\right]_D &= -2\lambda^2 t_\mu^{-2}t_s^{-1}\int d^2\mathbf{x}\left\{\left[\left(\tilde{A}_\mu^x\right)^2+\left(\tilde{A}_\mu^y\right)^2\right]b(1+b)\right.\\
&\qquad\left.+\left(\tilde{A}_\mu^z\right)^2 2b(b-1)\right\}C^x(\mathbf{0}).
\end{aligned}$$

The sum of the above terms is (we now again set $t_\mu = t_s$)

$$\lambda t_s^{-2} \int d^2\mathbf{x} \left\{ \left[\left(\tilde{A}_\mu^x\right)^2 + \left(\tilde{A}_\mu^y\right)^2 \right] \left(1 + \frac{4(b-1)t_s + (b^2-3)\lambda}{t_s} C^x(\mathbf{0}) \right) \right.$$
$$\left. + \left(\tilde{A}_\mu^z\right)^2 \left((1+b)^2 - \frac{4(1+b)^3 t_s + (3+6b+b^2)\lambda}{t_s} C^x(\mathbf{0}) \right) \right\}. \qquad \text{(A.23)}$$

On the calculation of disorder terms

As an illustration, we give details for the calculation of the variance terms for a relatively simple term, $\left[\langle H_{c3}\rangle_{\varphi c} H_{c0}\right]_D$, and a more involved one, $\left[\langle H_{c1} H_{c2}^2 H_{c4}\rangle_{\varphi c} H_{c0}\right]_D$. For $\left[\langle H_{c3}\rangle_{\varphi c} H_{c0}\right]_D$ we have

$$\begin{aligned}
\left[\langle H_{c3}\rangle_{\varphi c} H_{c0}\right]_D &= 8 \int d^2\mathbf{x} d^2\mathbf{x}' p_{k\mu} p_{k'\mu'} \epsilon_{ijk} \epsilon_{i'j'k'} \epsilon_{abc} \epsilon_{a'b'c'} C^l(\mathbf{0}) \tilde{n}_{j'}^{a'} \tilde{n}_{k'}^{c'} \tilde{A}_{\mu'}^{i'} \times \\
&\quad \left\{ 2\epsilon_{jlm}\epsilon_{klq} \tilde{n}_m^a \tilde{n}_q^c \tilde{A}_\mu^i + 2\epsilon_{ilm}\epsilon_{klq} \tilde{n}_q^c \tilde{n}_j^a \tilde{A}_\mu^m + 2\epsilon_{ilm}\epsilon_{jlq} \tilde{n}_q^a \tilde{n}_k^c \tilde{A}_\mu^m \right. \\
&\quad \left. - \tilde{n}_j^a \tilde{n}_k^c \tilde{A}_\mu^i \left((\epsilon_{ilm})^2 + (\epsilon_{jlm})^2 + (\epsilon_{klm})^2 \right) \right\} \left[Q_\mu^b(\mathbf{x}) Q_{\mu'}^{b'}(\mathbf{x}') \right]_D \\
&= 16\lambda \int d^2\mathbf{x} p_{k\mu} p_{k'\mu} \epsilon_{ijk} \epsilon_{i'j'k'} \epsilon_{abc} \epsilon_{a'bc'} \tilde{n}_{j'}^{a'} \tilde{n}_{k'}^{c'} \tilde{A}_\mu^{i'} \times \\
&\quad \left\{ \left(\epsilon_{jlm}\epsilon_{klq} \tilde{n}_m^a \tilde{n}_q^c \tilde{A}_\mu^i + \epsilon_{ilm}\epsilon_{klq} \tilde{n}_q^c \tilde{n}_j^a \tilde{A}_\mu^m + \epsilon_{ilm}\epsilon_{jlq} \tilde{n}_q^a \tilde{n}_k^c \tilde{A}_\mu^m \right) C^l(\mathbf{0}) \right. \\
&\quad \left. - \tilde{n}_j^a \tilde{n}_k^c \tilde{A}_\mu^i \left(2 + (1+b)^{-1} \right) C^x(\mathbf{0}) \right\} \\
&= 16\lambda \int d^2\mathbf{x} \left(\epsilon_{ijk}\right)^2 \left(\tilde{A}_\mu^i\right)^2 \left\{ p_{k\mu} p_{j\mu} C^i(\mathbf{x}) + p_{k\mu}^2 C^i(\mathbf{x}) + p_{k\mu} p_{i\mu} C^j(\mathbf{x}) \right. \\
&\quad + p_{k\mu} p_{i\mu} C^k(\mathbf{x}) + p_{k\mu}^2 C^k(\mathbf{x}) + p_{k\mu} p_{j\mu} C^k(\mathbf{x}) \\
&\quad \left. - \left(2 + (1+b)^{-1} \right) C^x(\mathbf{0}) \left(p_{k\mu}^2 + p_{k\mu} p_{j\mu} \right) \right\}, \qquad \text{(A.24)}
\end{aligned}$$

where we again used the orthonormality of the $\mathbf{n}_k$. Performing the summation over the silent indices, one finally obtains

$$\begin{aligned}
&= 16\lambda \int d^2\mathbf{x} \left\{ \left[\left(\tilde{A}_\mu^x\right)^2 + \left(\tilde{A}_\mu^y\right)^2 \right] \left(p_{1\mu}^2 - p_{3\mu}^2 \right) + \left(\tilde{A}_\mu^z\right)^2 \left(4p_{3\mu} p_{1\mu} - 4p_{1\mu}^2 \right) \right\} C^x(\mathbf{0}) \\
&= 4\lambda t_\mu^{-2} \int d^2\mathbf{x} \left\{ \left[\left(\tilde{A}_\mu^x\right)^2 + \left(\tilde{A}_\mu^y\right)^2 \right] b - \left(\tilde{A}_\mu^z\right)^2 2b(1+b) \right\} C^x(\mathbf{0}).
\end{aligned}$$

We now turn to the more lengthy evaluation of $\left[\langle H_1 H_{c2}^2 H_{c4}\rangle_{\varphi c} H_{c0}\right]_D$. We have

$$\begin{aligned}
H_1 H_{c2}^2 H_{c4} &= 16 \int d^2\mathbf{x} d^2\mathbf{x}' d^2\mathbf{x}'' d^2\mathbf{x}''' p_{k\mu} t_{\mu'}^{-1} p_{k'\mu'} p_{k''\mu''} p_{k'''\mu'''} \epsilon_{ijk} \epsilon_{i'j'k'} \epsilon_{i''j''k''} \epsilon_{i'''j'''k'''} \times \\
&\quad \epsilon_{abc} \epsilon_{a'b'c'} \epsilon_{a''b''c''} \epsilon_{a'''b'''c'''} \tilde{A}_{\mu'}^{i'} \left(1 - b\delta_{i'z} + 2b\delta_{j'z} \right) \tilde{n}_{j''}^{a''} \tilde{n}_{k''}^{c''} \tilde{n}_{j'''}^{a'''} \tilde{n}_{k'''}^{c'''} \times \\
&\quad \left\{ 2\partial_\mu \varphi^i \varphi^d \left(\epsilon_{kdl} \tilde{n}_l^c \tilde{n}_j^a + \epsilon_{jdl} \tilde{n}_l^a \tilde{n}_k^a \right) + \varphi^d \partial_\mu \varphi^l \epsilon_{idl} \tilde{n}_j^a \tilde{n}_k^c \right\} \times \\
&\quad \partial_{\mu'} \varphi^{j'} \varphi^{k'} \partial_{\mu''} \varphi^{i''} \partial_{\mu'''} \varphi^{i'''} Q_\mu^b Q_{\mu''}^{b''} Q_{\mu'''}^{b'''}. \qquad \text{(A.25)}
\end{aligned}$$

We now need to perform the average over the φ fields. For convenience, we split $H_1 H_{c2}^2 H_{c4} = \mathcal{A} + \mathcal{B}$ into two terms, where $\mathcal{A}$ corresponds to the part of $H_1 H_{c2}^2 H_{c4}$ which involves the first term in the curly brackets in Eq. (A.25) and $\mathcal{B}$ corresponds to the second term in the curly brackets. For $\langle \mathcal{A} \rangle_{\varphi c}$, we need to calculate the average

$$\left\langle \partial_\mu \varphi^i(\mathbf{x}) \varphi^d(\mathbf{x}) \partial_{\mu'} \varphi^{j'}(\mathbf{x}') \varphi^{k'}(\mathbf{x}') \partial_{\mu''} \varphi^{i''}(\mathbf{x}'') \partial_{\mu'''} \varphi^{i'''}(\mathbf{x}''') \right\rangle_\varphi , \tag{A.26}$$

which can be easily done via Wick's Theorem. However, not all possible permutations of pairings will contribute. All terms involving either of the contractions $\langle id \rangle$ or $\langle j'k' \rangle$ vanish as $\partial_\mu C^x(\mathbf{0}) = 0$. Although not immediately apparent, terms involving the pairing $\langle i''i''' \rangle$ also do not contribute to one loop order. This can be seen only after the computation of the disorder average $\left[\langle \mathcal{A} \rangle_{\varphi c} H_{c0} \right]_D$ and a gradient expansion similar to the one employed below Eq. (A.11). Using the same arguments as we used for the term (A.11), all $\langle i''i''' \rangle$ contractions can then be shown to give no contribution. Furthermore, all contractions which are identical up to a permutation of the indices i'' and i''' will give the same contributions after the disorder average is taken, as discussed below. We therefore only write down half of the permutations and indicate the others by $\{'' \leftrightarrow '''\}$. Thus, we only need to keep the following terms,

$$\begin{aligned}
&\left\langle \partial_\mu \varphi^i(\mathbf{x}) \varphi^d(\mathbf{x}) \partial_{\mu'} \varphi^{j'}(\mathbf{x}') \varphi^{k'}(\mathbf{x}') \partial_{\mu''} \varphi^{i''}(\mathbf{x}'') \partial_{\mu'''} \varphi^{i'''}(\mathbf{x}''') \right\rangle_\varphi \to \\
&\qquad \delta_{ij'} \delta_{di''} \delta_{k'i'''} \partial_\mu \partial_{\mu'} C^i(\mathbf{x}-\mathbf{x}') \partial_{\mu''} C^d(\mathbf{x}-\mathbf{x}'') \partial_{\mu'''} C^{i'''}(\mathbf{x}'-\mathbf{x}''') \\
&+ \delta_{ik'} \delta_{di''} \delta_{j'i'''} \partial_\mu C^i(\mathbf{x}-\mathbf{x}') \partial_{\mu''} C^d(\mathbf{x}-\mathbf{x}'') \partial_{\mu'} \partial_{\mu'''} C^{i'''}(\mathbf{x}'-\mathbf{x}''') \\
&+ \delta_{ii''} \delta_{dj'} \delta_{k'i'''} \partial_\mu \partial_{\mu''} C^i(\mathbf{x}-\mathbf{x}'') \partial_{\mu'} C^d(\mathbf{x}-\mathbf{x}') \partial_{\mu'''} C^{i'''}(\mathbf{x}'-\mathbf{x}''') \\
&+ \delta_{ii''} \delta_{dk'} \delta_{j'i'''} \partial_\mu \partial_{\mu''} C^i(\mathbf{x}-\mathbf{x}'') C^d(\mathbf{x}-\mathbf{x}') \partial_{\mu'} \partial_{\mu'''} C^{i'''}(\mathbf{x}'-\mathbf{x}''') \\
&+ \{'' \leftrightarrow '''\}
\end{aligned} \tag{A.27}$$

Let us now perform the disorder average $\left[\langle \mathcal{A} \rangle_{\varphi c} H_{c0} \right]_D$. For this, we need to calculate

$$\left[Q^{\tilde{b}}_{\tilde{\mu}}(\tilde{\mathbf{x}}) Q^b_\mu(\mathbf{x}) Q^{b''}_{\mu''}(\mathbf{x}'') Q^{b'''}_{\mu'''}(\mathbf{x}''') \right]_D \tag{A.28}$$

where the variables carrying a tilde arise from the H_{c0} term. Again, we can use Wick's Theorem to decompose the average. Of the three possible permutations of pairings, two involve either of the two contractions $\langle bb'' \rangle$ or $\langle bb''' \rangle$. Neither permutation contributes. This is easily seen for the $\langle bb'' \rangle$ contraction and the explicitly written terms in (A.27) because they all involve after the contraction a derivative of $C^x(\mathbf{0})$ and thus vanish. The same terms also do not contribute for the case of a $\langle bb''' \rangle$ contraction, which again can be seen with a gradient expansion and using arguments analogous to those below Eq. (A.11). Therefore, only one term of the disorder average must be kept,

$$\left[Q^{\tilde{b}}_{\tilde{\mu}}(\tilde{\mathbf{x}}) Q^b_\mu(\mathbf{x}) Q^{b''}_{\mu''}(\mathbf{x}'') Q^{b'''}_{\mu'''}(\mathbf{x}''') \right]_D \to \lambda^2 \delta_{b\tilde{b}} \delta_{b''b'''} \delta_{\mu\tilde{\mu}} \delta_{\mu''\mu'''} \delta(\mathbf{x}-\tilde{\mathbf{x}}) \delta(\mathbf{x}''-\mathbf{x}''') \tag{A.29}$$

The terms in (A.27) which only differ by a permutation of the double primed and triple primed variables give then identical contributions, as such a permutation simply relabels the variables associated with the two H_{c2} terms in $\left[\langle\mathcal{A}\rangle_{\varphi c} H_{c0}\right]_D$. With (A.27, A.29) we then have

$$\begin{aligned}\left[\langle\mathcal{A}\rangle_{\varphi c} H_{c0}\right]_D &= 128\lambda^2 \int d^2\mathbf{x} d^2\mathbf{x}' d^2\mathbf{x}'' t_{\mu'}^{-1} \left(p_{k''\mu''}^2 + p_{k''\mu''} p_{j''\mu''}\right)^2 \left(\epsilon_{i''j''k''}\right)^2 \epsilon_{i'j'k'} \tilde{A}_{\mu'}^{i'} \times \\ &\quad (1 - b\delta_{i'z} + 2b\delta_{j'z}) \left\{-\tilde{A}_\mu^k p_{i\mu} p_{k\mu} \epsilon_{kdi} + \tilde{A}_\mu^k p_{d\mu} p_{k\mu} \epsilon_{idk} - \tilde{A}_\mu^j p_{d\mu}^2 \epsilon_{ijd} \right. \\ &\quad \left. -\tilde{A}_\mu^j p_{i\mu} p_{d\mu} \epsilon_{jdi}\right\} \times \\ &\quad \Big[\delta_{ij'}\delta_{di''}\delta_{k'i''} \partial_\mu \partial_{\mu'} C^i(\mathbf{x}-\mathbf{x}') \partial_{\mu''} C^d(\mathbf{x}-\mathbf{x}'') \partial_{\mu''} C^{i''}(\mathbf{x}'-\mathbf{x}'') \\ &\quad +\delta_{ik'}\delta_{di''}\delta_{j'i''} \partial_\mu C^i(\mathbf{x}-\mathbf{x}') \partial_{\mu''} C^d(\mathbf{x}-\mathbf{x}'') \partial_{\mu'}\partial_{\mu''} C^{i''}(\mathbf{x}'-\mathbf{x}'') \\ &\quad +\delta_{ii''}\delta_{dj'}\delta_{k'i''} \partial_\mu \partial_{\mu''} C^i(\mathbf{x}-\mathbf{x}'') \partial_{\mu'} C^d(\mathbf{x}-\mathbf{x}') \partial_{\mu''} C^{i''}(\mathbf{x}'-\mathbf{x}'') \\ &\quad +\delta_{ii''}\delta_{dk'}\delta_{j'i''} \partial_\mu \partial_{\mu''} C^i(\mathbf{x}-\mathbf{x}'') C^d(\mathbf{x}-\mathbf{x}') \partial_{\mu'}\partial_{\mu''} C^{i''}(\mathbf{x}'-\mathbf{x}'')\Big]. \end{aligned} \tag{A.30}$$

The integration over $\mathbf{x}''$ can now be performed with

$$t_{\mu''}^{-1} \int d^2\mathbf{x}'' \partial_{\mu''} C^x(\mathbf{x}-\mathbf{x}'') \partial_{\mu''} C^x(\mathbf{x}'-\mathbf{x}'') = \frac{1}{2} C^x(\mathbf{x}-\mathbf{x}') + \mathcal{O}(\kappa^2). \tag{A.31}$$

The remaining double integral over $\mathbf{x}$ and $\mathbf{x}'$ can then again be approximated with a gradient expansion in the relative coordinate and employing Eq. (A.31). We then obtain (we denote the center of mass coordinate again by $\mathbf{x}$)

$$\begin{aligned}\left[\langle\mathcal{A}\rangle_{\varphi c} H_{c0}\right]_D &\simeq 16\lambda^2 t_s \int d^2\mathbf{x} \left(p_{k''}^2 + p_{k''} p_{j''}\right)^2 \left(\epsilon_{i''j''k''}\right)^2 \epsilon_{i'j'k'} \tilde{A}_\mu^{i'} (1 - b\delta_{i'z} + 2b\delta_{j'z}) \times \\ &\quad \beta_i \beta_d \epsilon_{idk} \left\{\tilde{A}_\mu^k p_{i\mu} p_{k\mu} + \tilde{A}_\mu^k p_{d\mu} p_{k\mu} + \tilde{A}_\mu^j p_{d\mu}^2 + \tilde{A}_\mu^j p_{i\mu} p_{d\mu}\right\} \times \\ &\quad [\delta_{ij'}\delta_{di''}\delta_{k'i''}\beta_{k'} - \delta_{ik'}\delta_{di''}\delta_{j'i''}\beta_{j'} - \delta_{ii''}\delta_{dj'}\delta_{k'i''}\beta_{k'} + \delta_{ii''}\delta_{dk'}\delta_{j'i''}\beta_{j'}] \times \\ &\quad \times C^x(\mathbf{0}). \end{aligned} \tag{A.32}$$

where β_k is defined through $\beta_1 = \beta_2 = 1$, $\beta_3 = (1+b)^{-1}$ and $p_k t_s / t_\mu = p_{k\mu}$. After some straightforward algebra, one finally finds

$$\begin{aligned}\left[\langle\mathcal{A}\rangle_{\varphi c} H_{c0}\right]_D &\simeq 32\lambda^2 t_\mu^{-2} t_s^3 \int d^2\mathbf{x} \left\{\left[\left(\tilde{A}_\mu^x\right)^2 + \left(\tilde{A}_\mu^y\right)^2\right] \times \right. \\ &\quad \left(\left(p_1+p_3\right)^2 + \frac{4p_1^2}{1+b}\right)\left(\left(p_1+p_3\right)^2 + 2p_1^2 + 2p_1 p_3\right) + \\ &\quad \left.\left(\tilde{A}_\mu^z\right)^2 8(1-b)\left(p_1^2 + p_1 p_3\right)\left(p_1+p_3\right)^2\right\} C^x(\mathbf{0}). \end{aligned} \tag{A.33}$$

The calculation of $\left[\langle\mathcal{B}\rangle_{\varphi c} H_{c0}\right]_D$ can be done in much the same way as just shown for $\left[\langle\mathcal{A}\rangle_{\varphi c} H_{c0}\right]_D$. One arrives at

$$\begin{aligned}\left[\langle\mathcal{B}\rangle_{\varphi c} H_{c0}\right]_D &\simeq -32\lambda^2 t_\mu^{-2} t_s^3 \int d^2\mathbf{x} \left\{\left[\left(\tilde{A}_\mu^x\right)^2 + \left(\tilde{A}_\mu^y\right)^2\right]\left(\left(p_1+p_3\right)^2 + \frac{4p_1^2}{1+b}\right)\left(p_1+p_3\right)^2 \right. \\ &\quad \left. + \left(\tilde{A}_\mu^z\right)^2 8(1-b) p_1^2 \left(p_1+p_3\right)^2\right\} C^x(\mathbf{0}). \end{aligned} \tag{A.34}$$

Finally, expressing all p_k through b and t_s, one obtains for $\left[\langle \mathcal{A}+\mathcal{B}\rangle_{\varphi c} H_{c0}\right]_D$

$$\left[\left\langle H_1 H_{c2}^2 H_{c4}\right\rangle_{\varphi c} H_{c0}\right]_D = 2\lambda^2 t_\mu^{-2} t_s^{-1} \int d^2\mathbf{x} \left\{\left[\left(\tilde{A}_\mu^x\right)^2 + \left(\tilde{A}_\mu^y\right)^2\right](1+b)(2+b) + \left(\tilde{A}_\mu^z\right)^2 2(1+b)(1-b)^2\right\} C^x(\mathbf{0}). \quad \text{(A.35)}$$

Appendix B

RG calculation for disordered stripes

B.1 Evaluation of integrals

We want to evaluate the integrals in Eq. (4.24). We begin with

$$P = \sum_{\epsilon_3,\epsilon_4=\pm 1} \int d\tau_3 d\tau_4 dy_3 dy_4 \left\langle e^{i\sqrt{2}\phi_1 - i\sqrt{2}\phi_2 + i2\epsilon_3\sqrt{\pi}\phi_3 + i2\epsilon_4\sqrt{\pi}\phi_4} \right\rangle_0 \tag{B.1}$$

which has nonzero contributions only for $\epsilon_3 + \epsilon_4 = 0$. Thus,

$$\begin{aligned} P &= e^{-F(y_1-y_2,\tau_1-\tau_2)} \sum_{\pm} \int d\tau_3 d\tau_4 dy_3 dy_4 e^{-2\pi F(y_3-y_4,\tau_3-\tau_4) \pm \sqrt{2\pi} F(y_1-y_3,\tau_1-\tau_3)} \times \\ &\quad \times e^{\mp\sqrt{2\pi}F(y_1-y_4,\tau_1-\tau_4) \mp \sqrt{2\pi}F(y_2-y_3,\tau_2-\tau_3) \pm \sqrt{2\pi}F(y_2-y_4,\tau_2-\tau_4)}. \end{aligned} \tag{B.2}$$

The dominant contributions to the integral come from small $|\mathbf{x}_3 - \mathbf{x}_4|$ where we introduced $\mathbf{x}_j := (c\tau_j, y_j)$ (it can be shown that contribution arising from e. g. small $\mathbf{x}_1 - \mathbf{x}_3$ and $\mathbf{x}_2 - \mathbf{x}_4$ cancel at the lowest order with the contributions arising from small $\mathbf{x}_2 - \mathbf{x}_3$ and $\mathbf{x}_1 - \mathbf{x}_4$ [144]). We therefore introduce $\mathbf{R} = \frac{1}{2}(\mathbf{x}_3 + \mathbf{x}_4)$ and expand in the relative coordinate $\mathbf{r} = \mathbf{x}_3 - \mathbf{x}_4$. We obtain

$$\begin{aligned} P &\simeq \frac{2}{c^2} e^{-F(\mathbf{x}_1-\mathbf{x}_2)} \int d^2\mathbf{R} d^2\mathbf{r} e^{-2\pi F(\mathbf{r})} \left[1 + \pi \left(\mathbf{r} \cdot \nabla_{\mathbf{R}} \left[F(\mathbf{x}_1 - \mathbf{R}) - F(\mathbf{x}_2 - \mathbf{R})\right]\right)^2\right] \\ &= P_1 + P_2 \end{aligned} \tag{B.3}$$

The first term P_1 is proportional to the volume $\int d^2\mathbf{R}$ but it is canceled by the perturbative expansion of Z^{-1} present in Eq. (4.24), see also [144]. The remaining term P_2 can then be written, after taking the angular average of $\mathbf{r}$ and performing a partial integration, as

$$\begin{aligned} P_2 = \frac{\pi}{c^2} e^{-F(\mathbf{x}_1-\mathbf{x}_2)} \int dr\ r^3 e^{-2\pi F(\mathbf{r})} \int d^2\mathbf{R} \left[F(\mathbf{x}_1 - \mathbf{R}) - F(\mathbf{x}_2 - \mathbf{R})\right] \times \\ \times \nabla_R^2 \left[F(\mathbf{x}_2 - \mathbf{R}) - F(\mathbf{x}_1 - \mathbf{R})\right]. \end{aligned} \tag{B.4}$$

Using $\nabla^2 F(\mathbf{x}) = 2\pi\mu\delta(\mathbf{x})$ we obtain

$$P_2 = \frac{4\pi^2 a^4 \mu}{c^2} e^{-F(\mathbf{x}_1-\mathbf{x}_2)} F(\mathbf{x}_1-\mathbf{x}_2) \int \frac{dr}{a} \left(\frac{r}{a}\right)^{3-2\pi\mu}. \tag{B.5}$$

We now turn to the other integral in Eq. (4.24),

$$\begin{aligned} Q &= \sum_{\pm} \int d\tau_3 d\tau_4 dy_3 dy_4 \delta(y_3-y_4) \left\langle e^{i\sqrt{2}\phi_1 - i\sqrt{2}\phi_2 \pm i2\sqrt{\pi}\delta\phi_3 \pm i2\sqrt{\pi}\delta\phi_4} \right\rangle_0 \\ &= e^{-F(\mathbf{x}_1-\mathbf{x}_2)} \sum_{\pm} \int d\tau_3 dy_3 d\tau_4 e^{-2\pi\delta^2 F(0,\tau_3-\tau_4)} e^{\pm\sqrt{2\pi}\delta F(y_1-y_3,\tau_1-\tau_3) \mp \sqrt{2\pi}\delta F(y_1-y_3,\tau_1-\tau_4)} \\ &\times e^{\mp\sqrt{2\pi}\delta F(y_2-y_3,\tau_2-\tau_3) \pm \sqrt{2\pi}\delta F(y_2-y_3,\tau_2-\tau_4)}. \end{aligned} \tag{B.6}$$

We introduce $\mathcal{T} = \frac{1}{2}(\tau_3+\tau_4)$ and$\tau = \tau_3 - \tau_4$ and expand Q in τ,

$$\begin{aligned} Q &\simeq 2e^{-F(\mathbf{x}_1-\mathbf{x}_2)} \int d\tau d\mathcal{T} dy e^{-2\pi\delta^2 F(0,\tau)} \times \\ &\quad \left[1 + \pi\delta^2\tau^2 \left(\partial_{\mathcal{T}} \left[F(y_1-y,\tau_1-\mathcal{T}) - F(y_2-y,\tau_2-\mathcal{T})\right]\right)^2\right] \\ &= Q_1 + Q_2. \end{aligned} \tag{B.7}$$

Again, the volume term Q_1 can be shown to cancel a similar term from Z^{-1} and we need only consider Q_2. We go to isotropic variables $\mathbf{R} = (X,Y) = (c\mathcal{T}, y)$, introduce $x = c\tau$ and write

$$\begin{aligned} Q_2 &\simeq \frac{\pi\delta^2}{c^2} e^{-F(\mathbf{x}_1-\mathbf{x}_2)} \int dx e^{-2\pi\delta^2 F(x)} x^2 \int d^2\mathbf{R} \left[F(\mathbf{x_1}-\mathbf{R}) - F(\mathbf{x_2}-\mathbf{R})\right] \times \\ &\quad \times \left[\left(\partial_X^2 + \partial_Y^2\right) + \left(\partial_X^2 - \partial_Y^2\right)\right] \left[F(\mathbf{x_1}-\mathbf{R}) - F(\mathbf{x_2}-\mathbf{R})\right]. \end{aligned} \tag{B.8}$$

Using [113]

$$\int d^2\mathbf{R} \ln|\mathbf{x}_1-\mathbf{R}| \left(\partial_Y^2 - \partial_X^2\right) \ln|\mathbf{x}_2-\mathbf{R}| = \pi\cos\left(2\theta_{\mathbf{x}_1\mathbf{x}_2}\right), \tag{B.9}$$

where $\theta_{\mathbf{x}_1\mathbf{x}_2}$ is the angle between $\mathbf{x}_1-\mathbf{x}_2$ and the y axis, we find

$$Q_2 \simeq \frac{8\pi^2 a^3 \delta^2 \mu^2}{c^2} e^{-F(\mathbf{x}_1-\mathbf{x}_2)} \left[\ln|\mathbf{x}_1-\mathbf{x}_2| - \frac{1}{2}\cos\left(2\theta_{\mathbf{x}_1\mathbf{x}_2}\right)\right] \int d\left(\frac{x}{a}\right) \left(\frac{x}{a}\right)^{2-2\pi\mu\delta^2} \tag{B.10}$$

B.2 Calculation of renormalized parameters

Combining Eq. (4.24, B.5, B.10) we have

$$\begin{aligned} \left\langle e^{i\sqrt{2}(\phi_1-\phi_2)} \right\rangle &\simeq \left\langle e^{i\sqrt{2}(\phi_1-\phi_2)} \right\rangle_0 \left(1 + \frac{g^2\pi^2\mu^2 a^2}{2c^2} \ln|\mathbf{x}_1-\mathbf{x}_2| \int \frac{dr}{a} \left(\frac{r}{a}\right)^{3-2\pi\mu} \right. \\ &\quad + \frac{2\pi^2 a^2 \delta^2 \mu^2 D}{c^2 L} \ln|\mathbf{x}_1-\mathbf{x}_2| \int d\left(\frac{x}{a}\right) \left(\frac{x}{a}\right)^{2-2\pi\mu\delta^2} \\ &\quad \left. - \frac{\pi^2 a^2 \delta^2 \mu^2 D}{c^2 L} \cos\left(2\theta_{\mathbf{x}_1\mathbf{x}_2}\right) \int d\left(\frac{x}{a}\right) \left(\frac{x}{a}\right)^{2-2\pi\mu\delta^2} \right). \end{aligned} \tag{B.11}$$

Re-exponentiating the term in brackets, we thus find Eq. (4.25),

$$\left\langle e^{i\sqrt{2}(\phi(y_1,\tau_1)-\phi(y_2,\tau_2))}\right\rangle \simeq \exp\left(-\frac{\tilde{\mu}}{2}\ln\left(\frac{(y_1-y_2)^2+c^2(\tau_1-\tau_2)^2}{a^2}\right)-\tilde{\kappa}\cos(2\theta)\right) \quad \text{(B.12)}$$

and

$$\tilde{\mu} = \mu-\frac{1}{2}\mathcal{D}\mu^2\int_{x>a}d\left(\frac{x}{a}\right)\left(\frac{x}{a}\right)^{2-2\pi\mu\delta^2}-\frac{1}{2}\mathcal{G}^2\mu^2\int_{x>a}d\left(\frac{x}{a}\right)\left(\frac{x}{a}\right)^{3-2\pi\mu} \quad \text{(B.13)}$$

$$\tilde{\kappa} = \kappa+\frac{1}{4}\mathcal{D}\mu^2\int_{x>a}d\left(\frac{x}{a}\right)\left(\frac{x}{a}\right)^{2-2\pi\mu\delta^2} \quad \text{(B.14)}$$

with $\mathcal{D}=4\pi^2\delta^2a^2D/(c^2L)$ and $\mathcal{G}=\pi ga/c$.

B.3 Derivation of scaling equations

To obtain the scaling equations, we look at how $\tilde{\mu}$ and $\tilde{\kappa}$ change under a rescaling $a\to\lambda a$. We therefore introduce $\varphi=x/a$ and split the integrals $\int_{x>a}d(x/a)\ldots=\int_1^\lambda d\varphi\ldots+\int_\lambda^\infty\ldots$ so that e. g.

$$\begin{aligned}\int_{x>a}d\left(\frac{x}{a}\right)\left(\frac{x}{a}\right)^{2-2\pi\mu\delta^2} &= \int_1^\lambda d\varphi\ \varphi^{2-2\pi\mu\delta^2}+\int_\lambda^\infty d\varphi\ \varphi^{2-2\pi\mu\delta^2}\\ &= \frac{\lambda^{3-2\pi\mu\delta^2}-1}{3-2\pi\mu\delta^2}+\lambda^{3-2\pi\mu\delta^2}\int_1^\infty d\varphi\ \varphi^{2-2\pi\mu\delta^2}\\ &\simeq \ln\lambda+\left(1+\ln\lambda\left[3-2\pi\mu\delta^2\right]\right)\int_1^\infty d\varphi\ \varphi^{2-2\pi\mu\delta^2}. \quad \text{(B.15)}\end{aligned}$$

We thus can rewrite Eq. (B.14) as

$$\tilde{\kappa}=\kappa_\lambda+\frac{1}{4}\mathcal{D}_\lambda\mu_\lambda^2\int_1^\infty d\varphi\ \varphi^{2-2\pi\mu\delta^2}, \quad \text{(B.16)}$$

where

$$\kappa_\lambda = \kappa+\frac{1}{4}\mathcal{D}\mu^2\ln\lambda, \quad \text{(B.17)}$$

$$\mathcal{D}_\lambda\mu_\lambda^2 = \mathcal{D}\mu^2+\mathcal{D}\mu^2\left[3-2\pi\mu\delta^2\right]\ln\lambda. \quad \text{(B.18)}$$

Similarly, we can rewrite Eq. (B.13) as

$$\tilde{\mu}=\mu_\lambda-\frac{1}{2}\mathcal{D}_\lambda\mu_\lambda^2\int_1^\infty d\varphi\ \varphi^{2-2\pi\mu\delta^2}-\frac{1}{2}\mathcal{G}_\lambda^2\mu_\lambda^2\int_1^\infty d\varphi\ \varphi^{3-2\pi\mu}, \quad \text{(B.19)}$$

with

$$\mu_\lambda = \mu-\frac{1}{2}\mathcal{D}\mu^2\ln\lambda-\frac{1}{2}\mathcal{G}^2\mu^2\ln\lambda, \quad \text{(B.20)}$$

$$\mathcal{G}_\lambda^2\mu_\lambda^2 = \mathcal{G}^2\mu^2+\mathcal{G}^2\mu^2\left[4-2\pi\mu\right]\ln\lambda. \quad \text{(B.21)}$$

For $\lambda = e^{\ell}$, $\ell \ll 1$, Eqs. (B.17, B.18, B.20, B.21) can be written in differential form as

$$\frac{\partial}{\partial \ell}\kappa = \frac{1}{4}\mathcal{D}\mu^2, \tag{B.22}$$

$$\frac{\partial}{\partial \ell}\left(\mathcal{D}\mu^2\right) = \left(3 - 2\pi\mu\delta^2\right)\mathcal{D}\mu^2, \tag{B.23}$$

$$\frac{\partial}{\partial \ell}\mu = -\frac{1}{2}\mu^2\left(\mathcal{D} + \mathcal{G}^2\right), \tag{B.24}$$

$$\frac{\partial}{\partial \ell}\left(\mathcal{G}^2\mu^2\right) = (4 - 2\pi\mu)\,\mathcal{G}^2\mu^2. \tag{B.25}$$

To linear order in $\mathcal{G}^2$ and $\mathcal{D}$, these equations reduce to Eqs. (4.27-4.30).

Bibliography

[1] E. Dagotto, Rev. Mod. Phys. **66**, 763 (1994).

[2] S. A. Trugman, Phys. Rev. B **37**, 1597 (1988).

[3] B. I. Shraiman and E. D. Siggia, Phys. Rev. Lett. **61**, 467 (1988).

[4] B. I. Shraiman and E. D. Siggia, Phys. Rev. Lett. **62**, 1564 (1989).

[5] B. I. Shraiman and E. D. Siggia, Phys. Rev. B **40**, 9162 (1989).

[6] F. C. Zhang and T. M. Rice, Phys. Rev. B **37**, R3759 (1988).

[7] S. Chakravarty, B. I. Halperin, and D. R. Nelson, Phys. Rev. B **39**, 2344 (1989).

[8] R. J. Birgeneau *et al.*, Phys. Rev. B **59**, 13788 (1999).

[9] F. C. Chou *et al.*, Phys. Rev. Lett. **71**, 2323 (1993).

[10] F. Borsa *et al.*, Phys. Rev. B **52**, 7334 (1995).

[11] C. Niedermayer *et al.*, Phys. Rev. Lett. **80**, 3843 (1998).

[12] C. Y. Chen *et al.*, Phys. Rev. B **51**, 3671 (1995).

[13] S. Wakimoto, S. Ueki, Y. Endoh, and K. Yamada, Phys. Rev. B **62**, 3547 (2000).

[14] M. Matsuda *et al.*, Phys. Rev. B **62**, 9148 (2000).

[15] K. Yamada *et al.*, Phys. Rev. B **57**, 6165 (1998).

[16] J. M. Tranquada *et al.*, Nature (London) **375**, 561 (1995).

[17] J. M. Tranquada, P. Wochner, and D. J. Buttrey, Phys. Rev. Lett. **79**, 2133 (1997).

[18] T. Suzuki *et al.*, Phys. Rev. B **57**, R3229 (1998).

[19] H. Kimura *et al.*, Phys. Rev. B **59**, 6517 (1999).

[20] H. Kimura *et al.*, Phys. Rev. B **61**, 14366 (2000).

[21] Y. S. Lee *et al.*, Phys. Rev. B **60**, 3643 (1999).

[22] G. F. Reiter, Phys. Rev. B **49**, R1536 (1994).

[23] A. Ramsak and P.Horsch, Phys. Rev. B **57**, 4308 (1998).

[24] R. J. Gooding, Phys. Rev. Lett. **66**, 2266 (1991).

[25] J. Villain, Zeit. f. Phys. B **33**, 31 (1979).

[26] L. I. Glazman and A. S. Ioselevich, Zeit. f. Phys. B **80**, 133 (1990).

[27] V. Cherepanov, I. Y. Korenblit, A. Aharony, and O. Entin-Wohlman, Eur. Phys. J. B **8**, 511 (1999).

[28] C. Goldenberg and A. Aharony, Phys. Rev. B **56**, 661 (1997).

[29] N. Hasselmann, A. H. Castro Neto, and C. Morais Smith, to appear in Europhys. Lett. , Preprint cond. mat. **0005486**, (2001).

[30] N. Hasselmann, A. H. Castro Neto, and C. Morais Smith, "Studies of High Temperature Superconductors", inv. contr., Ed. A. V. Narlikar, Nova Science Pub. **34**, (2000).

[31] M. Matsuda *et al.*, Phys. Rev. B **61**, 4326 (2000).

[32] P. Azaria, B. Delamotte, F. Delduc, and T. Jolicoeur, Nucl. Phys. B **408**, 485 (1993).

[33] S. Klee and A. Muramatsu, Nucl. Phys. B **473**, 539 (1996).

[34] T. Dombre and N. Read, Phys. Rev. B **39**, 6797 (1989).

[35] J. A. Hertz, Phys. Rev. B **18**, 4875 (1978).

[36] W. Apel, M. Wintel, and H. U. Everts, Zeit. f. Phys. B **86**, 139 (1992).

[37] K. Binder and A. P. Young, Rev. Mod. Phys. **58**, 801 (1986).

[38] A. M. Polyakov, Phys. Lett. **59B**, 79 (1975).

[39] Y. Imry and S. K. Ma, Phys. Rev. Lett. **35**, 1399 (1975).

[40] M. Wintel, H. U. Everts, and W. Apel, Europhys. Lett. **25**, 711 (1994).

[41] J. M. Kosterlitz and D. J. Thouless, J. Phys. C **6**, L97 (1973).

[42] H. Kawamura, J. Phys.: Condens. Matter **10**, 4707 (1998).

[43] M. Wintel, H. U. Everts, and W. Apel, Phys. Rev. B **52**, 13480 (1995).

[44] M. Wintel, PhD thesis, Univ. Hannover 93U7008 (1993).

[45] S. Scheidl, Phys. Rev. B **55**, 457 (1997).

[46] D. S. Fisher, Phys. Rev. B **31**, 7233 (1985).

[47] T. Nattermann, S. Scheidl, S. E. Korshunov, and M. S. Li, J. Phys. I France **5**, 565 (1995).

[48] M.-C. Cha and H. A. Fertig, Phys. Rev. Lett. **74**, 4867 (1995).

[49] B. W. Southern and A. P. Young, Phys. Rev. B **48**, 13170 (1993).

[50] B. W. Southern and H.-J. Xu, Phys. Rev. B **52**, R3836 (1995).

[51] B. Keimer *et al.*, Phys. Rev. B **46**, 14034 (1992).

[52] S.-W. Cheong *et al.*, Phys. Rev. B **44**, 9739 (1991).

[53] M. Hücker *et al.*, Phys. Rev. B **59**, R725 (1999).

[54] I. Y. Korenblit, A. Aharony, and O. Entin-Wohlmann, Phys. Rev. B **60**, R15017 (1999).

[55] J. Zaanen and O. Gunnarsson, Phys. Rev. B **40**, 7391 (1989).

[56] D. Poilblanc and T. M. Rice, Phys. Rev. B **39**, 9749 (1989).

[57] H. J. Schulz, J. Phys. (Paris) **50**, 2833 (1989).

[58] H. J. Schulz, Phys. Rev. Lett. **64**, 1445 (1990).

[59] S. A. Kivelson and V. J. Emery, Synth. Metals **80**, 151 (1996).

[60] W. P. Su, J. R. Schrieffer, and A. J. Heeger, Phys. Rev. B **22**, 2099 (1980).

[61] V. J. Emery, S. A. Kivelson, and H. Q. Lin, Phys. Rev. Lett. **64**, 1993 (1990).

[62] U. Löw, V. J. Emery, K. Fabricius, and S. A. Kivelson, Phys. Rev. Lett. **72**, 1918 (1994).

[63] S. R. White and D. J. Scalapino, Phys. Rev. B **61**, 6320 (2000).

[64] C. S. Hellberg and E. Manousakis, Phys. Rev. Lett. **78**, 4609 (1997).

[65] K. Nakajima *et al.*, J. Phys. Soc. Jap. **66**, 809 (1997).

[66] E. G. Nikolaev, H. B. Brom, and A. A. Zakharov, Preprint cond. mat. **0003165**, (2000).

[67] S. R. White and D. J. Scalapino, Phys. Rev. Lett. **80**, 1272 (1998).

[68] G. B. Martins *et al.*, Phys. Rev. Lett. **84**, 5844 (2000).

[69] M. P. Gelfand, R. R. P. Singh, and D. A. Huse, Phys. Rev. B **40**, 10801 (1989).

[70] N. Read and S. Sachdev, Phys. Rev. B **42**, 4568 (1990).

[71] N. Read and S. Sachdev, Phys. Rev. Lett. **66**, 1773 (1991).

[72] M. Vojta and S. Sachdev, Phys. Rev. B **61**, 3699 (2000).

[73] M. Vojta, Y. Zhang, and S. Sachdev, Preprint cond. mat. **0003163**, (2000).

[74] D. K. Morr, J. Schmalian, and D. Pines, Preprint cond. mat. **0002164**, (2000).

[75] S. Wakimoto *et al.*, Phys. Rev. B **61**, 3699 (2000).

[76] D. K. Morr and D. Pines, Phys. Rev. Lett. **81**, 1086 (1998).

[77] J. Zaanen and P. B. Littlewood, Phys. Rev. B **50**, 7222 (1994).

[78] C. H. Chen, S.-W. Cheong, and A. S. Cooper, Phys. Rev. Lett. **71**, 2461 (1993).

[79] J. M. Tranquada, D. J. Buttrey, V. Sachan, and J. E. Lorenzo, Phys. Rev. Lett. **73**, 1003 (1994).

[80] J. M. Tranquada, D. J. Buttrey, and V. Sachan, Phys. Rev. B **54**, 12318 (1996).

[81] V. I. Anisimov, M. A. Korotin, J. Zaanen, and O. K. Andersen, Phys. Rev. Lett. **68**, 345 (1992).

[82] P. Wochner, J. M. Tranquada, D. J. Buttrey, and V. Sachan, Phys. Rev. B **57**, 1066 (1998).

[83] J. M. Tranquada *et al.*, Phys. Rev. B **50**, 6340 (1994).

[84] T. Katsufuji *et al.*, Phys. Rev. B **54**, R14230 (1996).

[85] G. Blumberg, M. V. Klein, and S.-W. Cheong, Phys. Rev. Lett. **80**, 564 (1998).

[86] J. M. Tranquada *et al.*, Phys. Rev. Lett. **78**, 338 (1997).

[87] Y. Koike *et al.*, Int. J. Mod. Phys. B **13**, 3546 (1999).

[88] M. Akoshima *et al.*, J. of Low Temp. Physics **117**, 1163 (1999).

[89] J. M. Tranquada *et al.*, Phys. Rev. B **54**, 7489 (1996).

[90] J. M. Tranquada, N. Ichikawa, and S. Uchida, Phys. Rev. B **59**, 14712 (1999).

[91] R. J. Birgeneau *et al.*, Phys. Rev. B **39**, 2868 (1989).

[92] T. E. Mason, G. Aeppli, and H. A. Mook, Phys. Rev. Lett. **68**, 1414 (1992).

[93] G. Aeppli *et al.*, Science **278**, 1432 (1997).

[94] J. Zaanen, M. L. Horbach, and W. van Saarloos, Phys. Rev. B **53**, 8671 (1996).

[95] S. A. Kivelson, E. Fradkin, and V. J. Emery, Nature (London) **393**, 550 (1998).

[96] B. J. Suh *et al.*, Phys. Rev. B **61**, R9265 (2000).

[97] B. Nachumi *et al.*, Phys. Rev. B **58**, 8760 (1998).

[98] D. Haskel, E. A. Stern, F. Dŏgan, and A. R. Moodenbaugh, Phys. Rev. B **61**, 7055 (2000).

[99] Y. Yoshinari, P. C. Hammel, and S.-W. Cheong, Phys. Rev. Lett. **82**, 3536 (1999).

[100] S. H. Lee and S.-W. Cheong, Phys. Rev. Lett. **79**, 2514 (1997).

[101] V. Sachan *et al.*, Phys. Rev. B **51**, 12742 (1995).

[102] B. O. Wells *et al.*, Science **277**, 1067 (1997).

[103] N. J. Curro *et al.*, Phys. Rev. Lett. **85**, 642 (2000).

[104] H. Eskes, R. Grimberg, W. van Saarloos, and J. Zaanen, Phys. Rev. B **54**, R724 (1996).

[105] H. Eskes *et al.*, Phys. Rev. B **58**, 6963 (1998).

[106] R. Rajaraman, *Solitons and Instantons* (North-Holland, Amsterdam, 1982).

[107] J. Zinn-Justin, *Quantum Field Theory and Critical Phenomena* (Clarendon Press, Oxford, 1989).

[108] Y. A. Dimashko, C. Morais Smith, N. Hasselmann, and A. O. Caldeira, Phys. Rev. B **60**, 88 (1999).

[109] N. Hasselmann, A. H. Castro Neto, C. Morais Smith, and Y. Dimashko, Phys. Rev. Lett. **82**, 2135 (1999).

[110] T. Nattermann, I. Lyuksyutov, and M. Schwartz, Europhys. Lett. **16**, 295 (1991).

[111] S. N. Coppersmith *et al.*, Phys. Rev. B **25**, 349 (1982).

[112] M. P. A. Fisher, P. B. Weichman, G. Grinstein, and D. S. Fisher, Phys. Rev. B **40**, 546 (1989).

[113] T. Giamarchi and H. J. Schulz, Phys. Rev. B **37**, 325 (1988).

[114] J. V. José, L. P. Kadanoff, S. Kirkpatrick, and D. R. Nelson, Phys. Rev. B **16**, 1217 (1977).

[115] C. Morais Smith, N. Hasselmann, and A. H. Castro Neto, to appear in "Physics in Local Lattice Distortions", Ed. by H. Oyanagi, Am. Inst. of Phys. (2001).

[116] C. Morais Smith, N. Hasselmann, and Y. Dimashko, Journal de Physique IV (Colloques) IV **9**, (1999).

[117] M. Fujita *et al.*, Preprint cond. mat. **0101320**, (2001).

[118] N. Hasselmann, A. H. Castro Neto, and C. Morais Smith, "Stripes and Related Phenomena", Ed. by A. Bianconi and N. L. Saini, Kluwer Academic/Plenum Publishers (2000).

[119] J. Zaanen and W. van Saarloos, Physica C **282-287**, 178 (1997).

[120] S. M. Hayden *et al.*, Phys. Rev. Lett. **76**, 1344 (1996).

[121] T. E. Mason *et al.*, Phys. Rev. Lett. **77**, 1604 (1996).

[122] P. Bourges *et al.*, Science **288**, 1234 (2000).

[123] R. P. Sharma *et al.*, Nature (London) **404**, 736 (2000).

[124] C. Morais Smith, Y. Dimashko, N. Hasselmann, and A. O. Caldeira, "Stripes and Related Phenomena", Ed. by A. Bianconi and N. L. Saini, Kluwer Academic/Plenum Publishers (2000).

[125] C. Morais Smith, Y. Dimashko, N. Hasselmann, and A. O. Caldeira, Phys. Rev. B **58**, 453 (1998).

[126] A. I. Larkin and Y. N. Ovchinnikov, J. of Low Temp. Physics **34**, 409 (1979).

[127] H. Fukuyama and P. A. Lee, Phys. Rev. B **17**, 535 (1978).

[128] P. A. Lee and T. M. Rice, Phys. Rev. B **19**, 3970 (1979).

[129] G. Blatter *et al.*, Rev. Mod. Phys. **66**, 1125 (1994).

[130] C. Y. Chen *et al.*, Phys. Rev. Lett. **63**, 2307 (1989).

[131] D. A. Huse, C. L. Henley, and D. S. Fisher, Phys. Rev. Lett. **55**, 2924 (1985).

[132] M. Kardar, Nucl. Phys. B **290**, 582 (1987).

[133] J. S. Langer, Ann. Phys. **41**, 108 (1967).

[134] H. J. Schulz, Phys. Rev. B **34**, 6372 (1986).

[135] L. P. Kadanoff and A. C. Brown, Ann. Phys. **121**, 318 (1979).

[136] M. den Nijs, Physica A **111**, 273 (1982).

[137] M. den Nijs and K. Rommelse, Phys. Rev. B **40**, 4709 (1989).

[138] F. D. M. Haldane, Phys. Rev. B **25**, R4925 (1982).

[139] D. Loss and T. Martin, Phys. Rev. B **50**, 12160 (1994).

[140] J. Voit, Phys. Rev. Lett. **64**, 323 (1990).

[141] H. J. Schulz, Phys. Rev. B **22**, 5274 (1980).

[142] V. L. Pokrovsky and A. L. Talapov, Phys. Rev. Lett. **42**, 65 (1979).

[143] A. M. Polyakov, *Gauge Fields and Strings* (Harwood Academic Publishers, Chur, 1987).

[144] D. R. Nelson, Phys. Rev. B **18**, 2318 (1978).

Acknowledgements

I would especially like to thank Prof. Hartwig Schmidt, Prof. Cristiane Morais Smith and Prof. Antonio Castro Neto for their advice and support of this thesis. I profitted from many discussions with Prof. Hartwig Schmidt, especially during the initial phase of the thesis. His comments and suggestions served as an important compass for my work. I benefitted very much from a close collaboration with Prof. Cristiane Morais Smith, especially during the time I stayed in Hamburg but also during my entire thesis. She was a very supportive supervisor and the many discussions with her helped to shape the thesis. Prof. Antonio Castro Neto inspired and guided much of the work presented here. His enthusiasm and many inspirational ideas were an essential ingredient for this work and I thank him for being much more than a host during my stay in Riverside.

A fruitful collaboration with Prof. Amir Caldeira, which also gave me the opportunity to work with him for two months in Campinas, is gratefully acknowledged. I extend my thanks to Dr. Yuri Dimashko for many discussions and a collaboration during his stay in Hamburg. I thank Prof. Dionys Bariswyl for his unmatched hospitality and the possibility to work for two months in Fribourg. I enjoyed a very productive three months stay at Los Alamos and I thank Prof. Allan Bishop for this opportunity. I thank Prof. Chris Hammel and Dr. Nick Curro for helpful explanations and discussions on their experimental data during this visit.

Especially I wish to thank Dr. Guillermo Castilla, Dr. Alexander Chernyshev, Dr. Eduardo Novais and Dr. Thorsten Dröse for numerous discussions and suggestions.

This thesis was financially supported by the Graduiertenkolleg ,,Physik nanostrukturierter Festkörper" (Univ. Hamburg) and by a Gottlieb Daimler- und Karl Benz-Stiftung scholarship which supported me during my stay in Riverside. Further I acknowledge financial support from a DAAP/CAPES scholarship, from the Université de Fribourg and from the Los Alamos National Laboratory.